NONLINEAR STOCHASTIC DYNAMICS OF A NANOMECHANICAL RESONATOR COUPLED TO A SINGLE ELECTRON TRANSISTOR

BY SUBRAMANIAN RAMAKRISHNAN

A dissertation submitted to the

Graduate School—New Brunswick

Rutgers, The State University of New Jersey

in partial fulfillment of the requirements

for the degree of

Doctor of Philosophy

Graduate Program in Mechanical and Aerospace Engineering

Written under the direction of

Professor Haym Benaroya

and approved by

_____

_____

_____

_____

New Brunswick, New Jersey

October, 2007

ABSTRACT OF THE DISSERTATION

Nonlinear Stochastic Dynamics of a Nanomechanical Resonator Coupled to a Single Electron Transistor

by Subramanian Ramakrishnan

Dissertation Director: Professor Haym Benaroya

Nanoelectromechanical systems (NEMS) comprise nanometer to micrometer scale mechanical oscillators coupled to electronic devices of comparable dimensions. NEMS have great potential for sensor applications as well as for exploring fundamental physics. The dynamics of a nanomechanical resonator coupled to a single electron transistor (SET) is considered in the Duffing regime using a master equation approach and a Langevin approach. In the first approach, the master equations are derived and solved using a finite element method as well as a moment approximation method for both the single-well and the (inverted) double-well Duffing potentials. It is observed that the SET damps the resonator motion much more effectively in the single-well Duffing case in comparison with the linear case. In the double-well case we observe the existence of a limit cycle wherein the SET and the resonator exist in a state of dynamic equilibrium. This is followed by the onset of instability in the numerical solutions. The results from the master equation approach are used in a numerical fitting procedure to characterize the damping term in the averaged equations of motion of the system. It is observed that a linear damping term provides the best fit in all cases except for the strongly nonlinear regime. Based on this result, a Langevin equation is written down from which

a Fokker-Planck equation is derived for the system. The Fokker-Planck equation is solved analytically, in closed form, for the steady state. In the time dependent case, the equation is solved using a finite element method and the results are shown to be in qualitative agreement with those obtained using the master equation approach. Therefore it is established that the SET-resonator system attains a steady state much more rapidly in the single-well Duffing regime. Finally, the steady state analytical solution to the Fokker-Planck equation is utilized to show that the steady state effective temperature is lower in the presence of the single-well Duffing nonlinearity.

Acknowledgements

I have dreamed of earning a doctorate in the mathematical sciences since I was seventeen. As the dream is finally being realized at the young age of thirty five plus (during which I studied in three countries, obtained two master's degrees and worked in spells in the industry), so many kind faces light up the landscape of memory and I struggle to express my gratitude in full measure.

Undoubtedly, my first vote of thanks goes to my advisor at Rutgers, Prof. Haym Benaroya. I shall remain indebted to him for the rest of my life. The intellectual freedom he afforded me, the support and encouragement with respect to the research, his patience with my mistakes and his kindness as a human being are all qualities that I shall strive to emulate. Coming back into academia after an innings in the industry with a young family to attend to at home (and commuting from Brooklyn to New Brunswick, to boot), it would've been nigh impossible to complete the doctorate in three years but for Haym's pivotal role as my advisor.

I am grateful to our graduate director Prof. Haim Baruh for being instrumental in my admission to Rutgers and for introducing me to Prof. Benaroya. In addition, Prof. Baruh's doors were always open to me for a discussion on matters academic and otherwise.

It is a pleasure to record my gratitude to Dr. Yuriy Gulak, post-doc in our Center who has been immensely generous with his time and his wisdom. In particular, the numerical aspects of this work would've been hard to accomplish without his unstinted support and patience, not to mention his expertise.

The interdisciplinary nature of the research implied that I could not have gone forward without extended interactions with good physicists. Accordingly, I am grateful

to Prof. Bala Sundaram (UMass-Boston) for introducing me to the world of nanoresonators, to Prof. Miles Blencowe (Dartmouth College) for being so generous with his time and for inviting me to give a talk, to Prof. Andrew Armour (Univ. of Nottingham, UK) for useful discussions and to Prof. Keith Schwab (Cornell Univ.) for enlightening me on the experimental aspects of nanoresonators. I would like to add to this list Prof. Dan Ocone (Rutgers) and Prof. Joel Lebowitz (Rutgers).

It is a pleasure to record my thanks to the friends I have made here at Rutgers. Praveen Subramanian, Doddi Sai Kumar, Arvind Ayyer, Pradeep George , Shankar Salvady, Guru Srinivasan, Alisar Tuncer, Elan Borenstein are some of the names that immediately spring to the fore. On the administrative side, I am truly thankful to Ms. Aeisha Jenkins for being such a splendid graduate secretary and to Ms. Trisha Mazzucco for being so supportive as our Center administrative assistant.

It is with deep gratitude that I acknowledge the graduate fellowship from the School of Engineering that financially sustained me during my years at Rutgers. Again, it was Prof. Benaroya who recommended me for the fellowship and I am thankful to him for that as well.

On the home front, my gratitude to my dear wife Vidya simply defies words. Without her faith in me and her unconditional love and support, this dissertation could not have been written. Thanks are due to my little son Hari who always stopped crying when told that his father had to go to the university.

I owe most of what I know to my father, Late S. Ramakrishnan. The brilliance and purity of his intellect were always an inspiration. In particular, his almost poetic approach to mathematics lit a fire in me that continues to burn today. This dissertation is dedicated to his memory in gratitude and fond remembrance. I am also grateful to my mother, Ms. Ponna Ramakrishnan who underwent deep struggles of solitude so that her son could reach his goals in a far away land.

And last but not the least, I am grateful to the Almighty from Whom all emerges and in Whom all converges.

Dedication

To the memory of my beloved father Late S. Ramakrishnan, an outstanding mathematician and an excellent teacher who taught me most of what I know.

Table of Contents

List of Figures

List of Abbreviations

NEMS is for Nanoelectromechanical systems

FEM is for Finite Element Method

MEM is for Moment Evolution Method

Chapter 1

Introduction

1.1 Nanoelectromechanical Systems

Nanoelectromechanical systems (NEMS) comprise nanometer to micrometer scale mechanical oscillators coupled to electronic devices of comparable dimensions. The motion of such an oscillator leaves its signature on the current characteristics of the electronic device and hence the latter may be used as a measurement device for the motion characteristics of the oscillator. Quantitatively, NEMS have ushered in the era of numbers hitherto unheard of in technology. For instance, the typical dimensions of a NEMS oscillator is a few microns and frequencies in the range of a few MHz to a GHz have been achieved [16], [37]. Indeed, the spectrum of functionalities that such numbers imply have been exploited and the proven and potential applications of these systems include ultrasensitive motion detection, mass sensing, bio-molecular studies and quantum enabled technologies.

In keeping with the current fascination with the nanoscale in general, NEMS have witnessed an enormous amount of research activity in recent times. In a fundamental sense, the unique feature of these systems is the coupling achieved between mechanical and electronic degrees of freedom. While the idea has been around for a while, NEMS have become a reality due to the recent spectacular advances in semiconductor fabrication technology and are poised to play a pivotal role in one of the pet themes of the present time namely minaturization.

There exists a vast literature on NEMS. In 2000, Craighead [23] published a review that surveyed the field at that time. The book of Cleland [15] provides a comprehensive introduction to various aspects of the subject. Blick and co-workers [10] review

experimental methods in NEMS while Blencowe [9] presents a more recent survey.

We now turn to some specific applications of NEMS in the next section.

1.2 Applications of NEMS

Among the most spectacular applications of NEMS is motion sensing. For instance, in 2003, Knobel and Cleland [40] reported nanometer scale displacement sensing using an electronic device known as the single electron transistor (SET). The resonator in their experiment was a "3μm long $\times$ 250 nm wide $\times$ 200 nm thick doubly clamped beam of single-crystal GaAs, capacitively coupled to an aluminum SET, located 250 nm from the beam." A displacement sensitivity of 2.0×10^{-15} m $Hz^{\frac{-1}{2}}$ at 116.7 MHz resonant frequency of the beam was reported.

In another remarkable experiment in 2004, LaHaye and co-workers [41] reported an experiment in which they used a vibrating nano-beam about a hundredth of a millimeter long as a displacement sensor. The beam had a frequency of 20 million cycles per second (20 MHz), was cooled in the experiment to about 60 millikelvins and had a measured displacement sensitivity of 10^{-5} nanometers. This displacement sensitivity corresponds to about 1/1000 the diameter of a single hydrogen atom.

Another area of application is mass sensing. Ekinci and co-workers [26] reported an experiment in which a modulated flux of atoms was adsorbed onto the surface of a nanomechanical resonator in an ultrahigh-vacuum environment. The mass-induced resonance frequency shifts of the resonator due to the adsorption process was measured to report a mass sensitivity of 2.53×10^{-18} g.

In the area of charge sensing, Cleland and Roukes [17] reported a NEMS based charge detector that achieved a charge sensitivity of $0.1e$, where e is the unit electron charge.

It is clear from our discussion thus far that NEMS have revolutionized sensing technology. However, the utility of these devices is not restricted to practical applications and NEMS have implications for fundamental physics. We now turn to a discussion of those implications.

From a theoretical point of view, NEMS straddle the classical and the quantum worlds since while the oscillator is a macroscopic object, the processes that take place in the electronic device are essentially quantum mechanical [14]. On the one hand, despite quantum mechanics having been formulated almost 75 years ago, fundamental questions regarding the interface between the classical and quantum regimes of mechanics remain yet unanswered. The precise nature of the relationship between the macroscopic (classical) and microscopic (quantum) worlds, whether the transition from one to the other is governed by yet to be discovered physics or whether classical physics is just a true approximation to quantum physics are all open questions [8]. On the other hand, questions in quantum measurement (the interaction of a microscopic system with a macroscopic measurement apparatus) and quantum control (could one control the evolution of a quantum system from a given state to a desired one?) have profound implications for futuristic technologies such as the design of truly nano-devices and, on further extrapolation, for the fantastic possibilities perceived by quantum computation. The point of all this is that, owing to the scale at which they function, NEMS provide a rich arena for research in all of the above areas both as a test bed for the validation of practical ideas as well as to navigate theoretical efforts.

If classical physics is a faithful approximation of quantum physics at the macroscopic scale, then, in principle, one should be able to observe quantum phenomena in the motion of macroscopic objects. Precisely, one should be able to validate the Heisenberg uncertainty principle in the macroscopic domain. Let us consider the motion of a nanomechanical oscillator. Due to its extremely small size, the oscillator is to be considered as executing thermal Brownian motion under the influence of stochastic atmospheric forces and defects in its own structure. This motion is dictated by the laws of statistical mechanics and it follows that, if cooled sufficiently under controlled conditions, the amplitude of this motion will tend to vanish. The temperature that defines this threshold is determined by the resonant frequency of the oscillator. If the laws of quantum physics are valid, what remains when the Brownian motion subsides is the quantum zero point fluctuation of the oscillator in its lowest energy state. The

key point is that, as a consequence of the uncertainty principle, this zero point state is not the state of absolute rest. In other words, the laws of quantum physics prohibit the oscillator from being in a state of total rest. It is now straightforward to see how NEMS experiments can play a crucial role in validating the uncertainty principle for macroscopic systems. If displacement measurements can be made on the beam, at temperatures that guarantee the absence of Brownian motion, then those measurements can be compared to the zero point displacements predicted by quantum physics. It is important to note here that in their experiment with the 20 MHz beam, LaHaye and co-workers [41] reported a measured displacement sensitivity within an astonishing factor of 10 of the zero point amplitude predicted by the uncertainty principle for their system. Hence it is fair to conclude that the state-of-the-art in this enterprise stands on the threshold of actually testing the laws of quantum mechanics in a macroscopic system. In this context, we also note here that the quantum measurement aspect is a significant contributor to the importance of cooling effects in NEMS [46].

Having provided an overview of the applications of NEMS and established that they are of interest from both the practical and theoretical points of view, we now embark on a discussion of theoretical models of NEMS in the next section.

1.3 Theoretical Models of NEMS

Due to the scales in which they operate and the fact that they couple the mechanical and electronic degrees of freedom, NEMS are complex and interesting dynamical systems in their own right. Nevertheless, a number of open questions remain and analytical modelling of NEMS is well acknowledged as a fertile area of current research (see, for instance [9]).

In an abstract sense, the dynamics of NEMS is a vibration problem since, after all, one is dealing with an oscillator. However, the typical sizes of NEMS oscillators, the extraordinarily high frequencies and the defining characteristic of interaction with the electronic device all conspire to negate a straightforward treatment of the problem. A robust analytical model, while addressing all of the above, should also account for the

following unique features of NEMS dynamics.

Firstly, while the oscillator is expected to behave as a classical dynamical system, the electronic processes occuring in the device that are responsible for driving the oscillator are inherently quantum mechanical. Moreover, the oscillator motion influences the electronic process as well (which is the basis for using NEMS as sensors) making the oscillator and the device a genuinely coupled system. Therefore, analytical models have to deal with this situation. Furthermore, it is observed in experiments (see, for instance [46]) that interaction with the electronic device under extreme conditions (typically characterized by operating temperatures in the millikelvin range) can push the oscillator to purely quantum states.

Secondly, the dynamical features of NEMS demand a stochastic treatment. This is due to the facts that the electronic processes involved are random processes [28] and that the typical size and frequency of the oscillator points to the importance of noise in the system [18].

In the absence of generic principles for the analytical modelling of NEMS, attempts have been mostly on a case by case basis and we now address the models relevant to our discussion.

Lifshitz and Cross [44] presented a deterministic model to explain the experimental results of Buks and Roukes [12] who studied the response of an array of 67 fully suspended, doubly clamped oscillators to parametric excitation. Each resonator was a $270\times1\times0.25$ μm beam spaced 4 μm away from its neighbors. Applied electrostatic forces induced coupling between the beams and the system was parametrically driven by an AC source. The response of the array was measured using diffraction techniques and showed the following features:(1) The typical response with increasing frequency had a small number of wide peaks where the response increased gradually and decreased abruptly, and (2) The coupled system showed response at frequencies higher than the expected ones. While the nonlinear model of Lifshitz and Cross qualitatively explains the features observed in the experiment, it is not applicable to the case of a NEMS oscillator actively coupled to an electronic device.

We now turn to a discussion of two analytical models of interest to us in this dissertation. In 2004, Armour, Blencowe and Zhang [3] proposed an interesting model that addressed the classical dynamics of a nanomechanical resonator coupled to an electronic device known as the single electron transistor (SET). The SET has proved to be an outstanding device in the context of NEMS in recent years [3], [19], [20], [36] and we discuss it in detail as part of our discussion of the Armour-Blencowe-Zhang (ABZ) model in Chapter 2. Here we note that the ABZ approach models the resonator as a stochastic linear oscillator subject to random forces imparted by the SET. In turn, the motion of the resonator influences the current in the transistor. The state of the coupled system is characterized by probability density functions which satisfy a pair of partial differential equations known as master equations. Solving the master equations, the model reaches the conclusion that interaction with the SET damps the resonator motion driving the coupled system to a steady state. The solution also determines the current through the SET as a function of the steady state probabilities. The two key assumptions of the ABZ model are that the SET and the resonator are weakly coupled and that there exists a wide separation of time scales between the frequency of the resonator and the electron tunnelling process in the SET. Indeed, despite the high frequency of NEMS oscillators, the electronic processes in the device occur at a much faster rate. Following the ABZ model there have been very recent attempts to study the motion of SET-resonator system in the strong coupling regime. For instance, in 2006, Doiron, Belzig and Bruder [25] presented a model extending the ABZ ideas to the strong coupling regime leading to a description of the damping process in the strong coupling regime.

The second model of interest to us is the one presented by Clerk and Bennett in 2005 [20] which adopts a Langevin approach to the SET-resonator system. This is based on the seminal work of Clerk [19] in quantum limited position detection. The Langevin equation is a classical equation well known in the context of stochastic dynamical systems in general and brownian motion in particular [31]. The key point of the Clerk-Bennett approach is that, starting from quantum theoretic considerations of

processes in the SET, it establishes rigorously that the dynamics of the resonator is well approximated by a classical Langevin equation. We discuss this approach in Chapter 2 but note here that as in the ABZ model, the resonator in modelled here as a stochastic linear harmonic oscillator. While concurring with the main conclusions of the ABZ model, the Clerk-Bennett model shows applicability to a broad spectrum of devices including a more sophisticated version of the SET known as the superconducting SET (SSET).

It is important to note here that the ABZ and Clerk-Bennett models make predictions on the behavior of the SET-resonator system in the readily accessible classical regime which have been confirmed by recent experiments (see, for instance, [46]).

1.4 Nonlinear Phenomena in NEMS

Given the typical operating frequencies of NEMS oscillators, it is natural to expect nonlinear phenomena to play an important role in the dynamics. In 2000, Erbe [27] and co-workers reported an experiment with a nonlinear nanomechanical resonator in which they showed the utility of the nonlinear response in an application for signal processing known as mixing, in the radio-frequency regime. They modelled the resonator as a deteministic Duffing system. The Duffing equation has for long served as an important paradigm for a broad class of nonlinear phenomena ([34], [57]) and this was among the first instances when it began to make its presence felt in NEMS. In 2002, Scheible and co-workers [52] reported evidence of a nanomechanical resonator transitioning to the chaotic regime. In the same year, Buks and Roukes [12] in their experiment with an array of resonators reported that nonlinear effects dominated the system response. Blick and co-workers [10], in their comprehensive review of NEMS, point to the Duffing equation as best suited to the study of nanoresonators in the nonlinear regime. In 2005, Aldridge and Cleland [1] reported an experiment which measured the nonlinear response of a nanoresonator with very high precision. They noted that, at large drive amplitudes, the behavior of doubly clamped resonators is similar to that of a Duffing oscillator. In the same year, Zaitsev and Buks [60], following the work of Lifshitz

and Cross [44], reported that introducing a nonlinear damping term into the Duffing equation better accounted for the behavior of a nanomechanical oscillator considered in their experiment.

The Duffing nonlinearity has been utilized in quantum models of NEMS as well. In 2004, Peano and Thorwat [49] theoretically investigated the nonlinear response of a driven nanomechanical beam, from a quantum mechanical point of view. Their results pointed to the importance of nonlinear considerations in NEMS.

We also note here that the Duffing oscillator is a Hamiltonian system characterized by a quartic term in the potential energy of the system. The Duffing regime can be naturally classified into two sub-cases depending on whether this quartic term is positive or negative and the two cases yield qualitatively different dynamics. Based on the geometry of the potential energy function, the case where the quartic term is positive may be termed the single-well Duffing case whereas the case where the quartic term is negative may be termed the double-well Duffing case. While most of the extant models in the Duffing regime treat the single-well case, the double-well case is interesting in its own right and is appropriate in models of strongly nonlinear behavior.

Thus, the importance of nonlinear phenomena in general and the Duffing regime in particular for NEMS is currently well recognized in the literature from both the theoretical and practical points of view. However, we note here that, to the best of our knowledge, no analytical model for NEMS exists in the nonlinear regime that accounts for the cardinal dynamical features of NEMS that were discussed in the previous section.

1.5 Motivation and Outline of the Dissertation

Our discussion so far points to the importance of the nonlinear regime with respect to NEMS, both from the theoretical and practical perspectives. Having observed the absence of analytical models for NEMS in the nonlinear regime that take into account the complexity of the coupled dynamics, we seek to develop in this dissertation, analytical nonlinear stochastic models for a nanomechanical resonator coupled to a SET. Specifically, we seek to generalize the Armour-Blencowe-Zhang (ABZ) model and the

Langevin approach of the Clerk-Bennett model to the Duffing regime of the NEMS under discussion.

Once the generalized dynamical equations are derived and the model is solved, aspects of particular interest to us are the following. The damping effects in resonator motion is a central issue in NEMS with direct implications for the efficacy of the system in sensory applications. Therefore, it is of interest to investigate the damping mechanism in the Duffing regime. Another important aspect of the Duffing resonator is the stability properties of the solutions. The onset of instability (a phenomenon frequently observed nonlinear systems), aside from being a phenomenon of theoretical interest, has a direct impact on the robustness of NEMS in applications. Also of great interest to us are temperature effects in the Duffing regime. There is a tremendous amount of current interest in cooling effects observed in NEMS and the question of the relationship between nonlinearity and temperature is one of importance.

The outline of the dissertation is as follows.

In Chapter 2 we first discuss the phenomenon of single electron tunnelling and the working of the SET. This is followed by detailed accounts of the Armour-Blencowe-Zhang model and the Langevin model proposed by Clerk and Bennett. Thus this chapter provides the analytical basis for the research carried out in this dissertation.

In Chapter 3 we first derive the dynamical equations of the generalized ABZ model (the master equations) in the Duffing regime. We define a new parameter η which naturally emerges from appropriate scaling of the master equations and characterizes the type and strength of the Duffing nonlinearity. We propose and develop two methods of solution for the master equations: a finite element method and a moment evolution method. We then solve the single-well case of the Duffing regime by the two methods and discuss the results. We also validate the results of the ABZ model by reducing our equations to the linear case and analyzing the solutions thence obtained.

In Chapter 4 we solve the double-well case of the Duffing regime and discuss the results. In this case, we observe the remarkable result that there exist regimes where the SET fails to damp the resonator and the coupled system settles into a state of

dynamical equilibrium. Our results also indicate the onset of instability as we vary the parameter η. Motivated by the observation of instability from the numerical results, we carry out a stability analysis of the moment evolution equations using Lyapunov's first method and conclude that the analytical results are consistent with the numerical ones with respect to the onset of instability.

In Chapter 5 we explore in further detail the phenomenon of damping of the resonator motion by the SET in the Duffing regime. We use the results of the resonator response obtained in the previous chapters to characterize the mathematical nature of the damping term in the equation of motion of the resonator by using a numerical fitting procedure. The results are then used to clarify the validity of using linear damping terms in analytical models of resonator motion.

In Chapter 6 we investigate the resonator dynamics in the Duffing regime using the Langevin method exemplified by the Clerk-Bennett model. Starting from a stochastic differential equation for the resonator motion, we first derive the corresponding Fokker-Planck equation satisfied by the probability density function that describes the resonator dynamics. We obtain an analytical closed form solution to the Fokker-Planck equation in the steady state. We then solve the equation in the time dependent case using the finite element method used in Chapter 3 and show that the results obtained for the resonator response are consistent with those obtained using the generalized ABZ model. Finally, we invoke a generalized version of the equipartition of energy theorem from statistical mechanics and exploit the closed form analytical solution of the steady state Fokker-Planck equation to show that the resonator attains a lower effective steady state temperature in the presence of the single-well Duffing nonlinearity.

In Chapter 7 we conclude the dissertation with a discussion of the results obtained in the previous chapters and suggestions for further research.

Chapter 2

Analytical Models For the SET-Nanoresonator System

2.1 Introduction

In this chapter we consider two analytical approaches to modeling the dynamics of the SET-nanoresonator system. These two models, which we generalize to the Duffing regime in this dissertation, are unique in that they attempt to capture the specifics of the dynamical interaction between the SET and the resonator. The SET being a key element of our system, it is essential to understand the principle behind its working. Hence, in Sec 2 of this chapter we provide an overview of the phenomenon of single electron tunneling and its realization in the SET. In Sec 3 we present the analytical model for a nanoresonator coupled to a SET enunciated by Armour *et al.* [3] which shall henceforth be referred to as the Armour-Blencowe-Zhang (ABZ) model. It is to be reiterated here that an ideal model for the system under consideration ought to be a hybrid between a classical and a quantum mechanical one. However, as discussed in Chapter 1, NEMS straddle the classical and quantum regimes of mechanics and the plethora of outstanding questions in the area of quantum-classical transitions present formidable challenges in representing them by analytical models valid in both regimes. Indeed, this statement currently applies to all NEMS.

In this context, the ABZ model achieves a compromise by representing the electron tunneling process using expressions arising from quantum mechanical calculations whilst the resonator is treated as a classical harmonic oscillator. Therefore the ABZ approach may be characterized as a semi-classical model that is explicitly valid in the classical regime. The central feature of the model is the recognition that since the electron tunneling process in the SET is a stochastic process [9],[28], the SET-resonator

coupled dynamics demand a stochastic treatment. Hence, in the model the dynamics is encoded into probability density functions associated with the process. These density functions satisfy a system of coupled, partial differential equations known as the master equations. Mathematically, the ABZ approach reduces to the derivation and the solution of the master equations. In Sec 4, we discuss an alternative, first principles approach to the SET-resonator system first discussed by Clerk and Bennett [20]. The main feature of this model is the treatment of the stochastic dynamics of the resonator using a classical Langevin equation and henceforth we refer to this approach as the Langevin model. While at first sight this model does not appear to address the electron tunneling phenomenon in as much detail as the ABZ model, the conclusions with respect to the dynamics turn out to be essentially the same in both approaches. Moreover, that a classical Langevin equation is an adequate approximation for the coupled dynamics is established in this model based on a rigorous quantum field theoretic calculation. In summary, the models discussed in this chapter form the basis for our treatment of the SET-nanoresonator system in the Duffing regime.

2.2 The SET-Nanoresonator System

2.2.1 Single Electron Tunneling and the SET

The phenomenon of single electron tunneling and its realization in the single electron transistor (SET) have elevated electronic detection capabilities to unprecedented levels. Our discussion of the topic is primarily based on the work of Ferry and Goodnick [28]. Other references include the fundamental work of Averin and Likharev [5] and Ben-Jacob et. al.[6].

A conventional MetalOxideSemiconductor Field Effect Transistor (MOSFET), the fundamental switching and amplification device of digital electronics, comprises three terminals viz. a source electrode, a drain electrode and a gate electrode and a channel of material (usually a semi-conductor) connecting the source and drain electrodes [28]. The gate voltage controls the density of electrons in the conduction channel and hence

the flow of current in the channel. The key point here is that the transfer of electrons in the channel is assumed to be a continuous process when the gate voltage is non-zero. The electrons behave like a compressible fluid with the only quantum mechanical constraint on their flow between the source and drain electrodes being the Pauli exclusion principle. In other words, there exists a 'conduction band continuum' of energy levels that the electrons in the channel are free to occupy.

A radical modification of this paradigm, known as the single electron tunneling transistor, was proposed by Averin and Likharev in 1985 [5] and realized and demonstrated by Fulton and Dolan in 1987 [30]. The idea is to exploit the phenomenon of quantum tunneling to achieve the transfer of electrons, one at a time, to and from a metallic island formed by joining together two tunnel junctions. This sandwich of the tunnel junctions replaces the conduction channel in a conventional transistor with the island. An important consequence is that the available energy levels in the island are discrete. Therefore, an electron tunneling onto the island inhabits a particular energy level in contrast to the conduction band in a conventional transistor. Hence, the tunneling of a single electron may be observed and controlled by varying the discrete energy levels through applying a potential difference in the vicinity of the island. A factor that could interfere with the phenomenon is the thermal noise that is ubiquitous in small scale devices. Random thermal fluctuations can affect the resolution of the discrete energy levels and hence the condition for single electron tunneling to take place is given by the following important inequality:

$$\Delta E \; >> \; k_B T, \tag{2.1}$$

where ΔE is the spacing of energy levels on the island (known as the Coulomb energy), k_B is the famous Boltzmann constant and T is the temperature of the island. Moreover, ΔE, which is the energy barrier that an electron needs to overcome before it can tunnel into the island, is given by the expression

$$\Delta E \; = \; \frac{e^2}{2C}, \tag{2.2}$$

where e is the charge of an electron and C is total capacitance of the gate capacitor

(the gate voltage is controlled using a capacitor) and the tunnel junctions, i.e., the net capacitance of the island.

The above formulae lead to interesting conclusions. Firstly, we note that ΔE is inversely proportional to C. In the light of this observation, let us consider the scenario that an electron inhabits the island. Now, even though e is very small, ΔE can become very large for very small C. This is precisely what is believed to happen in the nanoscale. The dimensions of the island reflect on its capacitance and hence ΔE becomes large for even the presence of a single electron in the island, thereby preventing further tunneling onto the island. This phenomenon, which is the basis for single electron tunneling, is called the Coulomb blockade. The central theme is to exploit this situation to observe the process and to control the current by providing the energy required for another electron to tunnel, at our discretion. Importantly, due to the Coulomb blockade effect, only a single electron tunnels onto or off the island at any given time and hence the name single electron transistor. In the context of a nanoresonator coupled to a SET, displacements of the resonator alter the gate capacitance. Hence, measuring the current through the SET yields a measure of the resonator displacement thereby facilitating the use of the system as a displacement detector.

Furthermore, the above equations, when viewed in conjunction, imply that for high enough ΔE, the phenomenon can be observed at high (room) temperatures. It is obvious that this aspect enhances the value of the process for real world applications.

The realization of such a device is contingent on the ability to fabricate and operate at nanoscales. Precisely, quantum tunneling occurs only when two electrodes are separated by an insulating barrier about 1 nm thick. At this scale, electrons (which obey Fermi-Dirac statistics and whose energy is known as the Fermi energy) can tunnel through the insulator even though in terms of classical physics such a phenomenon would be forbidden. The remarkable advances in nano-fabrication in the last few years have established the SET as an important nanoscale device in the present time.

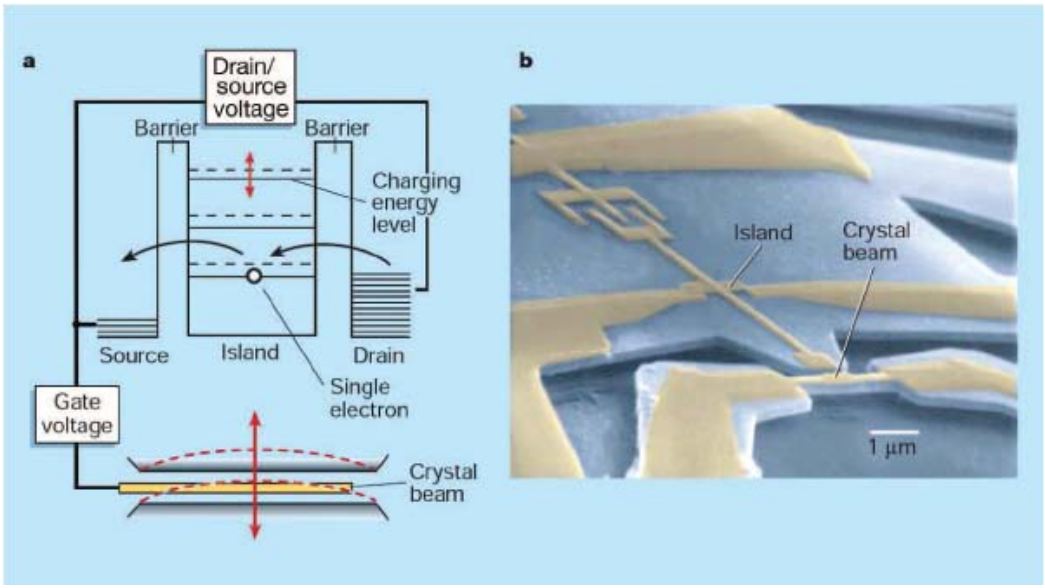

Figure 2.1: (**a**) Schematic of an SET-resonator system and (**b**) Experimental Realization

2.2.2 The SET Coupled to a Nanoresonator

We now discuss the system of interest to us, the SET coupled to a nanoresonator. A schematic of the arrangement and a single electron microscope (SEM) micrograph of an actual experimental realization of the system are provided in Fig 2.1 which is reproduced from [9]. The micrograph is from the experimental set up first reported by Knobel and Cleland [40]. Electrons quantum tunnel, one at a time, from the drain electrode to the SET island and then onto the source electrode. This flow of electrons is modulated by the drain-source voltage and the gate voltage. Essentially, the phenomenon of tunneling (both from the drain to the island as well as from the island to the source) occurs when an electron gains sufficient energy as to overcome the corresponding energy barrier. The energy levels of the barriers can be controlled by varying the gate voltage which, in turn, is dependent on the gate capacitance. The fundamental idea here, as already mentioned in the previous sub-section, is to let the displacement of the resonator control the gate capacitance. Thus, there exists a direct correlation between the motion of the resonator and the SET current. This current, when amplified and detected, serves as a signature of the resonator displacement.

It is of great interest and importance to understand the dynamical interaction between the SET and the resonator, both from the practical as well as the theoretical points of view. Given the scale and complexity of the interaction between the two components, one is confronted with a challenging dynamical system. The main features of the interaction that ought to be taken into account in a dynamical model are the following:

(1) While the motion of the resonator affects the SET current, the tunneling electrons in the SET provide a reaction force to the resonator which is known as back-action [3],[20]. Hence an analytical model should view the SET-resonator as a coupled dynamical system.

(2) Quantum tunneling is a random process. Therefore, the back-action force imparted on the resonator by the SET as well as the dynamical evolution of the coupled system demands treatment as a stochastic process.

(3) Given that the SET operates on the principle of single electron tunneling, the coupled dynamical system may be viewed as a two-state system; the two states defined by N or $N+1$ electrons in the central island. The initial island number N would depend on the specific properties of a given SET. It is to be noted, however, that given the time-scale of the tunneling processes, the switching between the two states is fast enough to appear as a continuous process at the classical level.

(4) It is not *a priori* clear whether, as the system evolves, the SET receives or provides energy to the resonator. A dynamical model needs to address this question as well as the important issues of whether the system ultimately reaches a steady state and if it does, the stability properties of the steady state.

In the following sections we discuss the ABZ model and the Langevin model with a closer look at how both address the above issues.

2.3 The Armour-Blencowe-Zhang (ABZ) Model

As a prelude to a discussion of the ABZ model we present a circuit diagram of the SET-resonator system in Fig 2.2, reproduced here from [9]. The SET comprises the

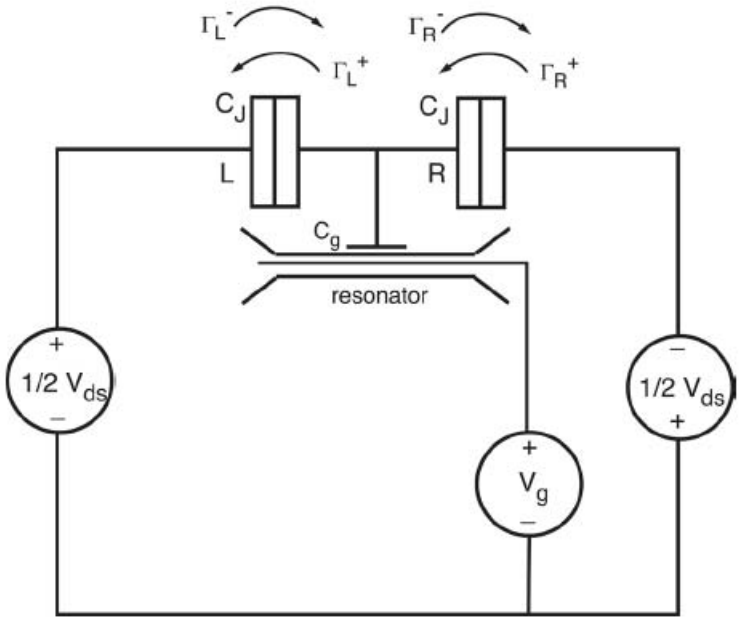

Figure 2.2: Circuit diagram of an SET-resonator system

left and right tunnel junctions (indicated by L and R in the figure) as well as the gate (island) whose capacitance is labeled C_g in the figure. The gate voltage is denoted by V_g and the drain-source voltage by V_{ds}. The tunneling rates across the left and right junctions are given by ${\Gamma_{L/R}}^{\pm}$ where the plus and minus signs indicate the direction of tunneling.

The starting point for the ABZ model is the so-called orthodox model [28] for a stand-alone SET. The only two accessible dynamical states of the SET being those with N or $N+1$ electrons in the central island, the orthodox model characterizes these mutually exclusive states by probabilities $p_N(t)$ and $p_{N+1}(t)$ that correspond to the probabilities of finding N or $N+1$ electrons in the island at time t, respectively. The time evolution of these probabilities are governed by a pair of coupled master equations given by [28]:

$$\frac{dp_N}{dt} = -\left({\Gamma_L}^- + {\Gamma_R}^+\right) p_N + \left({\Gamma_L}^+ + {\Gamma_R}^-\right) p_{N+1} \tag{2.3}$$

$$\frac{dp_{N+1}}{dt} = \left({\Gamma_L}^- + {\Gamma_R}^+\right) p_N - \left({\Gamma_L}^+ + {\Gamma_R}^-\right) p_{N+1}, \tag{2.4}$$

where ${\Gamma_{L/R}}^{\pm}$ represent the tunneling rates in the left (L) and right (R) junctions of the SET island. Here the $\pm$ signs indicate that tunneling, under very general conditions, is possible in both directions. The expressions for the tunneling rates emerge from a fully quantum mechanical calculation using Fermi's Golden Rule [28],[2] and take the final form:

$$ {\Gamma_{L/R}}^{\pm} = \frac{1}{e^2 R_J} \frac{{E_{L/R}}^{\pm}}{\left[1 - \exp\left(-E^{\pm}_{L/R}/k_B T_e\right)\right]}. \tag{2.5} $$

In the above expression e represents the electron charge, R_J the effective junction resistance (assumed identical for both junctions of the island), k_B the Boltzmann constant, T_e the temperature of the source, drain and island electron reservoirs (all assumed equal) and $E^{\pm}_{L/R}$ the energy gained by a single electron tunneling to the left (+) or to the right (−) across the left (L) or right (R) junction.

It is straightforward to observe from Eqns 2.3 and 2.4 that the probability of finding the SET in either of the two states given by $p = p_N + p_{N+1}$ is conserved since adding Eqns 2.3 and 2.4 leads to:

$$ \frac{dp}{dt} = 0. \tag{2.6} $$

The significant step taken in the ABZ model is the modification of the above master equations to incorporate the dynamics of the resonator. This is not straightforward to carry out primarily because once the SET is coupled to the resonator we have a hybrid between a continuous and a discrete system: the state of the SET shifts between the two discrete possibilities of N and $N+1$ electrons in the island while the resonator evolves in time as a continuous dynamical system, in principle having access to any point in the position-velocity (x, u) space. Under these circumstances, the ABZ model suggests a probabilistic description of the coupled system based on the following observations.

The state of the resonator can be described by a continuous probability density function $P(x, u; t)$ where x stands for the position and u stands for the velocity of the resonator. Therefore the dynamics of the resonator is fully described by $P(x, u; t)$ which, for all t, satisfies the normalization condition given by:

$$ \int_{-\infty}^{\infty} \int_{-\infty}^{\infty} P(x, u)\, dx du = 1. \tag{2.7} $$

Now, since for each state of the resonator the SET can be in either of the states N or $N+1$, one needs to be able to define the probability of finding the SET in either of these states, given that the probability density of the resonator is $P(x,u;t)$. To this end, the ABZ model defines a decomposition of P into $P(x,u;t) = P_N(x,u;t) + P_{N+1}(x,u;t)$ where the functions P_N and P_{N+1} are called sub-densities and are used to define the probabilities of the finding the SET in the N or $N+1$ states respectively, given that the resonator is in the state (x,u) at time t. The acutal probabilities may be denoted by p_N and p_{N+1} and of course, their sum is unity at a given instant in time and for any given state of the resonator.

Thus, $P(x,u;t) = P_N(x,u;t) + P_{N+1}(x,u;t)$ is a construction such that given that the resonator is in a state (x,u) at time t, we can compute the probabilities of the SET being in the N or $N+1$ state.

To proceed further, the model invokes a celebrated result from classical mechanics known as Liouville's theorem. Consider a Hamiltonian system with the Hamiltonian (the total energy) denoted by $H(p,q)$ where p is the generalized momentum corresponding to the generalized co-ordinate q. The Poisson bracket of a dynamical variable $Q(p,q)$ is defined as:

$$\{H,Q\} \;=\; \frac{\partial H}{\partial q}\,\frac{\partial Q}{\partial p} \;-\; \frac{\partial H}{\partial p}\,\frac{\partial Q}{\partial q}. \tag{2.8}$$

Liouville's theorem [32],[42],[59] states that the time evolution of the dynamical variable $Q(p,q)$ can be expressed as:

$$\frac{\partial Q}{\partial t} = \{H,Q\}. \tag{2.9}$$

Since the transition of the SET island from the N electron state to the $N+1$ electron state (and vice versa) is guaranteed to alter the dynamical state of the resonator, the resonator Hamiltonian corresponding to the two states is denoted by H_N and H_{N+1}. The key idea now is to treat the probability sub-densities P_N and P_{N+1} as dynamical variables evolving under the corresponding Hamiltonians H_N and H_{N+1}. At once, Liouville's theorem can be absorbed into the orthodox model master Equations 2.3 and

2.4 to write the generalized master equations for the SET-nanoresonator system as:

$$\frac{\partial P_N}{\partial t} = \{H_N, P_N\} - \left(\Gamma_L{}^- + \Gamma_R{}^+\right) P_N + \left(\Gamma_L{}^+ + \Gamma_R{}^-\right) P_{N+1} \tag{2.10}$$

$$\frac{\partial P_{N+1}}{\partial t} = \{H_{N+1}, P_N\} + \left(\Gamma_L{}^- + \Gamma_R{}^+\right) P_N - \left(\Gamma_L{}^+ + \Gamma_R{}^-\right) P_{N+1}. \tag{2.11}$$

A set of assumptions is introduced at this stage in order to obtain an explicit form of the master equations that is amenable to solution.

The first of these is the following. When the electron temperature T_e is small compared to the single electron charging energy (in other words, $k_B T_e << \frac{e^2}{2C}$ cf Eqns 2.1, 2.2) Eqn 2.5 for the tunneling rates, on substituting $T_e = 0$ becomes:

$$\Gamma_{L/R}{}^{\pm} = \frac{1}{e^2 R_J} E_{L/R}{}^{\pm}. \tag{2.12}$$

However, within the model, tunneling is allowed only when $E_{L/R}{}^{\pm}$ is positive. In order to reflect this requirement (in other words, to make $\Gamma_{L/R}{}^{\pm}$ vanish if $E_{L/R}{}^{\pm}$ is negative) the Heaviside step function is introduced as:

$$\Gamma_{L/R}{}^{\pm} = \frac{1}{e^2 R_J} E_{L/R}{}^{\pm} \Theta\left(E_{L/R}{}^{\pm}\right), \tag{2.13}$$

where $\Theta\left(E_{L/R}{}^{\pm}\right)$ is the Heaviside step function, which, by definition, vanishes when the argument is negative. Thus, this implies that in the ABZ model a given tunnel rate is negligible if the associated E is negative. For micron scale SETs, $C \approx 1$ femto F $\left(\equiv 10^{-15} F\right)$ yielding $T_e << 1K$. This condition being satisfied by most current experiments, the ABZ model uses Eqn 2.13 to calculate the tunneling rates.

The second assumption relates to the direction of tunneling. For electron temperature T_e of the order discussed in the previous paragraph and appropriately chosen drain-source voltage, it can be shown that tunneling occurs only in one direction. Hence only the Γ^+ terms are taken into account in the master equations.

The third assumption is that the resonator behaves as a linear harmonic oscillator. Hence, the resonator Hamiltonian corresponding to the N electron state is written as:

$$H_N = \frac{p^2}{2m} + \frac{1}{2} m\omega^2 x^2, \tag{2.14}$$

where m is the mass of the resonator, ω is its natural frequency, x the position co-ordinate and p the momentum conjugate to this position co-ordinate. Now, it is assumed that an electron tunneling onto the island (thereby changing the island electron number from N to $N+1$) induces a change in position of the resonator by a small distance x_0. Geometrically, this may be viewed as the tunneling electron shifting the origin of the harmonic oscillator potential by x_0. Indeed, this alters the resonator Hamiltonian which can now be written as:

$$H_{N+1} = \frac{p^2}{2m} + \frac{1}{2}m\omega^2 \left(x - x_0\right)^2 . \tag{2.15}$$

We now pause to examine the master equations 2.10 and 2.11 from the standpoint of the resonator dynamics in the light of our discussion thus far. Let us imagine for a moment that the tunneling terms are absent in the RHS of the master equations. Now, if the initial conditions for the sub-densities are taken to be $P_N\left(x, v, t_0\right) = \delta\left(x\right)\delta\left(v\right)$ and $P_{N+1} = 0$ (where $\delta\left(\right)$ stands for the Dirac delta function), this corresponds to the island number remaining fixed at N. Then, the evolving probability density remains a delta function for all time thereby describing deterministic harmonic oscillator motion of the resonator. What happens in the presence of the tunneling terms is that the evolving probability density begins to spread. The randomly fluctuating electron number of the island (between N and $N+1$) causes the evolution of the oscillator to be a stochastic process as it interrupts the deterministic evolution by causing the origin of the harmonic oscillator potential to shift randomly by an amount $\pm x_0$.

The final step needed before the master equations can be solved is to calculate the tunneling rates (established as well approximated by Eqn 2.13) in terms of the resonator Hamiltonians H_N and H_{N+1}. We note that, conceptually, this completes the circle in terms of the coupling between the tunneling process and the resonator motion. For, while the tunneling process influences the resonator dynamics (by altering the Hamiltonian) the tunneling rates themselves are calculated based on the resonator Hamiltonian.

In what follows we present a summary of the calculations that lead to the master equations and refer to [3],[9] for the details. The total energy of the SET-resonator

system corresponding to the N and $N+1$ states is given by the total Hamiltonians H'_N and H'_{N+1} as [3]:

$$\begin{aligned} H'_N &= E_c N' + H_N \\ H'_{N+1} &= -E_c N' - \frac{1}{2}\omega^2 {x_0}^2 - \omega^2 {x_0}^2 \left(N_g - N' - \frac{1}{2} \right) + H_{N+1}. \end{aligned} \tag{2.16}$$

In Eqns 2.16, H_N and H_{N+1} are the resonator Hamiltonians given by Eqns 2.14 and 2.15. The other terms are the contributions to the total energy by the island. Here, $E_c = e^2/2C$ is the island charging energy where e is the electron charge and C is the total SET capacitance. $N' = N_g - N - 1/2$ is a constant defined to simplify the expressions in Eqns 2.16. In the definition of N', the quantity N_g is called the charge induced by the gate voltage and is defined by $N_g = C_g V_g/e$ where C_g and V_g are the gate capacitance and the gate voltage, respectively. The only term that remains to be defined in Eqns 2.16 is x_0. This is the shift in resonator position induced by a tunneling electron and is explicitly defined as [3] $x_0 = -eN_g/Cm\omega^2 d$, where d is the resonator-SET island gap.

We now recall that tunneling rates of the model are given by Eqn 2.13 and that only positive values for ${E_{L/R}}^{\pm}$ enter the discussion (since otherwise the Heaviside function ensures that the tunneling rates vanish). Furthermore, for positive values of ${E_{L/R}}^{\pm}$ the Heaviside function returns the value of unity. Keeping in mind that tunneling is assumed to take place only in one direction, the tunneling terms to be considered now are ${E_{L/R}}^{+}$. Dropping the redundant superscript, the left (E_L) and right (E_R) tunneling rates are now calculated in the ABZ model as [3]:

$$E_L = H'_{N+1} - H'_N - \mu_L \tag{2.17}$$

$$E_R = H'_N - H'_{N+1} + \mu_R, \tag{2.18}$$

where μ_L (μ_R) is the chemical potential of the left(right)-hand lead. These potentials enter into the calculation because they contribute to the net energy of the SET island and hence need to be taken into account in calculating the tunneling rates [28]. These potentials can be expressed in terms of the drain-source voltage V_{ds} and the electron

charge e as [3]:

$$-\mu_L = \mu_R = eV_{ds}/2. \tag{2.19}$$

Substituting the expressions for the Hamiltonians given by Eqns 2.16 into Eqns 2.17 and 2.18 the ABZ model obtains the master equations in explicit form as (Eqns. 15 and 16 in [3]):

$$\frac{\partial P_N}{\partial t} = {\omega_0}^2(x)\frac{\partial P_N}{\partial u} - u\frac{\partial P_N}{\partial x} + \frac{1}{e^2R}\left[E_L P_{N+1} - E_R P_N - m{\omega_0}^2 x_0 x P\right] \tag{2.20}$$

$$\frac{\partial P_{N+1}}{\partial t} = {\omega_0}^2(x - x_0)\frac{\partial P_{N+1}}{\partial u} - u\frac{\partial P_{N+1}}{\partial x} - \frac{1}{e^2R}\left[E_L P_{N+1} - E_R P_N - m{\omega_0}^2 x_0 x P\right], \tag{2.21}$$

where,

$$E_L = -2E_c N' - m{\omega_0}^2 {x_0}^2\left(N_g - N' - 1/2\right) + eV_{ds}/2 \tag{2.22}$$

$$E_R = 2E_c N' + m{\omega_0}^2 {x_0}^2\left(N_g - N' - 1/2\right) + eV_{ds}/2. \tag{2.23}$$

The tunnelling rates in the master equations in the form given by Eqns. 2.20 and 2.21 are the ones we use in our generalization of the ABZ model to the Duffing regime.

However, the master equations may also be written in in non-dimensional form as [9]:

$$\frac{\partial P_N}{\partial t} = \epsilon^2 x\frac{\partial P_N}{\partial u} - u\frac{\partial P_N}{\partial x} + \tilde{E}_L P_{N+1} - \tilde{E}_R P_N \tag{2.24}$$

$$\frac{\partial P_{N+1}}{\partial t} = \epsilon^2(x-1)\frac{\partial P_{N+1}}{\partial u} - u\frac{\partial P_{N+1}}{\partial x} - \tilde{E}_L P_{N+1} + \tilde{E}_R P_N, \tag{2.25}$$

where the new dimensionless parameters ϵ and κ have been introduced. We note that all the variables in the above equations are scaled variables. The parameter ϵ, defined as $\epsilon = \omega\,\tau_t$, characterizes the separation between the resonator and SET dynamical timescales. We note that τ_t, the time taken by an electron to tunnel on to or off of the island, defines the characteristic timescale of the SET. The other dimensionless parameter is defined as $\kappa = m\omega^2 {x_0}^2/eV_{ds}$ and characterizes the coupling strength between the resonator and the SET and is within the terms $\tilde{E}_L$ and $\tilde{E}_R$ defined below. As mentioned earlier, the shift in resonator position induced by a tunneling electron has the explicit form $x_0 = -eN_g/Cm\omega^2 d$, where d is the resonator-SET island gap. Hence, it follows that the

coupling strength κ can be controlled by varying the gate voltage V_g. The significance of these parameters will be discussed momentarily.

With respect to the master Equations 2.24 and 2.25 it remains to define the dimensionless energy terms $\tilde{E}_L$ and $\tilde{E}_R$. These can be expressed in terms of the parameters defined so far, as [3]:

$$\tilde{E}_L = -\frac{e}{CV_{ds}}\left(N_g - N - \frac{1}{2}\right) - \kappa N + \frac{1}{2} - \kappa x \tag{2.26}$$

$$\tilde{E}_R = +\frac{e}{CV_{ds}}\left(N_g - N - \frac{1}{2}\right) + \kappa N + \frac{1}{2} + \kappa x. \tag{2.27}$$

The main point to be noted from the master Equations 2.24 and 2.25 is that the parameters κ and ϵ hold the key to describing the coupled SET-resonator dynamics. The importance of these parameters can be seen from the following. In essence, the SET and the resonator are two dynamical systems in mutual interaction. Two characteristics of each of the systems that can be expected to influence the coupled dynamics are the timescale and the total energy. The parameter ϵ compares the relative timescales of the oscillator period and the electron tunneling time. On the other hand κ compares the energy scale of the oscillator motion (note that the numerator in the definition of κ is twice the potential energy corresponding to a displacement of x_0) to the energy scale defined by the drain-source voltage. In general, the electron tunneling time is much smaller compared to the oscillator period and hence practical situations are best described by small values for ϵ. Likewise, strong interaction between the SET and the resonator complicate the dynamics to the extent that models such as the ABZ are likely to lose their validity. Hence it is important to consider small values for κ as well.

Having derived the master equations, the ABZ model proceeds to solve them under the fortunate circumstance that the master equations yield a closed set of moment equations. While it is a standard technique in stochastic analysis to attempt to solve for the moments of an unknown density when confronted with a complicated partial differential equation governing the evolution of the density itself (the point being that a system of simpler ordinary differential equations uniquely satisfied by the moments can usually be derived from the partial differential equation), the fact that one obtains a

closed system of moment equations in this case is a consequence of the assumption that the resonator is a linear harmonic oscillator. As will be seen in our generalization of the ABZ model to the Duffing regime, the hierarchy of moment equations turns out to be an infinite one in that case thereby raising significant analytical challenges in solving the master equations.

The ABZ model is solved for the moment equations using an analytical approximation as well as numerically. The approximate analytical solution for the mean displacement of the resonator is given by:

$$\langle x(t)\rangle = e^{-\kappa\epsilon^2 t/2\tau_t}\left[x(0)\cos\left(\sqrt{1-\kappa}\,\epsilon t/\tau_t\right) + \frac{u(0)\,\tau_t}{\sqrt{1-\kappa}\,\epsilon}\sin\left(\sqrt{1-\kappa}\,\epsilon t/\tau_t\right)\right], \quad (2.28)$$

where $\langle . \rangle$ represents the ensemble average. Here $x(0)$ and $u(0)$ are the initial conditions on the position and velocity, respectively. A comparison of this approximate analytical solution with an exact numerical one is reproduced from [3] in the following figure.

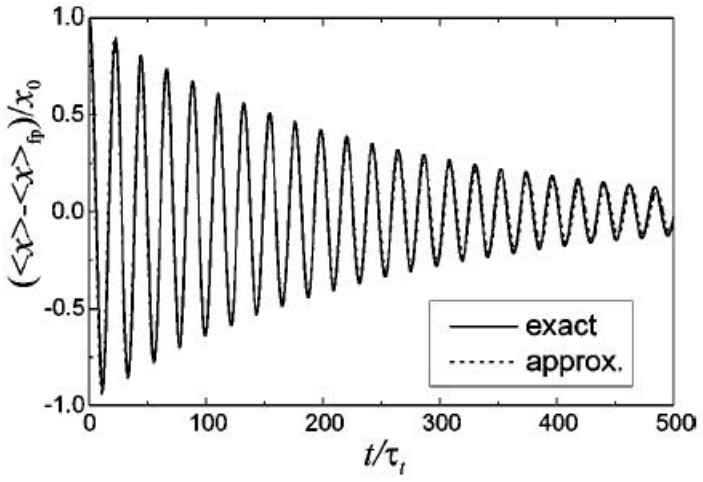

Figure 2.3: Mean Displacement of Resonator

In Fig 2.3 the displacement co-ordinate is taken such that it is centered around the fixed point $\langle x\rangle_{fp}$ of the system of moment equations and scaled with respect to x_0, the shift in resonator position induced by a tunneling electron. This, as well as the scaling of the temporal variable in terms of the electron tunneling time, is carried out

for convenience and does not affect the qualitative nature of the dynamics. We now discuss the main conclusions of the ABZ model.

As seen from Fig 2.3, the interaction with the SET damps the oscillator and the system reaches a steady state. This is a significant conclusion since, as discussed in Sec 2.2.1, it was not *a priori* clear that interaction with the SET would provide a damping mechanism for the resonator. It is of interest to note that the analytical solution given by Eqn 2.28 corresponds to the motion of a damped harmonic oscillator with damping constant $\kappa\ \epsilon^2/\tau_t$ and frequency $\sqrt{1-\kappa}\ \epsilon/\tau_t$. The damping constant may be viewed as an intrinsic damping rate for the SET-resonator system. It is to be emphasized here that the model, to begin with, made no assumptions whatsoever about damping in the system. Practically, for the system to be of value as a sensor it is imperative that a steady state is reached since the transients of the complicated dynamics between the SET and the resonator cannot be allowed to interfere with the sensing process. We also note here that, in the broad context of nanomechanical resonators coupled to mesoscopic devices, most of the earlier models, for instance (Gorelik *et al.* [33], Isacsson *et al.* [38], Nord *et al.* [47], Armour and MacKinnon [4], Brandes and Lambert [11]) do not discuss the possibility of interaction with the device damping the resonator motion. The ABZ model is novel in this respect.

That the system reaches a steady state is further evidenced by the steady state densities depicted in Fig 2.4.

Recalling that the frequency of the resonator was expressed in terms of ϵ and τ_t as $\omega = \epsilon/\tau_t$, we can conclude that interaction with the SET alters the frequency of the oscillator by a factor of $\sqrt{1-\kappa}$. It is immediate then that the model is valid only in the regime of weak coupling ($\kappa < 1$) since otherwise we are led to the physically untenable conclusion that the frequency of the resonator vanishes. A wide separation of time scales ($\epsilon < 1$) is also a necessary condition for the assumptions of the model to hold. However, this is readily achieved in practice since, despite having frequencies in the GHz range, the time period of the resonator is still significantly large compared to the electron tunneling time. In the case of the results shown in Fig 2.3, the values of

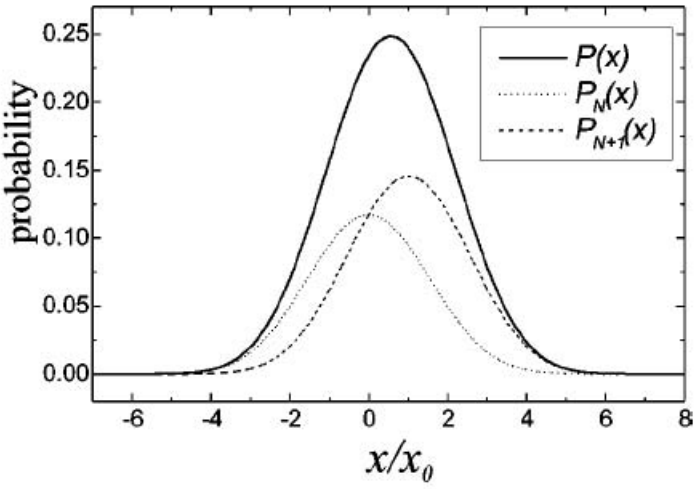

Figure 2.4: Steady State Sub-densities

the parameters are taken to be $\kappa = 0.1$ and $\epsilon = 0.3$.

Further evidence that the model breaks down in the strong coupling regime is provided by the behavior of the variance of the displacement in the steady state with respect to increasing coupling strength κ [3]. This is shown in Fig 2.5. The curve shows the effect of κ on the (scaled) variance in the steady state based on the analytical solution while the points show the corresponding results from the numerical solution. Evidently, the numerical and analytical results diverge from each other as the coupling strength is increased.

Thus we are led to the important conclusion that the ABZ model is valid in the regime where the SET is weakly coupled to the resonator and when there is a wide separation of timescales between the two. This serves as a useful guideline in choosing the parameters in our generalization to the Duffing case.

The next point relates to the definition of an effective temperature of the resonator. It is a fundamental result in statistical mechanics that in the steady state, a relationship between the average energy and the absolute temperature of the system can be established using the equipartition of energy theorem [39], [58]. We examine this theorem and its generalization for the nonlinear potentials in detail in Chapter 6. Here we point

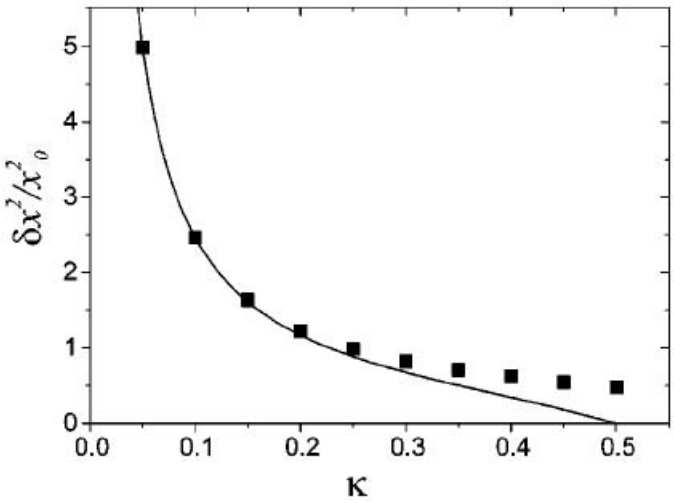

Figure 2.5: Comparison of Variance in Steady State

out that the ABZ model exploits the existence of a steady state to define an effective temperature T_{eff} of the system given by:

$$k_B T_{eff} = eV_{ds} p_N p_{N+1}. \tag{2.29}$$

Here k_B is the Boltzmann constant, V_{ds} is the drain-source voltage and p_N and p_{N+1} are the steady state probabilities of finding the SET in the N and $N+1$ state respectively obtained from the ABZ model. The point of view that the above result affords is that the SET acts like a thermal bath for the oscillator. While Eqn 2.29 implies that the coupling strength κ does not explicitly influence the effective temperature, it is to be noted that the steady state probabilities p_N and p_{N+1} are, indeed, dependent on the coupling strength. The characterization of the system using an effective temperature is very useful, particularly in the context of using NEMS as a test bed for observing explicit quantum behavior.

The final conclusion relates to the effect of the coupled SET-resonator dynamics on the SET current. It is known from the orthodox model [3] that the mean value of the current, assuming very low electron temperature is given by:

$$\langle I \rangle = \frac{e}{\tau_t} p_N^{st} p_{N+1}^{st}, \tag{2.30}$$

where e is the electron charge, τ_t is the tunneling time and p_N^{st} and p_{N+1}^{st} are the steady state probabilities obtained from the orthodox model. The ABZ model shows that due to the SET-resonator coupling the averaged current gets modified as:

$$\langle I \rangle = \frac{e}{\tau_t} p_N p_{N+1} \left(1 - \kappa\right), \tag{2.31}$$

where e is the electron charge, τ_t is the tunneling time and p_N and p_{N+1} are the steady state probabilities obtained from the ABZ model (same as those in Eqn 2.29). From Eqn 2.31 it is observed that coupling to the resonator slightly reduces the current flowing through the SET. Moreover, this is yet another indication that the model is valid in the weak coupling regime since the current vanishes as κ tends to unity.

This concludes our discussion of the ABZ model.

2.4 The Langevin Model

The Langevin model for the stochastic motion of a dynamical system goes back to the classical work of Langevin that addressed Brownian motion. The starting point is a differential equation of motion the forcing term in which is a stochastic process known as the white noise process. In modern terminology such a differential equation is known as a stochastic differential equation (SDE). We discuss SDEs and the associated Fokker-Planck equations in Chapter 6 as a prelude to our treatment of the Duffing resonator using the Langevin approach and suffice it to mention here that the Fokker-Planck equation is a partial differential equation governing the evolution of the probability density corresponding to the stochastic process represented by the Langevin equation. Hence, the Fokker-Planck equation in the Langevin approach is equivalent to the master equations in the ABZ model.

In the context of the SET-resonator system, the Langevin model presents an *ab initio* formulation of the problem. The motion of the resonator would be described by the following Langevin equation:

$$\ddot{x} + \gamma \dot{x} + {\omega_0}^2 x = F\left(t\right). \tag{2.32}$$

Here, γ is the damping coefficient, ω_0 is the natural frequency of the oscillator and $F(t)$ is the random force imparted by the tunneling electrons in the SET on the oscillator. We note that here no specific assumptions are made about the SET-resonator interaction but for the customary one in stochastic analysis that $F(t)$ is a zero mean, delta correlated, white noise process. Hence it is reasonable to expect that this equation of motion holds across the spectrum of coupling strengths. Moreover this eliminates the need for specific assumptions regarding the nature of the SET-resonator interaction. However, we note that the damping term in the equation has been introduced by hand whereas the ABZ model did not assume that the SET damps the resonator. Furthermore, Eqn 2.32 is inherently a classical equation and hence does not reflect the essentially quantum mechanical nature of the process of electron tunneling in the SET.

It is in this context that an aspect of the work of Clerk and Bennett [20] enters our discussion. In the last few years Clerk [19] and co-workers [21] in a series of papers have investigated various aspects of measurements in mesoscopic systems whose working principles are explicitly quantum mechanical. It is a fundamental tenet of theoretical formulations of interacting quantum Hamiltonian systems that the interaction is captured by adding an interaction term to the system Hamiltonian. For instance, if systems A and B interact with each other, the effective Hamiltonian of the interaction H (from which the coupled dynamics follows) is written as:

$$H = H_A + H_B + H_{int}, \tag{2.33}$$

where H_A and H_B are the respective Hamiltonians of systems A and B and H_{int} is the interaction term. This principle has met with great success in modeling even the complex interactions arising in quantum field theories. Clerk and co-workers adopt this abstract approach to the generic situation of a macroscopic system (say, a nanoresonator) interacting with an electronic device (e.g., a SET). Thus the interaction between the resonator and the SET is accounted for by a term:

$$H_{int} = -A\hat{x} \cdot \hat{F}, \tag{2.34}$$

where the operator $\hat{x}$ corresponds to the position of the resonator and $\hat{F}$ corresponds to

the quantity in the device that drives the interaction which is the number of electrons in the island in the case of the SET. A is a dimensionless coupling constant akin to κ in the ABZ model. Germane to the present discussion is the remarkable conclusion from rigorous theoretical calculations in the above formalism that the motion of the resonator is well approximated by the classical Langevin equation very similar to Eqn 2.32 [19],[20].

Having thus established that the Langevin model is a reasonable approach to the SET-resonator system, the rest of the tale unfolds in a straightforward manner. Using the theory of stochastic processes one obtains passage to the Fokker-Planck equation from the Langevin equation 2.32. While this is discussed in further detail in Chapter 6, here we write down the Fokker-Planck equation as:

$$\frac{\partial P}{\partial t} = -y\frac{\partial P}{\partial x} + \gamma\left(P + y\frac{\partial P}{\partial y}\right) + {\omega_0}^2 x\frac{\partial P}{\partial y} + \frac{1}{2}\frac{\partial^2 P}{\partial y^2}. \tag{2.35}$$

where P is the probability density corresponding to the resonator motion and we have used the notation $\dot{x} = y$.

The work of Clerk and Bennett [20] proceeds to discuss how the definition of an effective temperature of the oscillator emerges from their model. The conclusions with respect to the SET-resonator system are in consonance with those of the ABZ model. Furthermore, the Clerk-Bennett work enters into a discussion of a more advanced version of the SET known as a superconducting SET (SSET). The key difference between the two is that the leads in a SSET are superconducting. The tunneling scenario changes in that instead of single electrons, it is electron pairs (also known as Cooper pairs) that tunnel in the SSET. The main advantage of using a SSET is that substantially lower temperatures are obtained for the system. Perhaps, the most interesting dynamical aspect of a SSET coupled to a nanoresonator is that there exist unstable regimes in which, instead of damping the resonator motion, the SSET actually pumps energy into the resonator. Interestingly, these conclusions were demonstrated by Naik *et al.* [46] in a remarkable experiment in 2006. While some of these ideas enter our discussions in later chapters, here we conclude with the note that solving Eqn 2.35 completely solves the dynamical aspect of the problem.

Chapter 3

Generalization of the ABZ Model - The Single-Well Duffing Case

3.1 Introduction

In this chapter we consider the nonlinear extension of the ABZ model [3] where we model the resonator as a Duffing oscillator. As discussed in Chapter 1, our motivation springs from the facts that the Duffing is the most important type of nonlinearity in the context of NEMS and that the coupled dynamics of the SET-resonator system in this regime has not been studied so far in the literature.

The Duffing oscillator is characterized by a quartic potential term in the Hamiltonian and naturally gives rise to two distinct sub-cases - those represented by whether the quartic term is added or subtracted from the harmonic oscillator potential. The distinction is important since the former subcase corresponds to a single-well shaped potential (hardening stiffness) while the latter corresponds to an inverted double-well shaped potential (softening stiffness) and the two cases engender qualitatively different dynamics. In this chapter we derive the master equations for the generic Duffing case, applicable to both the subcases. However, the analysis and discussion of the results here is focused on the single well Duffing case and the double-well case is treated in the next chapter.

In our analysis of the Duffing resonator motion we retain the framework and assumptions of the ABZ model that was discussed in detail in Chapter 2. We assume that the island charging energy E_c of the SET is large in comparison with the electronic thermal energy $k_B T_e$ and the drain-source bias eV_{ds}. We do not consider external damping effects. Moreover, since little is currently known about nonlinear behavior of the

SET, we neglect the nonlinear terms in the Hamiltonian in calculating the tunneling rates in the device. In other words, in our approach the nonlinear effects are confined to the resonator motion via the Poisson bracket terms in the master equations derived in [3]. This important assumption is further buttressed by the fact that in all the current models of the SET-resonator system, the gate capacitance of the SET is assumed to be a linear function of the oscillator displacement. This is tantamount to our approach of considering only the linear terms of the Hamiltonian in calculating the SET tunneling rate.

Based on the above assumptions we first derive the master equations. We then proceed to solve them to obtain the resonator response using two distinct methods - a finite element method (FEM) and a moment equations method (MEM). The FEM solves the master equations directly while the MEM provides the solution to a set of moment evolution equations that are generated from the master equations. It is important to observe here that, in sharp contrast to the resonator dynamics in the linear regime, one obtains an infinite hierarchy of moment equations in the Duffing regime. Indeed, this is a characteristic feature of all nonlinear systems. Therefore, in our case the MEM requires a set of approximations in order to obtain moment closure. However, we validate these approximations by invoking the results of the FEM. Of the two methods, while the FEM, in principle, provides more accurate solutions, the MEM is analytically more tractable. We first demonstrate that our results are in consonance with those of the ABZ model when we collapse our equations to obtain the linear case. This exercise also serves as an independent validation of the ABZ model. We then proceed to solve the Duffing case dealing with the sub-cases in detail and discuss the interesting dynamical behavior that emerges.

This chapter is organized as follows. In Sec 2 we derive the master equations for the general Duffing case. In Sec 3 we obtain the master equations in their non-dimensionalized form. In Sec 4 we show that a new parameter η that characterizes the nonlinearity naturally emerges from the scaling of the equations carried out in Sec 3. The entire analysis and discussion in this chapter is pivoted on this parameter η and

the unique nonlinear effects that arise as a consequence of its existence and variations. Moreover the two sub-cases of the Duffing correspond to η being positive or negative. In Sec 5 we derive the moment evolution equations for a generic η that are then solved in the later sections for the single-well Duffing subcase. A set of detailed calculations that lead to the moment evolution equations presented in this section are furnished in Appendix A. In Sec 6 we present an overview of the finite element method used to solve the master equations. The finite element code used and details regarding initial conditions are provided in Appendix B. In Sec 7 we validate the key results of the ABZ model from the standpoint of our generalization by considering the linear case. In Sec 8 we solve the single-well Duffing (hardening stiffness) case and discuss the results. We conclude the chapter in Sec 9 with an overview of our main results and a discussion.

3.2 The Master Equations

Consider a Duffing nanoresonator with resonator Hamiltonians for the N and $N+1$ states of the system given by:

$$H_N = \frac{p^2}{2m} + \frac{1}{2}m{\omega_0}^2[x^2 + \beta x^4] \tag{3.1}$$

$$H_{N+1} = \frac{p^2}{2m} + \frac{1}{2}m{\omega_0}^2[(x - x_0)^2 + \beta(x - x_0)^4]. \tag{3.2}$$

Here p represents the momentum, m the mass and ω_0 the frequency of the resonator. As in the ABZ model, x_0 is the distance between the equilibrium positions of the resonator corresponding to the N and $N+1$ states of the SET island. In comparison with a linear harmonic oscillator, the difference is the added term βx^4 in the potential energy. This is the generic potential for a Duffing system and β is a constant the magnitude of which determines the strength of the quartic order term in the potential function. The sign of β determines the geometry of the potential function and the two cases of β being positive or negative engender qualitatively different dynamics. We also note here that, by definition, the Hamiltonian is a function of the momentum p and the co-ordinate x where both are treated as independent variables.

We first compute the Poisson brackets of H_N and H_{N+1} with P_N and P_{N+1} where

P_N and P_{N+1} represent the density functions corresponding to the N and $N+1$ states of the system. We recall from our discussion in Chapter 2 that the term resulting from the Poisson brackets of the Hamiltonians with the corresponding density functions is the dynamical contribution of the resonator motion to the master equations. The Poisson bracket of a dynamical variable $Q(x,p)$ with the system Hamiltonian $H(p,x)$ is defined as:

$$\{H,Q\} \;=\; \frac{\partial H}{\partial x}\,\frac{\partial Q}{\partial p} \;-\; \frac{\partial H}{\partial p}\,\frac{\partial Q}{\partial x}. \tag{3.3}$$

Considering P_N as a dynamical variable, the Poisson bracket of P_N and the corresponding Hamiltonian H_N can be written as:

$$\{H_N,P_N\} \;=\; \frac{\partial H_N}{\partial x}\,\frac{\partial P_N}{\partial p} \;-\; \frac{\partial H_N}{\partial p}\,\frac{\partial P_N}{\partial x}. \tag{3.4}$$

In order to compute each of the terms in Eqn 3.4 we first note that, by definition,

$$p = \; mu \tag{3.5}$$

$$\Rightarrow\; \frac{\partial u}{\partial p} = \frac{1}{m}, \tag{3.6}$$

where u is the velocity of the resonator. Using Eqn 3.1, Eqn 3.5 and Eqn 3.6 we can now compute,

$$\frac{\partial H_N}{\partial p} = \; \frac{p}{m} \; = u. \tag{3.7}$$

$$\begin{aligned}\frac{\partial P_N}{\partial p} &= \frac{\partial P_N}{\partial u}\frac{\partial u}{\partial p}\\ &= \frac{1}{m}\frac{\partial P_N}{\partial u}.\end{aligned} \tag{3.8}$$

We also obtain:

$$\frac{\partial H_N}{\partial x} = m{\omega_0}^2(x+2\beta x^3). \tag{3.9}$$

Substituting Eqn 3.9, Eqn 3.7 and Eqn 3.8 into Eqn 3.4 we get:

$$\begin{aligned}\{H_N,P_N\} &= m{\omega_0}^2(x+2\beta x^3)\frac{1}{m}\frac{\partial P_N}{\partial u} - u\frac{\partial P_N}{\partial x}\\ &= {\omega_0}^2(x+2\beta x^3)\frac{\partial P_N}{\partial u} - u\frac{\partial P_N}{\partial x}.\end{aligned} \tag{3.10}$$

In Eqn 3.10, for convenience we introduce the constant $\alpha = 2\beta$ without loss of generality. Indeed, α faithfully reflects changes in the nonlinear coefficient β in terms of

both magnitude and sign. Thus $\alpha > 0$ corresponds to a single-well potential (hardening stiffness) while $\alpha < 0$ indicates the double-well potential (softening stiffness). We write:

$$\{H_N, P_N\} = {\omega_0}^2(x + \alpha x^3)\frac{\partial P_N}{\partial u} - u\frac{\partial P_N}{\partial x}. \tag{3.11}$$

An identical calculation using H_{N+1} given by Eqn 3.2 yields the other Poisson bracket term as:

$$\{H_{N+1}, P_{N+1}\} = {\omega_0}^2\left[(x - x_0) + \alpha(x - x_0)^3\right]\frac{\partial P_{N+1}}{\partial u} - u\frac{\partial P_{N+1}}{\partial x}. \tag{3.12}$$

We now have the dynamical contribution of the Duffing resonator motion to the master equations for both states N and $N + 1$. We recall from Chapter 2 that the general form of the coupled master equations are given by Eqns. 2.10 and 2.11. When one-way tunneling is assumed, the Γ^- terms vanish to yield :

$$\frac{\partial P_N}{\partial t} = \{H_N, P_N\} - \Gamma_R\, P_N + \Gamma_L\, P_{N+1} \tag{3.13}$$

$$\frac{\partial P_{N+1}}{\partial t} = \{H_{N+1}, P_{N+1}\} - \Gamma_L\, P_{N+1} + \Gamma_R\, P_N. \tag{3.14}$$

The second and third terms on the RHS of Eqn 3.13 and Eqn 3.14 arise from the tunneling process in the SET with Γ_L and Γ_R denoting the left and right tunneling rates respectively, across the SET junction. We recall from Chapter 2 that the tunneling rates from the ABZ model are given by the third terms on the RHS of Eqns. 2.20 and 2.21. As discussed in the introductory section of this chapter, we assume that the linear part of the potential term in the resonator Hamiltonian alone is involved in calculating the tunneling rates. Hence these terms remain unchanged from the ABZ model and, using Eqn 3.11 and Eqn 3.12 in Eqn 3.13 and Eqn 3.14, we obtain the master equations as:

$$\frac{\partial P_N}{\partial t} = {\omega_0}^2(x + \alpha x^3)\frac{\partial P_N}{\partial u} \;-\; u\frac{\partial P_N}{\partial x} + \;\frac{1}{e^2 R}\left[E_L P_{N+1} - E_R P_N - m{\omega_0}^2 x_0 x P\right] \tag{3.15}$$

$$\begin{aligned}\frac{\partial P_{N+1}}{\partial t} = {\omega_0}^2\left[(x - x_0) + \alpha(x - x_0)^3\right]\frac{\partial P_{N+1}}{\partial u} \;-\; u\frac{\partial P_{N+1}}{\partial x} \\ -\;\frac{1}{e^2 R}\left[E_L P_{N+1} - E_R P_N - m{\omega_0}^2 x_0 x P\right].\end{aligned} \tag{3.16}$$

In the above equations, the total probability density $P = P_N + P_{N+1}$. Among the other coefficients, e is the electron charge, R the junction resistance, E_L and E_R the position independent parts of the tunneling rates as detailed in Chapter 2.

3.3 The Nondimensionalized Master Equations

In order to minimize the number of parameters in the problem and to achieve a better understanding of the physical aspects of the solution, it is advantageous to nondimensionalize the master equations Eqn 3.15 and Eqn 3.16 derived in the previous section. As a result of this exercise we are able to introduce a new parameter η that comprehensively captures the nonlinearity in the problem thereby facilitating a clear discussion of nonlinear effects.

Consider the following scaling transformations:

$$\begin{aligned} u' &= \frac{u}{u_0} \\ x' &= \frac{x}{x_0} \\ t' &= \frac{t}{\tau_t} \\ \epsilon &= \omega_0 \tau_t. \end{aligned} \tag{3.17}$$

Here, τ_t is the electron tunneling time across the SET junction. Since ω_0 is the frequency of the resonator, the scaled parameter ϵ compares the relative timescales of the resonator period and the electron tunneling time. We also note that ϵ is introduced in an identical fashion in the ABZ model. The resonator motion being much slower than the electron tunneling time, in general we expect $\epsilon \ll 1$.

We now apply the scaling transformation Eqns. 3.17 to Eqn 3.15. Consider the first term on the RHS of Eqn 3.15. Due to the resonator being displaced by an amount x_0 in the time τ_t that it takes for an extra electron to tunnel on to the SET island, the speed corresponding to this displacement may be written as $u_0 = x_0/\tau_t$. Using this relation

we can write:

$$\begin{aligned}\omega_0{}^2\left(x+\alpha x^3\right)\frac{\partial P_N}{\partial u} &= \frac{\epsilon^2}{\tau_t{}^2}\left(x_0x'+\alpha x_0{}^3x'^3\right)\frac{1}{u_0}\frac{\partial P_N}{\partial u'}\\ &= \frac{\epsilon^2}{\tau_t{}^2}x_0\left(x'+\alpha x_0{}^2x'^3\right)\frac{\tau_t}{x_0}\frac{\partial P_N}{\partial u'}\\ &= \frac{\epsilon^2}{\tau_t}\left(x'+\alpha x_0{}^2x'^3\right)\frac{\partial P_N}{\partial u'}.\end{aligned} \tag{3.18}$$

Considering the second term on the RHS of Eqn 3.15 we obtain:

$$\begin{aligned}u\frac{\partial P_N}{\partial x} &= u_0u'\frac{1}{x_0}\frac{\partial P_N}{\partial x'}\\ &= \frac{1}{\tau_t}u'\frac{\partial P_N}{\partial x'}.\end{aligned} \tag{3.19}$$

Considering the third term on the RHS of Eqn 3.15 we first introduce a simplification by setting $E_L = E_R = eV_{ds}/2$. As discussed in Chapter 2, E_L and E_R are position independent parts of the tunneling rates and are essentially constants for a given drain-source voltage V_{ds} [3]. Hence this choice, while simplifying the calculations, does not constrain the scope of our discussion or the validity of our conclusions in any manner. We note here that the ABZ model also adopts the same choice in carrying out its computations [3]. We now write the third term as:

$$\begin{aligned}\frac{1}{Re^2}\left(E_LP_{N+1}-E_RP_N-m\omega_0{}^2x_0xP\right) &= \frac{eV_{ds}}{2Re^2}\left(P_{N+1}-P_N-\frac{2m\omega_0{}^2x_0}{eV_{ds}}xP\right)\\ &= \frac{V_{ds}}{2Re}\left(P_{N+1}-P_N-\frac{2m\omega_0{}^2x_0}{eV_{ds}}xP\right).\end{aligned} \tag{3.20}$$

Introducing the non-dimensional parameter $\kappa = m\omega_0{}^2x_0{}^2/eV_{ds}$ defined in the ABZ model into Eqn 3.20 we write:

$$\begin{aligned}\frac{1}{Re^2}\left(E_LP_{N+1}-E_RP_N-m\omega_0{}^2x_0xP\right) &= \frac{V_{ds}}{2Re}\left(P_{N+1}-P_N-2\frac{\kappa}{x_0}x'x_0P\right)\\ &= \frac{V_{ds}}{Re}\left(\frac{P_{N+1}}{2}-\frac{P_N}{2}-\kappa x'P\right).\end{aligned} \tag{3.21}$$

Applying the scaling transformation to the term on the LHS of Eqn 3.15 and collecting the transformed terms from Eqn 3.18, Eqn 3.19 and Eqn 3.21 we write the full transformed equation as:

$$\begin{aligned}\frac{1}{\tau_t}\frac{\partial P_N}{\partial t'} = &\frac{\epsilon^2}{\tau_t}\left[x'+\alpha x_0{}^2x'^3\right]\frac{\partial P_N}{\partial u'}\\ &-\frac{1}{\tau_t}u'\frac{\partial P_N}{\partial x'}+\frac{V_{ds}}{Re}\left[\frac{P_{N+1}}{2}-\frac{P_N}{2}-\kappa x'P\right].\end{aligned} \tag{3.22}$$

Multiplying both sides of Eqn 3.22 by τ_t we obtain:

$$\begin{aligned}\frac{\partial P_N}{\partial t'} &= \epsilon^2 \left[x' + \alpha {x_0}^2 {x'}^3\right] \frac{\partial P_N}{\partial u'} \\ &\quad - u' \frac{\partial P_N}{\partial x'} + \frac{\tau_t V_{ds}}{Re} \left[\frac{P_{N+1}}{2} - \frac{P_N}{2} - \kappa x' P\right].\end{aligned} \tag{3.23}$$

We now invoke Ohm's Law ($V = IR$) to observe that $\tau_t V_{ds}/Re = 1$. This follows from the fact that in this case, the current $I = e/\tau_t$. Hence we write Eqn 3.23 as:

$$\begin{aligned}\frac{\partial P_N}{\partial t'} &= \epsilon^2 \left[x' + \alpha {x_0}^2 {x'}^3\right] \frac{\partial P_N}{\partial u'} \\ &\quad - u' \frac{\partial P_N}{\partial x'} + \left[\frac{P_{N+1}}{2} - \frac{P_N}{2} - \kappa x' P\right].\end{aligned} \tag{3.24}$$

Starting with Eqn 3.16 and repeating the steps *mutatis mutandis* leads to the following equation for P_{N+1}:

$$\begin{aligned}\frac{\partial P_{N+1}}{\partial t'} &= \epsilon^2 \left[\left(x' - 1\right) + \alpha {x_0}^2 \left(x' - 1\right)^3\right] \frac{\partial P_{N+1}}{\partial u'} \\ &\quad - u' \frac{\partial P_{N+1}}{\partial x'} - \left[\frac{P_{N+1}}{2} - \frac{P_N}{2} - \kappa x' P\right].\end{aligned} \tag{3.25}$$

At this point we identify the primed variables in Eqn 3.24 and Eqn 3.25 to be dummy variables and hence write our master equations as:

$$\begin{aligned}\frac{\partial P_N}{\partial t} &= \epsilon^2 \left[x + \alpha {x_0}^2 x^3\right] \frac{\partial P_N}{\partial u} \\ &\quad - u \frac{\partial P_N}{\partial x} + \left[\frac{P_{N+1}}{2} - \frac{P_N}{2} - \kappa x P\right].\end{aligned} \tag{3.26}$$

$$\begin{aligned}\frac{\partial P_{N+1}}{\partial t} &= \epsilon^2 \left[(x - 1) + \alpha {x_0}^2 (x - 1)^3\right] \frac{\partial P_{N+1}}{\partial u} \\ &\quad - u \frac{\partial P_{N+1}}{\partial x} - \left[\frac{P_{N+1}}{2} - \frac{P_N}{2} - \kappa x P\right].\end{aligned} \tag{3.27}$$

3.4 The New Parameter η

Comparing Eqn 3.26 and Eqn 3.27 with the master equations of the ABZ model (Eqns. 2.24 and 2.25) it is evident that nonlinearity in the resonator (exemplified by the quartic terms in the resonator Hamiltonians given by Eqn 3.1 and Eqn 3.2) contributes the terms $\alpha {x_0}^2 x^3$ and $\alpha {x_0}^2 (x - 1)^3$ to the master equations. The only other parameters in the equations are κ and ϵ familiar to us from our study of the ABZ model. Hence we define:

$$\eta = \alpha {x_0}^2. \tag{3.28}$$

We make the following observations about η.

Firstly, since ${x_0}^2$ is always positive, η is guaranteed to faithfully reflect sign changes in α. Therefore, changing the sign of η allows us to unambiguously represent the single-well and double-well Duffing potentials.

Secondly, η is the true index of the effective nonlinearity in the SET-resonator system. Consider a weakly nonlinear resonator that corresponds to a relatively small value of α. However, a relatively high value of x_0 (resulting from a stronger coupling between the SET and the resonator since x_0 is the resonator displacement induced by the $(N+1)^{th}$ electron tunneling onto the SET island) even under this circumstance implies a higher value of η thereby amplifying the nonlinear effect. On the other hand, we have the expected conclusion that a higher value of α implies a higher η even if the coupling between the device and the resonator is weak (smaller x_0).

Thirdly, as a parameter that dictates the dynamics, η is to be treated on par with κ and ϵ. Indeed, in the sequel we discuss all uniquely nonlinear effects in terms of η. We now write the master equations in their final form as:

$$\begin{aligned}\frac{\partial P_N}{\partial t} &= \epsilon^2 \left[x + \eta x^3\right] \frac{\partial P_N}{\partial u} \\ &\quad - u\frac{\partial P_N}{\partial x} + \left[\frac{P_{N+1}}{2} - \frac{P_N}{2} - \kappa x P\right].\end{aligned} \tag{3.29}$$

$$\begin{aligned}\frac{\partial P_{N+1}}{\partial t} &= \epsilon^2 \left[(x-1) + \eta\,(x-1)^3\right] \frac{\partial P_{N+1}}{\partial u} \\ &\quad - u\frac{\partial P_{N+1}}{\partial x} - \left[\frac{P_{N+1}}{2} - \frac{P_N}{2} - \kappa x P\right].\end{aligned} \tag{3.30}$$

3.5 The Moment Evolution Equations

Having derived the coupled pair of master equations Eqn 3.29 and Eqn 3.30 in terms of the parameters κ, ϵ and η, our goal is to solve the equations. Once we obtain the probability densities P_N and P_{N+1} we can compute the mean response of the resonator $\langle x \rangle$ which is the quantity of prime interest. As mentioned in the introduction to this chapter, we adopt a two fold approach in obtaining solutions - a finite element method (FEM) and a moment equation method (MEM). In this section we obtain a set of ordinary differential equations for the time evolution of the moment equations from Eqn

3.29 and Eqn 3.30. The solution of these equations directly gives the time evolution of the moments.

We recall that $P_N(x,u;t)$ and $P_{N+1}(x,u;t)$ are sub-densities that correspond to the N and $N+1$ electron states of the SET-resonator system and that, by construction, $P(x,u;t) = P_N + P_{N+1}$. We will repeatedly use this equation in the following calculations. Adopting standard terminology from probability theory we define the mean value of an arbitrary random process $s(t)$ at time t, with respect to the density P as:

$$\langle s \rangle = \int dx \int du\ sP. \tag{3.31}$$

Similarly, the averages with respect to $P_N(x,u;t)$ and $P_{N+1}(x,u;t)$ are respectively defined as:

$$\begin{aligned} \langle s \rangle_N &= \int dx \int du\ sP_N \\ \langle s \rangle_{N+1} &= \int dx \int du\ sP_{N+1}. \end{aligned} \tag{3.32}$$

In Eqn 3.32 the limits of integration for both variables x and u are defined by the open interval $(-\infty, \infty)$. As our first step, we consider the sum of Eqn 3.29 and Eqn 3.30. The sum of the LHS is written down as:

$$\frac{\partial P_N}{\partial t} + \frac{\partial P_{N+1}}{\partial t} = \frac{\partial P}{\partial t}.$$

Now summing the RHS and equating to the LHS we write:

$$\begin{aligned} \frac{\partial P}{\partial t} &= \epsilon^2 \left[x + \eta x^3\right] \frac{\partial P_N}{\partial u} - u\frac{\partial P_N}{\partial x} + \epsilon^2 \left[(x-1) + \eta\,(x-1)^3\right] \frac{\partial P_{N+1}}{\partial u} - u\frac{\partial P_{N+1}}{\partial x} \\ &= \epsilon^2 \left[x + \eta x^3\right] \frac{\partial P_N}{\partial u} + \epsilon^2 \left[(x-1) + \eta\,(x-1)^3\right] \frac{\partial P_{N+1}}{\partial u} - u\frac{\partial P}{\partial x} \\ &= \epsilon^2 x\frac{\partial P}{\partial u} - \epsilon^2\frac{\partial P_{N+1}}{\partial u} + \epsilon^2\eta\left(x^3 - 1 - 3x^2 + 3x\right)\frac{\partial P_{N+1}}{\partial u} + \epsilon^2\eta x^3\frac{\partial P_N}{\partial u} - u\frac{\partial P}{\partial x} \\ &= \epsilon^2 x\frac{\partial P}{\partial u} - \epsilon^2\frac{\partial P_{N+1}}{\partial u} + \epsilon^2\eta x^3\frac{\partial P}{\partial u} - \epsilon^2\eta\frac{\partial P_{N+1}}{\partial u} \\ &\quad - 3\epsilon^2\eta x^2\frac{\partial P_{N+1}}{\partial u} + 3\epsilon^2\eta x\frac{\partial P_{N+1}}{\partial u} - u\frac{\partial P}{\partial x}. \end{aligned} \tag{3.33}$$

Rearranging the terms we can write the final form as:

$$\frac{\partial P}{\partial t} = \epsilon^2 x\frac{\partial P}{\partial u} + \epsilon^2\eta x^3\frac{\partial P}{\partial u} - \epsilon^2\left(1+\eta\right)\frac{\partial P_{N+1}}{\partial u} + 3\epsilon^2\eta x\frac{\partial P_{N+1}}{\partial u} - 3\epsilon^2\eta x^2\frac{\partial P_{N+1}}{\partial u} - u\frac{\partial P}{\partial x}. \tag{3.34}$$

In deriving the moment differential equations, along with Eqn 3.29, Eqn 3.30 and Eqn 3.34, we will use the following property of the mean of the derivative of an arbitrary random process $s(t)$ with an associated probability density function $P(x,u;t)$:

$$\int dx \int du\, s\frac{\partial P}{\partial t} = \frac{d\langle s\rangle}{dt}. \tag{3.35}$$

3.5.1 The Moment Evolution Equation for $\langle x\rangle$

To evaluate $d\langle x\rangle/dt$, we now multiply both sides of Eqn 3.34 by x, use Eqn 3.35 and integrate to write:

$$\begin{aligned}
\frac{d\langle x\rangle}{dt} &= -\int udu \int x\frac{\partial P}{\partial x}dx \\
&= -\int udu \int xdP \\
&= -\int udu \left[xP|_{-\infty}^{\infty} - \int Pdx\right] \\
&= \int\int uPdxdu \\
&= \langle u\rangle .
\end{aligned} \tag{3.36}$$

In deriving Eqn 3.36, we assume that $P(x,u;t)$ vanishes asymptotically. Therefore the product xP when evaluated between the limits $(-\infty,\infty)$ vanishes as well and we obtain the given result. To show that all the other terms on the RHS of Eqn 3.34 vanish under the integral to yield Eqn 3.36, we first observe that all the terms on the RHS of Eqn 3.34 except the last one are of the form $f(x)\partial G/\partial u$ where $G(x,u;t)$ represents any of the functions P_N, P_{N+1} or P and $f(x)$ is an arbitrary function of x. Assuming, as in the case of $P(x,u;t)$, that $G(x,u;t)$ vanishes asymptotically as well, consider:

$$\begin{aligned}
\int\int f(x)\frac{\partial G}{\partial u}dudx &= \int f(x)dx \int \frac{\partial G}{\partial u}du \\
&= \int f(x)dx \int dG \\
&= \int f(x)dx[G]_{-\infty}^{\infty} \\
&= 0.
\end{aligned} \tag{3.37}$$

3.5.2 The Moment Evolution Equation for $\langle u \rangle$

To evaluate $d\langle u \rangle/dt$, we now multiply both sides of Eqn 3.34 by u, use Eqn 3.35 and integrate to write:

$$\begin{aligned}\frac{d\langle u \rangle}{dt} = &\int\int dxdu \left[\epsilon^2 xu\frac{\partial P}{\partial u} + \epsilon^2\eta x^3 u\frac{\partial P}{\partial u} - \epsilon^2\left(1+\eta\right)u\frac{\partial P_{N+1}}{\partial u}\right] \\ &+ \int\int dxdu \left[3\epsilon^2\eta xu\frac{\partial P_{N+1}}{\partial u} - 3\epsilon^2\eta x^2 u\frac{\partial P_{N+1}}{\partial u} - u^2\frac{\partial P}{\partial x}\right].\end{aligned} \tag{3.38}$$

Considering the RHS of Eqn 3.38 term by term, for the first term we obtain:

$$\begin{aligned}\epsilon^2\int\int xdx\, u\frac{\partial P}{\partial u}du &= \epsilon^2\int xdx\int udP \\ &= \epsilon^2\int xdx\left[(uP)_{-\infty}^{\infty} - \int Pdu\right] \\ &= -\epsilon^2\int\int xPdxdu \\ &= -\epsilon^2\left\langle x\right\rangle.\end{aligned} \tag{3.39}$$

Similar calculations yield the other terms as :

$$\begin{aligned}\epsilon^2\eta\int\int x^3dx\, u\frac{\partial P}{\partial u}du &= \epsilon^2\eta\int x^3dx\int udP \\ &= \epsilon^2\eta\int x^3dx\left[(uP)_{-\infty}^{\infty} - \int Pdu\right] \\ &= -\epsilon^2\eta\int\int x^3Pdxdu \\ &= -\epsilon^2\eta\left\langle x^3\right\rangle.\end{aligned} \tag{3.40}$$

$$\begin{aligned}3\epsilon^2\eta\int\int xdx\, u\frac{\partial P_{N+1}}{\partial u}du &= 3\epsilon^2\eta\int xdx\int udP_{N+1} \\ &= 3\epsilon^2\eta\int xdx\left[(uP_{N+1})_{-\infty}^{\infty} - \int P_{N+1}du\right] \\ &= -3\epsilon^2\eta\int\int xP_{N+1}dxdu \\ &= -3\epsilon^2\eta\langle x\rangle_{N+1}.\end{aligned} \tag{3.41}$$

$$\begin{aligned}-3\epsilon^2\eta\int\int x^2dx\, u\frac{\partial P_{N+1}}{\partial u}du &= -3\epsilon^2\eta\int x^2dx\int udP_{N+1} \\ &= -3\epsilon^2\eta\int x^2dx\left[(uP_{N+1})_{-\infty}^{\infty} - \int P_{N+1}du\right] \\ &= 3\epsilon^2\eta\int\int x^2P_{N+1}dxdu \\ &= 3\epsilon^2\eta\langle x^2\rangle_{N+1}.\end{aligned} \tag{3.42}$$

$$
\begin{aligned}
-\epsilon^2 (1+\eta) \int\int dx\, u \frac{\partial P_{N+1}}{\partial u} du &= -\epsilon^2 (1+\eta) \int dx \int u dP_{N+1} \\
&= -\epsilon^2 (1+\eta) \int dx \left[(u P_{N+1})_{-\infty}^{\infty} - \int P_{N+1} du \right] \\
&= \epsilon^2 (1+\eta) \langle P \rangle_{N+1}.
\end{aligned}
\tag{3.43}
$$

$$
\begin{aligned}
-\int dx \int u^2 du \frac{\partial P}{\partial x} &= -\int u^2 du \int \frac{\partial P}{\partial x} dx \\
&= -\int u^2 du \int dP \\
&= -\int u^2 du [P]_{-\infty}^{\infty} \\
&= 0.
\end{aligned}
\tag{3.44}
$$

Substituting Eqns 3.39-3.44 in Eqn 3.38 we write the moment evolution equation for $\langle u \rangle$ as:

$$
\frac{d\langle u \rangle}{dt} = -\epsilon^2 \left[\langle x \rangle + \eta \left\langle x^3 \right\rangle \right] + \epsilon^2 (1+\eta) \langle P \rangle_{N+1} - 3\epsilon^2 \eta \langle x \rangle_{N+1} + 3\epsilon^2 \eta \left\langle x^2 \right\rangle_{N+1}. \tag{3.45}
$$

3.5.3 The Full Set of Moment Evolution Equations

It is evident from Eqn 3.36 and Eqn 3.45 that in order to generate a closed system of moment evolution equations, we need to evaluate $d\left\langle x^3 \right\rangle/dt$, $d\left\langle x^2 \right\rangle_{N+1}/dt$, $d\langle x \rangle_{N+1}/dt$ and $d\langle P \rangle_{N+1}/dt$ in terms of the moments appearing in Eqn 3.36 and Eqn 3.45. This involves calculations of considerable length and the details are provided in Appendix

A. Below we list the system of moment evolution equations that are finally obtained.

$$\frac{d\langle x\rangle}{dt} = \langle u\rangle \tag{3.46}$$

$$\frac{d\langle u\rangle}{dt} = -\epsilon^2\left[\langle x\rangle + \eta\left\langle x^3\right\rangle\right] + \epsilon^2(1+\eta)\left\langle P\right\rangle_{N+1} - 3\epsilon^2\eta\langle x\rangle_{N+1} + 3\epsilon^2\eta\left\langle x^2\right\rangle_{N+1} \tag{3.47}$$

$$\frac{d\langle P\rangle_{N+1}}{dt} = -\left\langle P\right\rangle_{N+1} + \frac{1}{2} + \kappa\langle x\rangle \tag{3.48}$$

$$\frac{d\left\langle x^3\right\rangle}{dt} = 3\left\langle x^2u\right\rangle \tag{3.49}$$

$$\frac{d\langle x\rangle_{N+1}}{dt} = \langle u\rangle_{N+1} - \langle x\rangle_{N+1} + \frac{1}{2}\langle x\rangle + \kappa\left\langle x^2\right\rangle \tag{3.50}$$

$$\frac{d\left\langle x^2\right\rangle_{N+1}}{dt} = 2\langle ux\rangle_{N+1} - \left\langle x^2\right\rangle_{N+1} + \frac{1}{2}\left\langle x^2\right\rangle + \kappa\left\langle x^3\right\rangle \tag{3.51}$$

$$\frac{d\left\langle x^2\right\rangle}{dt} = 2\langle ux\rangle \tag{3.52}$$

$$\frac{d\langle u\rangle_N}{dt} = -\epsilon^2\left[\langle x\rangle_N + \eta\left\langle x^3\right\rangle_N\right] + \frac{1}{2}\langle u\rangle - \kappa\langle xu\rangle + \langle u\rangle_N \tag{3.53}$$

$$\frac{d\left\langle x^3\right\rangle_N}{dt} = 3\left\langle x^2u\right\rangle_N. \tag{3.54}$$

In order to obtain closure for the above set of moment evolution equations, after exploring various possibilities, we arrived at the following decoupling approximations. As will be discussed in the sequel these approximations are justified based on the finite element solutions. It is also noted here that the approximations assume decoupling between moments of positions and velocities. Since position and velocity are independent variables in phase space, the assumptions of decoupling between their moments is more justifiable than similar assumptions between higher moments of the same variable. The approximations are:

$$\begin{aligned}
\left\langle x^2u\right\rangle &= \left\langle x^2\right\rangle\langle u\rangle \\
\langle ux\rangle_{N+1} &= \langle u\rangle_{N+1}\langle x\rangle_{N+1} \\
\langle ux\rangle &= \langle u\rangle\langle x\rangle \\
\left\langle x^2u\right\rangle_N &= \left\langle x^2\right\rangle_N\langle u\rangle_N.
\end{aligned} \tag{3.55}$$

Introducing the approximations Eqn 3.55 into the moment evolution equations we can write the decoupled system of equations as:

$$\frac{d\langle x\rangle}{dt} = \langle u\rangle \tag{3.56}$$

$$\frac{d\langle u\rangle}{dt} = -\epsilon^2\left[\langle x\rangle + \eta\left\langle x^3\right\rangle\right] + \epsilon^2(1+\eta)\langle P\rangle_{N+1} - 3\epsilon^2\eta\langle x\rangle_{N+1} + 3\epsilon^2\eta\left\langle x^2\right\rangle_{N+1} \tag{3.57}$$

$$\frac{d\langle P\rangle_{N+1}}{dt} = -\langle P\rangle_{N+1} + \frac{1}{2} + \kappa\langle x\rangle \tag{3.58}$$

$$\frac{d\left\langle x^3\right\rangle}{dt} = 3\left\langle x^2\right\rangle\langle u\rangle \tag{3.59}$$

$$\frac{d\langle x\rangle_{N+1}}{dt} = \langle u\rangle_{N+1} - \langle x\rangle_{N+1} + \frac{1}{2}\langle x\rangle + \kappa\left\langle x^2\right\rangle \tag{3.60}$$

$$\frac{d\left\langle x^2\right\rangle_{N+1}}{dt} = 2\langle u\rangle_{N+1}\langle x\rangle_{N+1} - \left\langle x^2\right\rangle_{N+1} + \frac{1}{2}\left\langle x^2\right\rangle + \kappa\left\langle x^3\right\rangle \tag{3.61}$$

$$\frac{d\left\langle x^2\right\rangle}{dt} = 2\langle u\rangle\langle x\rangle \tag{3.62}$$

$$\frac{d\langle u\rangle_N}{dt} = -\epsilon^2\left[\langle x\rangle_N + \eta\left\langle x^3\right\rangle_N\right] + \frac{1}{2}\langle u\rangle - \kappa\langle x\rangle\langle u\rangle + \langle u\rangle_N \tag{3.63}$$

$$\frac{d\left\langle x^3\right\rangle_N}{dt} = 3\left\langle x^2\right\rangle_N\langle u\rangle_N. \tag{3.64}$$

We now make note of the following identities that arise from the construction $P(x,u;t) = P_N + P_{N+1}$:

$$\langle u\rangle = \langle u\rangle_N + \langle u\rangle_{N+1} \tag{3.65}$$

$$\left\langle x^2\right\rangle = \left\langle x^2\right\rangle_N + \left\langle x^2\right\rangle_{N+1}. \tag{3.66}$$

For convenience we now label the quantities in Eqns 3.56 - 3.64 as follows:

$$\begin{aligned}
\langle x \rangle &= X_1 \\
\langle u \rangle &= X_2 \\
\langle P \rangle_{N+1} &= X_3 \\
\left\langle x^3 \right\rangle &= X_4 \\
\langle x \rangle_{N+1} &= X_5 \\
\left\langle x^2 \right\rangle_{N+1} &= X_6 \\
\left\langle x^2 \right\rangle &= X_7 \\
\langle u \rangle_N &= X_8 \\
\left\langle x^3 \right\rangle_N &= X_9
\end{aligned} \tag{3.67}$$

Using Eqn 3.65, Eqn 3.66 and Eqns. 3.67 we write Eqns. 3.56 - 3.64 in the new variables as:

$$\begin{aligned}
\dot{X}_1 &= X_2 \\
\dot{X}_2 &= -\epsilon^2 \left[X_1 + \eta X_4 \right] + \epsilon^2 \left(1 + \eta \right) X_3 - 3\epsilon^2 \eta X_5 + 3\epsilon^2 \eta X_6 \\
\dot{X}_3 &= -X_3 + \frac{1}{2} + \kappa X_1 \\
\dot{X}_4 &= 3 X_2 X_7 \\
\dot{X}_5 &= \left[X_2 - X_8 \right] - X_5 + \frac{1}{2} X_1 + \kappa X_7 \\
\dot{X}_6 &= 2 \left[X_2 - X_8 \right] X_5 - X_6 + \frac{1}{2} X_7 + \kappa X_4 \\
\dot{X}_7 &= 2 X_1 X_2 \\
\dot{X}_8 &= -\epsilon^2 \left[X_1 - X_5 + \eta X_9 \right] + \frac{1}{2} X_2 - \kappa X_1 X_2 - X_8 \\
\dot{X}_9 &= 3 \left[X_7 - X_8 \right].
\end{aligned} \tag{3.68}$$

The nonlinear system Eqns. 3.68 is the set of moment evolution equations for the Duffing nanoresonator. We reiterate that positive and negative values for η correspond to the single-well and (inverted) double-well Duffing potentials. We solve the moment evolution equations for various values of η in the sequel, noting that the linear case is obtained by setting $\eta = 0$ in Eqns. 3.68.

To conclude this section, we note that in order to understand the effects of varying η (which represents the nonlinearity in the system), we set $\kappa = 0.1$ and $\epsilon = 0.3$ in all our cases. The choice of these values for κ (which measures the interaction strength between the SET and the resonator) and ϵ (which compares the relative timescales of the resonator period and the electron tunneling time) is guided by the corresponding choice in [3]. We recall from Chapter 2 that the ABZ model is only valid for both κ and ϵ much less than unity and our choice satisfies this constraint. However, extremely weak coupling between the SET and the resonator (for instance, say $\kappa = 0.01$) could mask the uniquely nonlinear effects and hence our choice is influenced by this aspect as well. In this context, we would like to draw a distinction between the coupling strength of the SET - resonator interaction and the dynamical effects that arise due to nonlinear resonator motion. We emphasize this important point in discussing our results.

3.6 The Finite Element Method

In this section we discuss the finite element method employed to directly solve the coupled master equations Eqn 3.29 and Eqn 3.30. We use the high-level open source finite element package **Freefem++** created by Hecht, Pironneau, Le Hyaric of the Universite Pierre et Marie Curie, France and Ohtsuka of Hiroshima University, Japan [35]. One of the advantages of using this package is that the equations can be directly fed into the program albeit in the variational form. To begin with, the boundary of the domain of integration is directly defined by the user as a parametric equation and given the number of points on the boundary as another input by the user, the program automatically generates an appropriate mesh in the domain. Next, the finite element space is created on the mesh using user-specified types of elements chosen from a wide variety built into the package. This finite element space is a space of polynomial functions for which a basis can be defined. All the functions involved in the problem are expressed in terms of this basis. In the next step, the differential equations defining the problem (in our case, the master equations) are defined in the variational (also known as weak) formulation. This implies that instead of dealing with the differential equation

directly, **Freefem++** solves for stationary values of a functional corresponding to the equation that emerges from variational considerations. The main advantage of this approach is that the problem of solving the differential equation is now mapped to a problem in linear algebra. Indeed, this principle is fundamental to the finite element method itself and we refer to [24] and [56] for the analytical details. Another highlight of **Freefem++** is that the built-in function *adaptmesh* can be used for mesh adaptation after any desired number of steps in the integration. Sample codes, representative of the ones we have used in our calculations are included in Appendix B. The number of points in the domain boundary, the time step of integration, the judicious use of mesh adaptation are all critical factors that determine the robustness of the solutions and we note here that our choice of values for each of these factors in all the cases as provided in Appendix B is a result of extensive numerical experimentation. The same applies to the initial conditions for P_N and P_{N+1} where we have consistently chosen sharply peaked Gaussian densities with mean 0.5 and variance 0.00625.

We now comment on the mathematical nature of the master equations Eqn 3.29 and Eqn 3.30. The terms involving the derivatives in Eqn 3.29 and Eqn 3.30 can be written in matrix form as:

$$\begin{pmatrix} P_N \\ P_{N+1} \end{pmatrix}_t = \begin{pmatrix} u & 0 \\ 0 & u \end{pmatrix} \begin{pmatrix} P_N \\ P_{N+1} \end{pmatrix}_x - \epsilon^2 \begin{pmatrix} x+\eta x^3 & 0 \\ 0 & (x-1)+\eta(x-1)^3 \end{pmatrix} \begin{pmatrix} P_N \\ P_{N+1} \end{pmatrix}_u \tag{3.69}$$

where the subscripts in Eqn 3.69 denote differentiation with respect to the indicated variable. Since the coefficient matrices in 3.69 are in diagonal form, it follows from the theory of partial differential equations [22], [43], [45] that the master equations Eqn 3.29 and Eqn 3.30 represent a system of hyperbolic partial differential equations.

Hyperbolic systems can be solved using the method of characteristics. We refer to [22], [45] for the details of the theoretical aspects and note that in **Freefem++** the method of characteristics can be employed to generate the finite element solutions.

We now make the following observations. The utility of the finite element solutions in the case of our master equations is multifold. Firstly, obtaining solutions to partial

differential equations of the kind that arise in our case is a formidable problem and the finite element approach solves our system of coupled partial differential equations. Secondly, the moment evolution equations were derived in their final form based on the approximations given by Eqns. 3.55 and the finite element solutions provide us with a way of validating these approximations. Finally, the agreement between the solutions obtained by the two methods in each of the cases considered allows us to confidently draw conclusions about the dynamical behavior of the SET-resonator system.

3.7 The Linear Case

In the case where the resonator is a linear harmonic oscillator, setting the parameter $\eta = 0$ in Eqn 3.29 and Eqn 3.30 we obtain the master equations as:

$$\frac{\partial P_N}{\partial t} = \epsilon^2 x \frac{\partial P_N}{\partial u} - u\frac{\partial P_N}{\partial x} + \left[\frac{P_{N+1}}{2} - \frac{P_N}{2} - \kappa x P\right] \tag{3.70}$$

$$\frac{\partial P_{N+1}}{\partial t} = \epsilon^2 (x-1) \frac{\partial P_{N+1}}{\partial u} - u\frac{\partial P_{N+1}}{\partial x} - \left[\frac{P_{N+1}}{2} - \frac{P_N}{2} - \kappa x P\right]. \tag{3.71}$$

Correspondingly, we obtain the moment evolution equations in the linear case by setting $\eta = 0$ in Eqns. 3.68 as:

$$\begin{aligned} \dot{X}_1 &= X_2 \\ \dot{X}_2 &= -\epsilon^2 [X_1 - X_3] \\ \dot{X}_3 &= -X_3 + \frac{1}{2} + \kappa X_1. \end{aligned} \tag{3.72}$$

We note here that when we set $\eta = 0$, we require only three equations for moment closure, just as in the ABZ model [3]. Hence the other equations in the system of Eqns. 3.68 become redundant and the moment evolution system collapses to the three equations given by Eqns. 3.72.

We solve the coupled Eqns. 3.70 and 3.71 using the FEM and obtain the mean displacement of the resonator $\langle x \rangle$ as a function of time. The initial conditions specified for P_N and P_{N+1} are Gaussian densities with mean 0.5 and variance 0.00625. In order to obtain a meaningful comparison of the mean displacement thus obtained with that given by the MEM, the initial conditions for X_1, X_2 and X_3 in Eqns. 3.72 are computed

using identical Gaussian distributions as in the FEM case. The values thus obtained are $X_1(0) = 0.5$, $X_2(0) = 0.0$ and $X_3(0) = 0.5$. We also note here that, as discussed in Section 2.5, we set $\kappa = 0.1$ and $\epsilon = 0.3$.

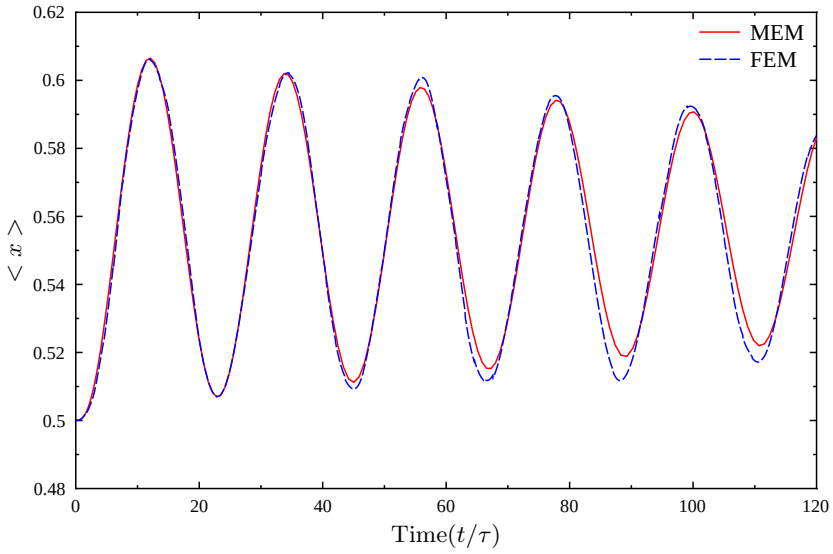

Figure 3.1: Mean Displacement of the Resonator: $\eta = 0$

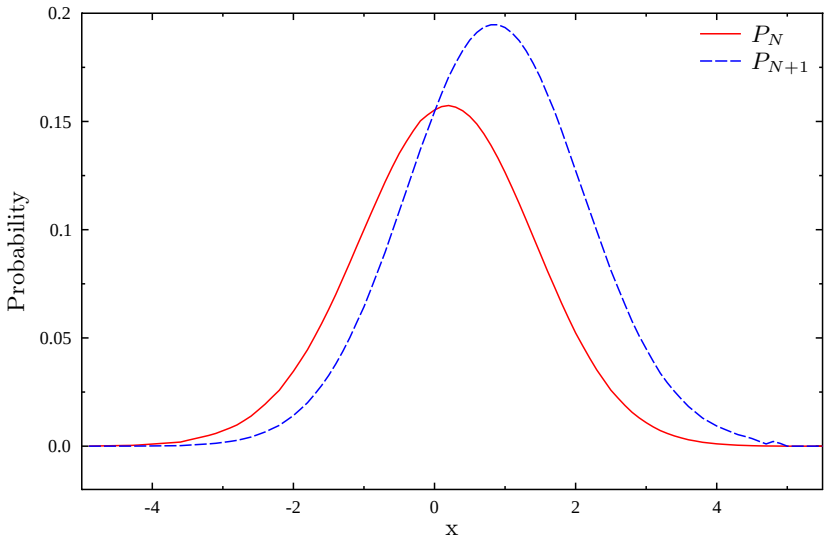

Figure 3.2: Steady State Probability Sub-Densities: $\eta = 0$

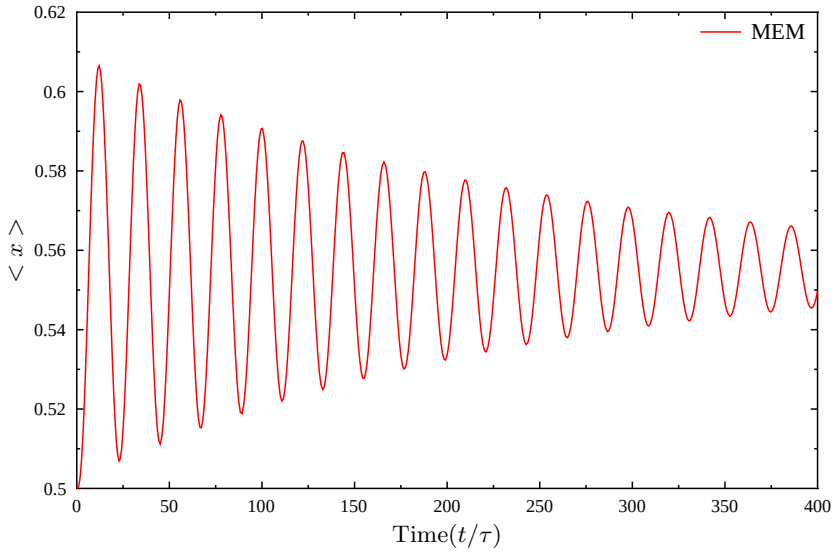

Figure 3.3: Mean Displacement of the Resonator: $\eta = 0$

A comparison of the evolution of the mean displacement in time obtained from both the FEM and the MEM is provided in Figure 3.1. In Figure 3.2 is presented the steady state probability sub-density functions obtained from the FEM. Figure 3.3 presents the MEM solution for mean displacement for up to $t/\tau = 400$.

Our main purpose in solving for the linear case is to validate the key results of the ABZ model that the resonator behaves like a damped linear harmonic oscillator due to the interaction with the SET and that the coupled SET-resonator system settles into a steady state. Our goal is achieved since both Figure 3.1 and Figure 3.3 clearly indicate that the resonator behaves as a damped harmonic oscillator in the linear regime. The first point that we would like to emphasize here is that this is hardly an obvious conclusion from a consideration of the coupled dynamics of the SET-resonator system. In other words, *a priori* there exists no indication in the master equation framework that the SET will damp the resonator due to the coupling between the two. The second point is that the result essentially follows from the master equations and hence is an exclusively probabilistic one. While it is natural to expect such motion in a damped, linear, deterministic model, it seems remarkable that the behavior emerges from a stochastic model of the coupled SET-resonator dynamics in the linear regime.

We now comment on the comparison of the solutions obtained by the two methods. From Figure 3.1 it is seen that while the solutions agree remarkably well for earlier times (until approximately $t/\tau = 40$), the same is not true for later times. We note here the limitations that are inherent in the finite element formulation and solution of the master equations. That we have had to impose vanishing spatial boundary conditions on a system of hyperbolic partial differential equations (the master equations), the choices related to the grid size, the time-step and the frequency of mesh-adaptation are all factors that affect the accuracy of the FEM solutions, particularly for later times. However, we note from Fig 3.1 that, qualitatively the two solutions are in good agreement.

3.8 The Single-Well Duffing Case

In this section we present the solutions to the master equations in the single-well (hardening stiffness) Duffing case. Our primary objective is to analyze the effect of nonlinearity on the dynamical behavior of the resonator. There also arises concomitantly, the question of the impact of the strength of the nonlinearity on the resonator response. Hence the main subsections of this section correspond to the nonlinear cases represented by $\eta = 0.5$, $\eta = 0.75$ and $\eta = 1$. In each of the cases, the main question of whether a steady state is attained is answered by observing the time evolution of the mean displacement of the resonator as well as the steady state density functions. Of these, the former is obtained from both the FEM and the MEM while the latter is provided directly by the FEM. Now, due to the fact that the MEM involves solving a system of ODEs, solutions that remain robust over longer times are easier to obtain using the method. Furthermore, the MEM solutions are valuable from the point of view of stability analysis as well. However, this method is hinged on the approximations given by Eqns. 3.55 and, in general, one ought to be chary about such moment approximations in the nonlinear regime. Therefore, in each of the cases considered, we validate the approximations given by Eqns. 3.55 by invoking the results from the FEM. Indeed, the moment of a product of random variables cannot be expected to be equal to the product of their moments and hence what is sought here is compelling qualitative agreement combined with reasonable quantitative agreement. It is to be noted here that the litmus test of the validity of the MEM is the direct comparison of the time evolution of mean resonator displacement obtained by the method with that obtained from the FEM.

It is an inherent characteristic of the analysis of random variables and processes (that are close to or truly normally distributed) that the behavior of both the mean and the variance are equally important in drawing conclusions. Hence we also discuss the time evolution of the variance of the resonator displacement.

3.8.1 $\eta = 0.5$

In this sub-section we consider our first case of the single-well Duffing regime represented by $\eta = 0.5$. We first discuss the evolution of the mean displacement of the resonator followed by a discussion of the moment approximations employed in this case in the MEM. We conclude the sub-section with the result on the evolution of the variance of the displacement.

Mean Displacement

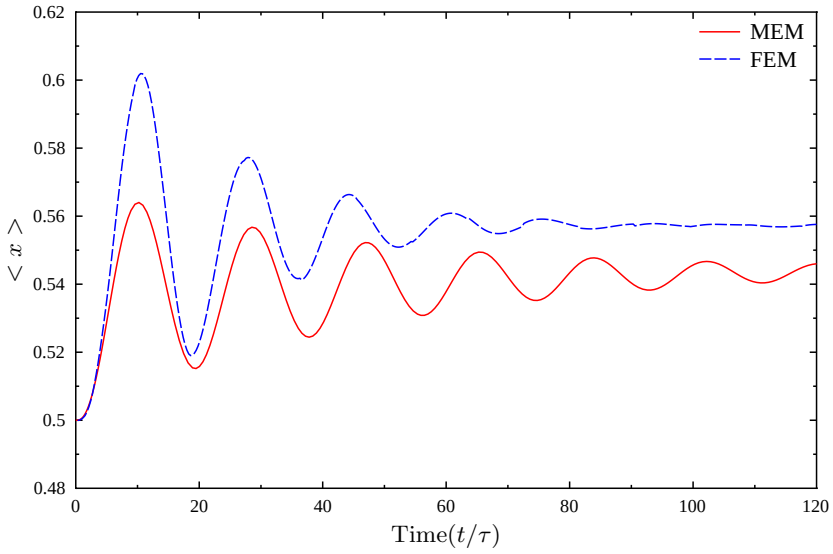

Figure 3.4: Mean Displacement of the Resonator: $\eta = 0.5$

In Fig 3.4 we present a comparison of the time evolution of the mean resonator displacement for the case $\eta = 0.5$ obtained from the FEM and the MEM. The first point to note is that the mean resonator displacement is asymptotically stationary implying that the system attains a steady state. Keeping in mind that the solutions obtained from the two methods cannot be expected to agree entirely due to the approximations involved in the MEM, the second point to note is that while the MEM solution is

non-conservative with respect to the magnitude of the displacement in comparison with the FEM solution, the maximum difference in peak amplitudes (which occurs in the first period) is about 6 percent. Furthermore, the difference in the (scaled) mean displacement when the system is very close to the steady state at time $t/\tau = 120$ is about 0.013. Therefore, we conclude that the two solutions are in good qualitative agreement and that the MEM solution is a good approximation to the resonator displacement in this case. Also, the feature that the two results reach the steady state at different times may be attributed to the limitations of the FEM. In Fig 3.5 we present the MEM solution for the resonator displacement plotted until $t/\tau = 400$.

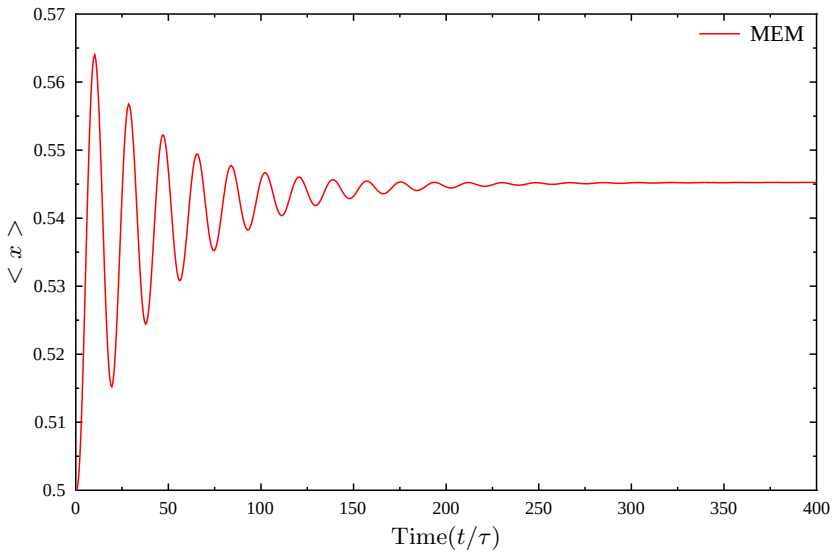

Figure 3.5: Mean Displacement of the Resonator: $\eta = 0.5$

The damping of the resonator motion observed in Fig 3.4 and Fig 3.5 clearly indicates that the resonator reaches a steady state. The probability density functions P_N and P_{N+1} corresponding to the steady state obtained from the FEM solution is presented in Fig 3.6.

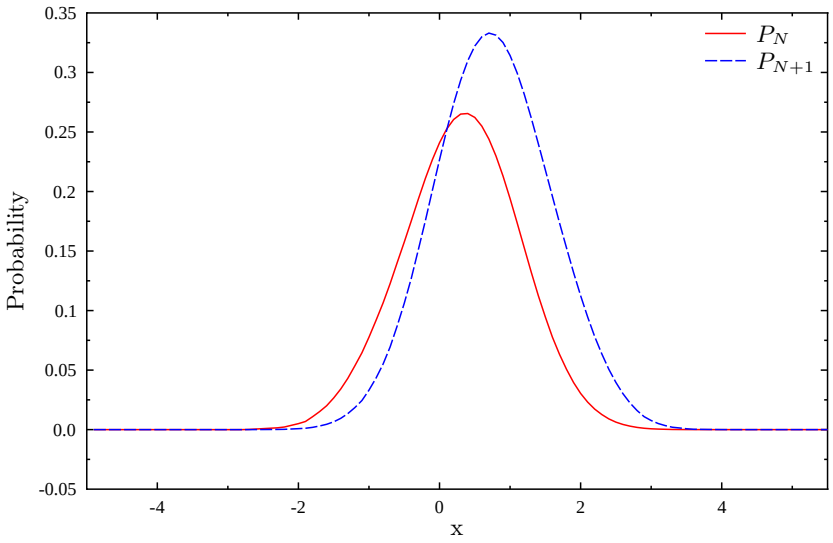

Figure 3.6: Steady State Probability Sub-Densities: $\eta = 0.5$

Moment Approximations

In order to further examine the validity of the moment approximations used in the MEM, we now plot the time evolution of each one of the approximations using the FEM solution. In other words, we know precisely the approximations that have been made in the MEM and we would like to examine their validity in the light of the FEM solution. We recall from Eqn 3.55 that the approximations used in deriving the moment evolution equations are given by:

$$\begin{aligned} \langle x^2 u \rangle &\approx \langle x^2 \rangle \langle u \rangle \\ \langle ux \rangle_{N+1} &\approx \langle u \rangle_{N+1} \langle x \rangle_{N+1} \\ \langle ux \rangle &\approx \langle u \rangle \langle x \rangle \\ \langle x^2 u \rangle_N &\approx \langle x^2 \rangle_N \langle u \rangle_N. \end{aligned} \tag{3.73}$$

We present a comparison of the time evolution of each one of the above approximations as computed from the FEM solution in Fig 3.7 - Fig 3.10.

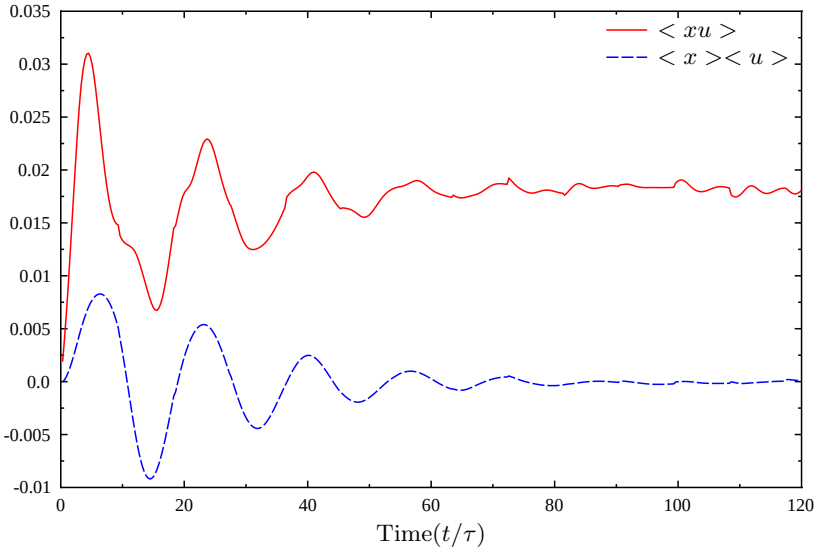

Figure 3.7: Comparison from FEM: $\eta = 0.5$

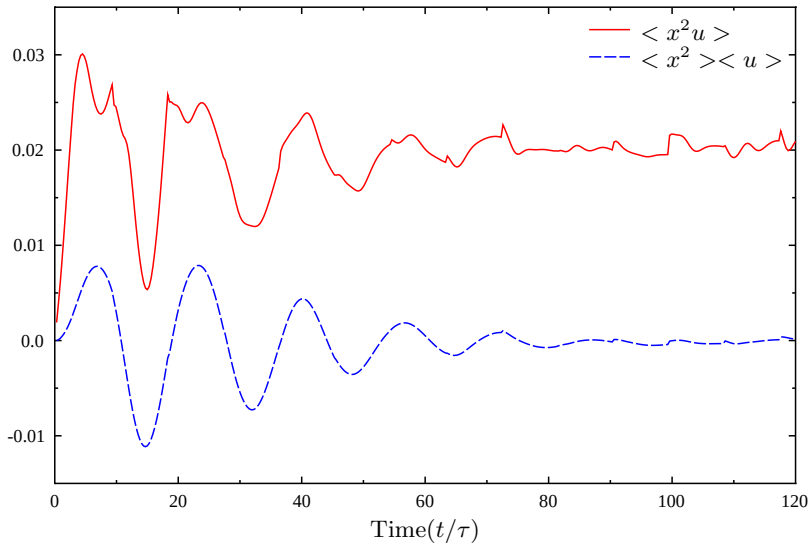

Figure 3.8: Comparison from FEM: $\eta = 0.5$

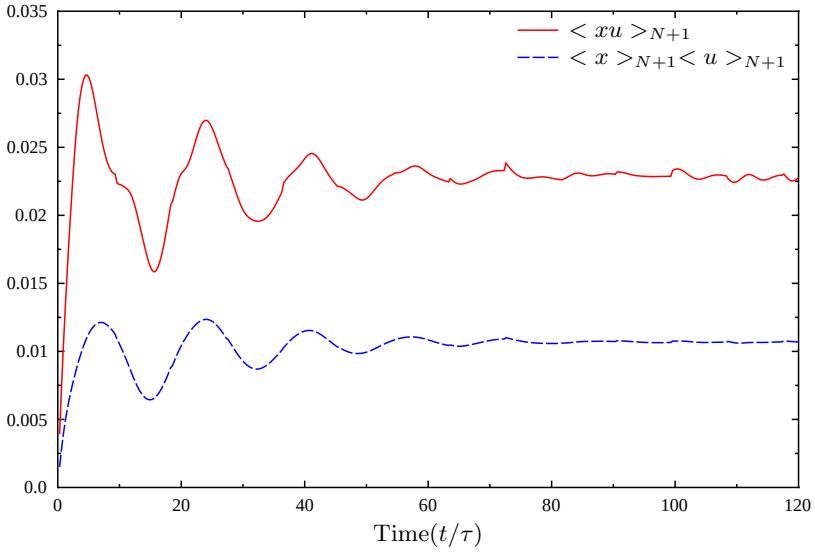

Figure 3.9: Comparison from FEM: $\eta = 0.5$

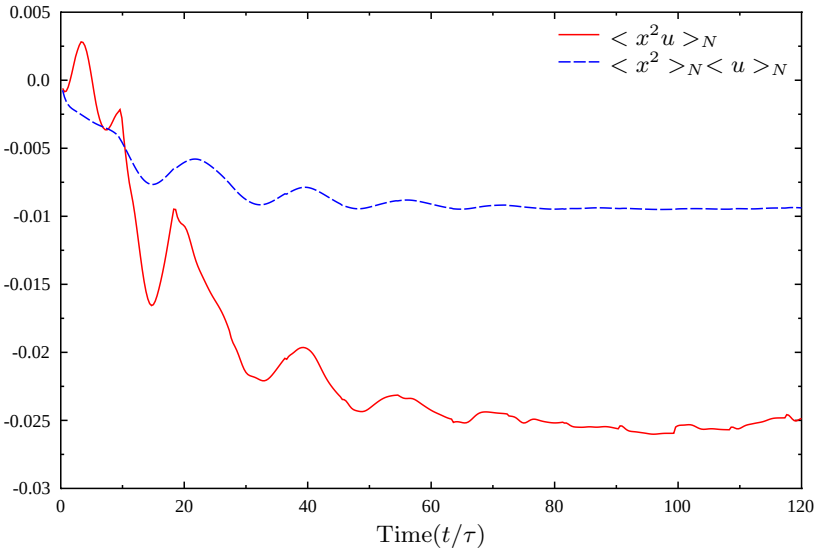

Figure 3.10: Comparison from FEM: $\eta = 0.5$

It is of interest to observe the qualitative similarity in Figs. 3.7 - 3.9 between the exact result (the moment of the products) and the approximation (the product of the moments). Furthermore, we observe from Figs 3.7 and 3.8 that the approximations tend to zero at $t/\tau = 120$ while the exact values are non-zero. This is explained based on the fact that in each of these cases the approximation involves a product, a term in which is the mean resonator velocity $\langle u \rangle$. The mean resonator velocity tends to zero in the steady state and the products involved in the approximation vanish as well. The numerical difference between the exact and approximate values in Fig 3.9 is 0.0125 at $t/\tau = 120$ while it is 0.0175 from Fig 3.10. The main point of this exercise is to buttress the moment approximations by demonstrating that the approximations do not lead to significant divergences. Indeed, this ultimately reflects in the agreement between the FEM and MEM solutions observed in Fig 3.4.

Variance

The time evolution of the variance of the displacement is presented in Fig 3.11. It is observed that the variance settles down to a constant value of 0.305 as the system approaches the steady state. This result, combined with the behavior of the mean displacement is further confirmation that, indeed, the system reaches a steady state. In this nonlinear case of $\eta = 0.5$, our analysis thus far has established that the MEM is a reasonable approximation and that the SET-resonator system attains a steady state. From comparing Figure 3.5 and Figure 3.3 we then draw the important conclusion that the SET damps the resonator at a significantly higher rate due to the nonlinearity in the resonator motion. As will be seen in the next subcases corresponding to $\eta = 0.75$ and $\eta = 1$, this is a consistent result since the rate at which the SET damps the resonator increases with η, the strength of the nonlinearity in the resonator motion.

3.8.2 $\eta = 0.75$

We now consider the case of a stronger nonlinearity given by $\eta = 0.75$. The analysis proceeds along the lines of the $\eta = 0.5$ case.

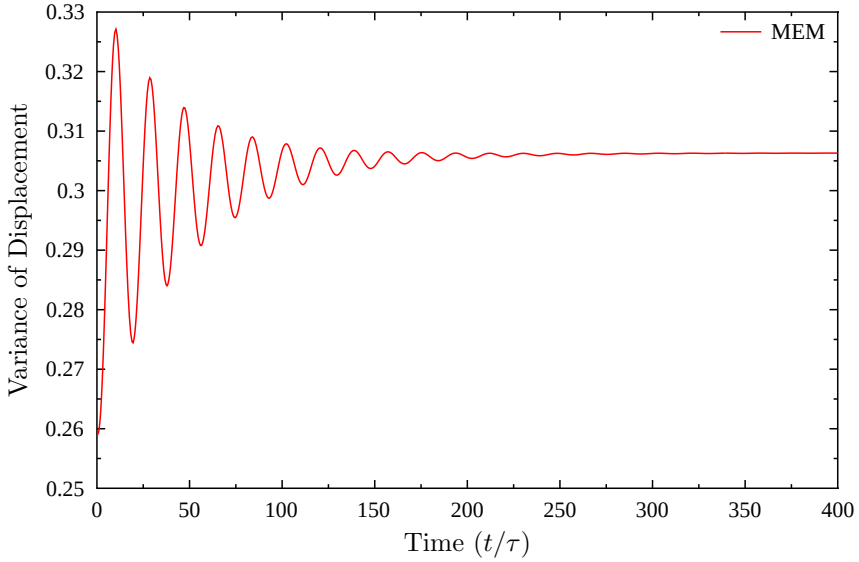

Figure 3.11: Evolution of Variance of Displacement: $\eta = 0.5$

Mean Displacement

In Fig 3.12 we present a comparison of the time evolution of the mean resonator displacement for the case $\eta = 0.75$ obtained from the FEM and the MEM. The maximum difference in peak amplitudes (which again occurs in the first period) is about 7.5 percent in this case. The difference in the (scaled) mean displacement when the system begins to approach the steady state at time $t/\tau = 120$ is about 0.018. These values are slightly higher than those obtained in the $\eta = 0.5$ case. This is to be expected since increasing the strength of the nonlinearity certainly implies more complicated dynamics. However, the two solutions are still in good qualitative agreement and hence the MEM solution continues to be a good approximation to the resonator displacement. In Fig 3.13 we present the MEM solution for the resonator displacement plotted until $t/\tau = 400$. The probability density functions P_N and P_{N+1} corresponding to the steady state obtained from the FEM solution is presented in Fig 3.14.

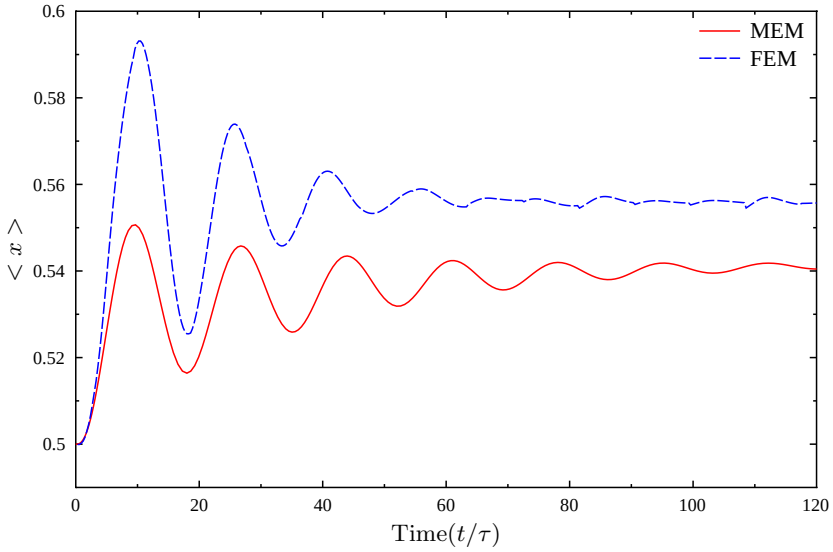

Figure 3.12: Mean Displacement of the Resonator: $\eta = 0.75$

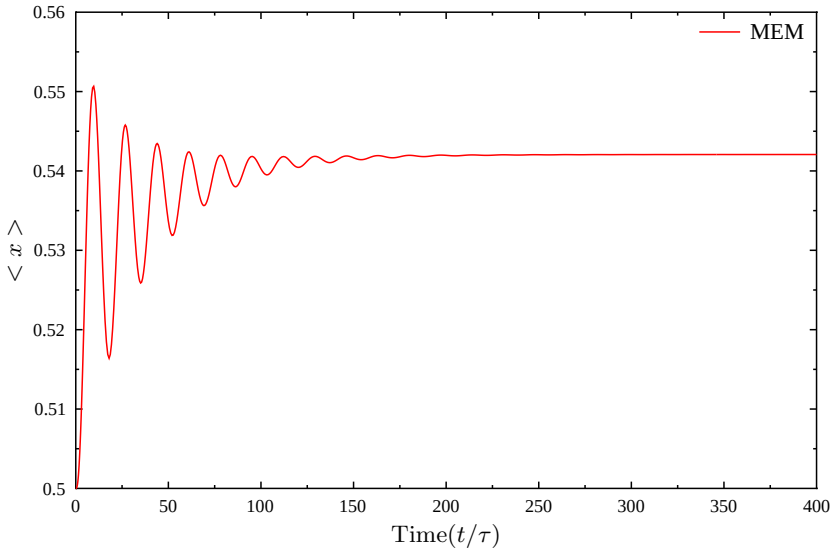

Figure 3.13: Mean Displacement of the Resonator: $\eta = 0.75$

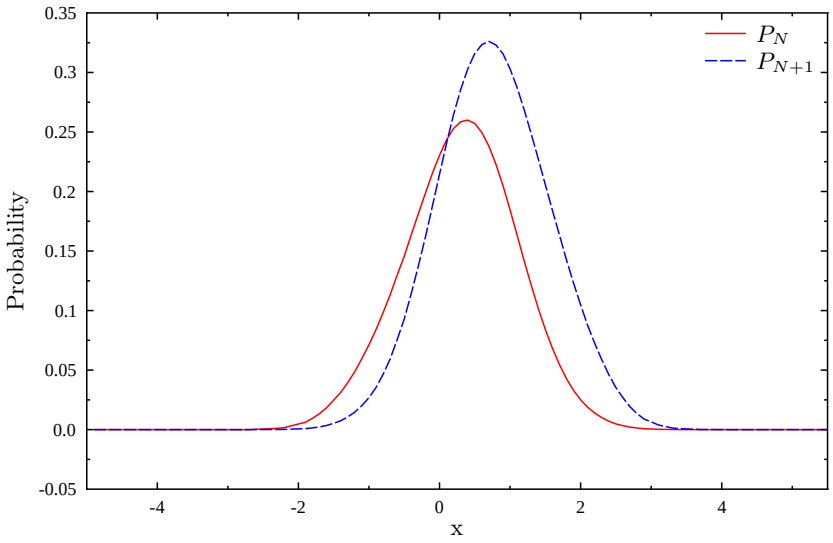

Figure 3.14: Steady State Probability Sub-Densities: $\eta = 0.75$

Moment Approximations

Since the consistency of the moment approximations is not guaranteed when the strength of the nonlinearity is increased, we examine the approximations in closer detail in the present case as well. We present a comparison of the time evolution of each one of the moment approximations as computed from the FEM solution in Fig 3.15 - Fig 3.18.

We observe that the qualitative similarity in Figs. 3.15 - 3.17 between the exact result (the moment of the products) and the approximation (the product of the moments) implies that our conclusions from the previous case of $\eta = 0.5$ continue to hold in this case as well. The disagreement between the exact and the approximate quantities is most severe in the case of the product $\langle x^2 \rangle_N \langle u \rangle_N$ (Fig 3.18). There exists even a qualitative difference between the moment of the product and the product of the moments as the former increases initially before showing a significant drop at around $t/\tau = 5$ whereas the latter decreases monotonically with respect to (scaled)

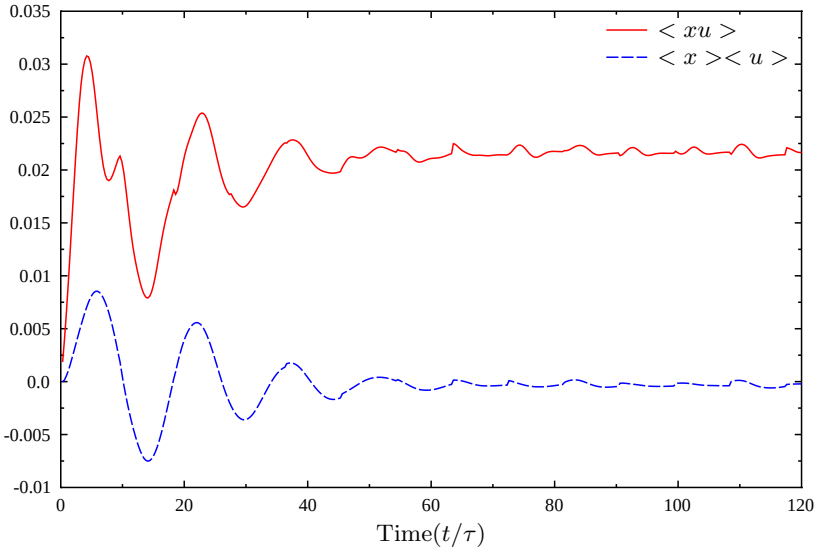

Figure 3.15: Comparison from FEM: $\eta = 0.75$

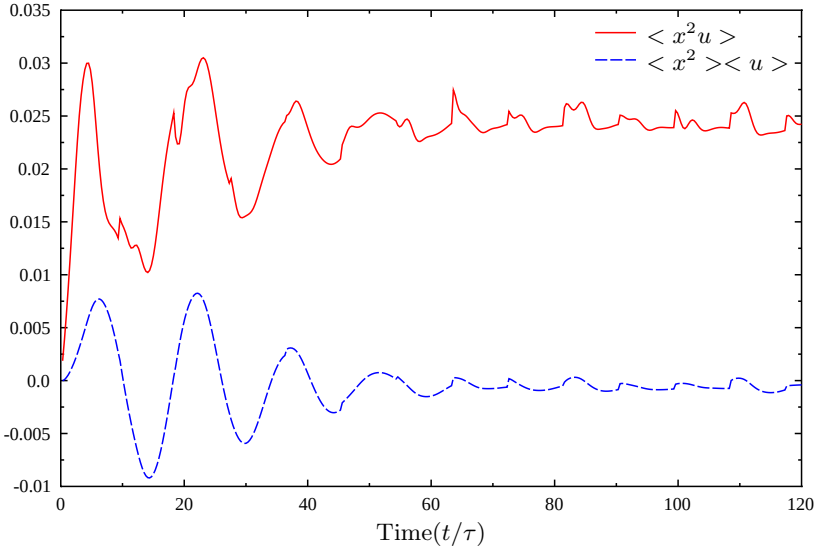

Figure 3.16: Comparison from FEM: $\eta = 0.75$

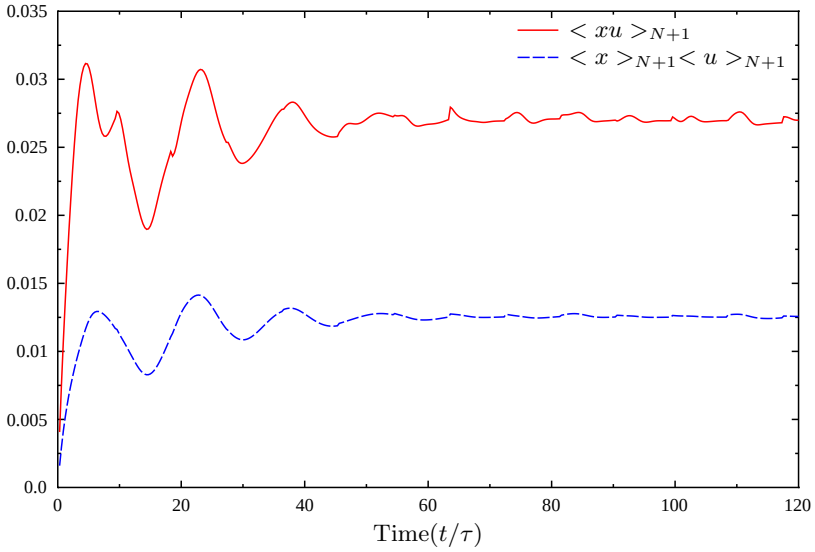

Figure 3.17: Comparison from FEM: $\eta = 0.75$

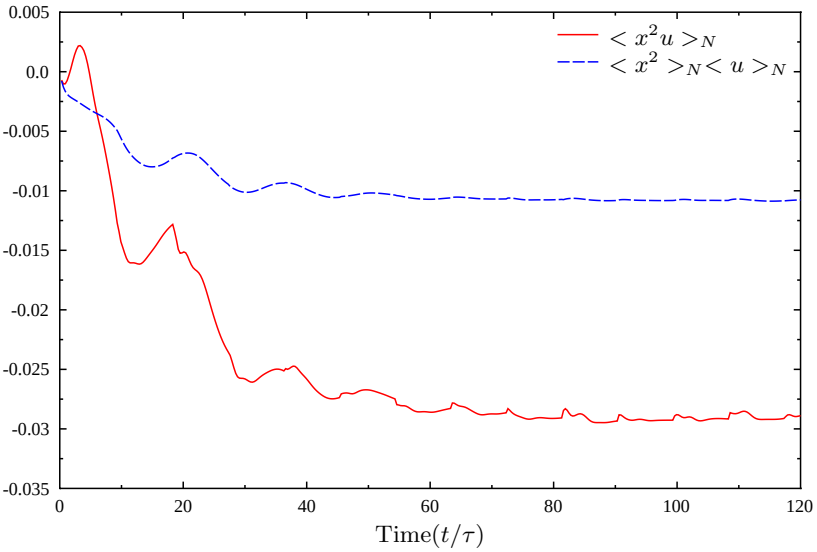

Figure 3.18: Comparison from FEM: $\eta = 0.75$

time. However, asymptotically both the exact and approximate quantities tend to constant values. Overall, even though the difference between the exact and approximate values in the steady state shows an increase (Figs. 3.15 - 3.18) when compared to the $\eta = 0.5$ case, the behavior is still not significantly different as to challenge the validity of the approximations.

Variance

The time evolution of the variance of the displacement is presented in Fig 3.19. It is observed that the variance settles down to a constant value of approximately 0.302 as the system approaches the steady state. This result, combined with the behavior of the mean displacement is further confirmation that, indeed, the system reaches a steady state. When we compare Figure 3.13 with Figure 3.3 and Figure 3.5 it is clear that the

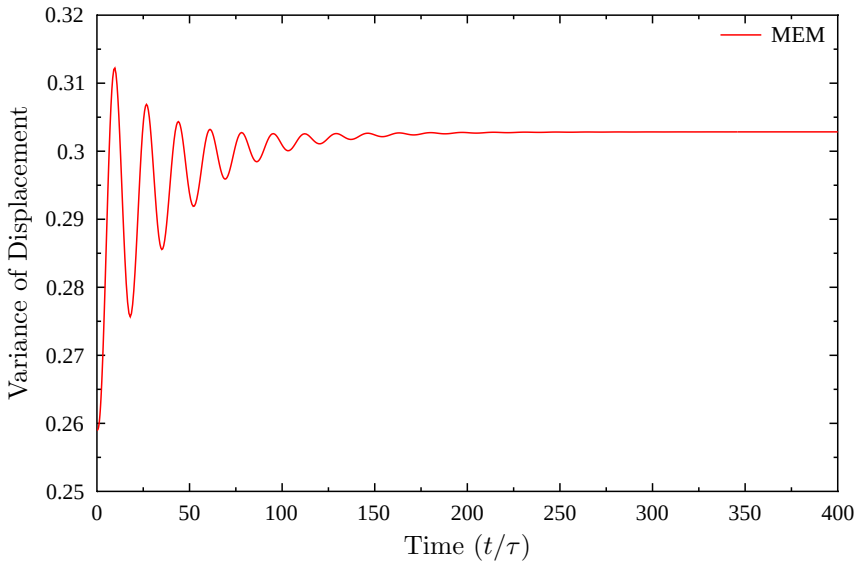

Figure 3.19: Evolution of Variance of Displacement: $\eta = 0.75$

rate at which the SET damps the resonator motion increases with increasing η. As a final case in our analysis we consider $\eta = 1$ in the next subsection.

3.8.3 $\eta = 1$

We now present the strongest nonlinear case that we consider, given by $\eta = 1.0$. The analysis is very similar to that carried out for the previous cases. In Fig 3.20 we

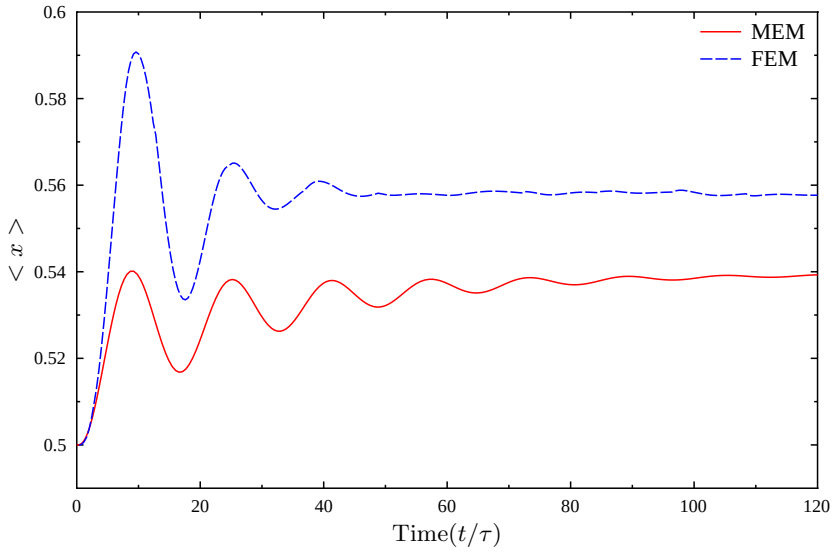

Figure 3.20: Mean Displacement of the Resonator: $\eta = 1$

present a comparison of the time evolution of the mean resonator displacement for the case $\eta = 1.0$ obtained from the FEM and the MEM. The maximum difference in peak amplitudes (which again occurs in the first period) is about 9.2 percent in this case. The difference in the (scaled) mean displacement when the system is begins to approach the steady state at time $t/\tau = 120$ is about 0.019. As is to be expected, these values are slightly higher than those obtained in the previous cases. However, the two solutions continue to be in good qualitative agreement and hence the MEM solution continues to be a good approximation to the resonator displacement. In Fig 3.21 we present the MEM solution for the resonator displacement plotted until $t/\tau = 400$.

The probability sub-density functions P_N and P_{N+1} corresponding to the steady state obtained from the FEM solution is presented in Fig 3.22.

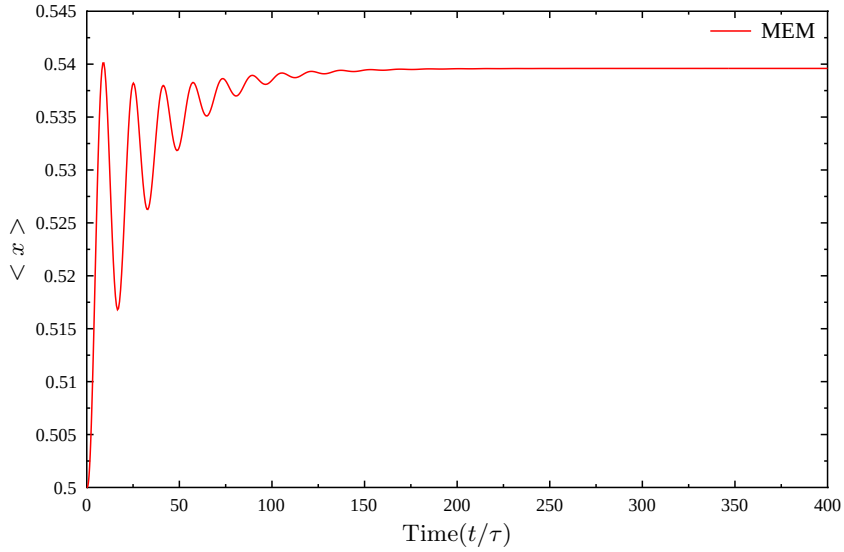

Figure 3.21: Mean Displacement of the Resonator: $\eta = 1$

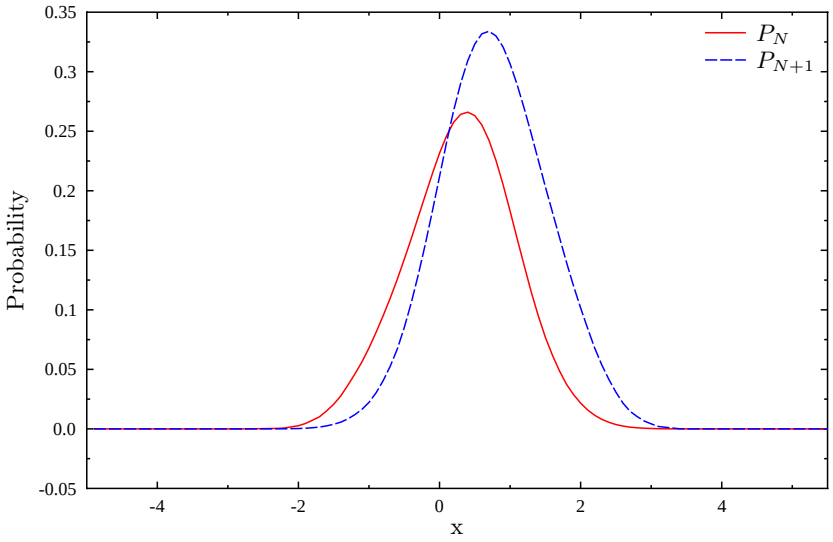

Figure 3.22: Steady State Probability Sub-Densities: $\eta = 1$

Moment Approximations

As in the previous cases, we present a comparison of the time evolution of each one of the moment approximations as computed from the FEM solution in Fig 3.23 - Fig 3.26.

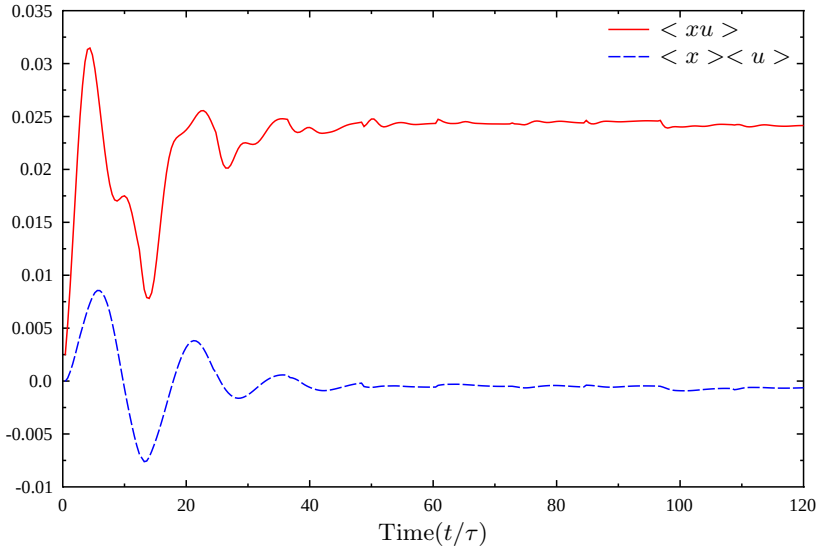

Figure 3.23: Comparison from FEM: $\eta = 1$

The behavior of the moments in Figs 3.23 - 3.26 confirms that the approximations continue to hold in the qualitative sense. However, quantitatively the difference between the steady state values of the exact and approximate quantities has increased compared to all the previous cases. Therefore the approximation, while still valid, becomes increasingly divergent from the exact value as the strength of the nonlinearity is increased.

Variance

The time evolution of the variance of the displacement is presented in Fig 3.27. It is observed that the variance settles down to a constant value of approximately 0.3

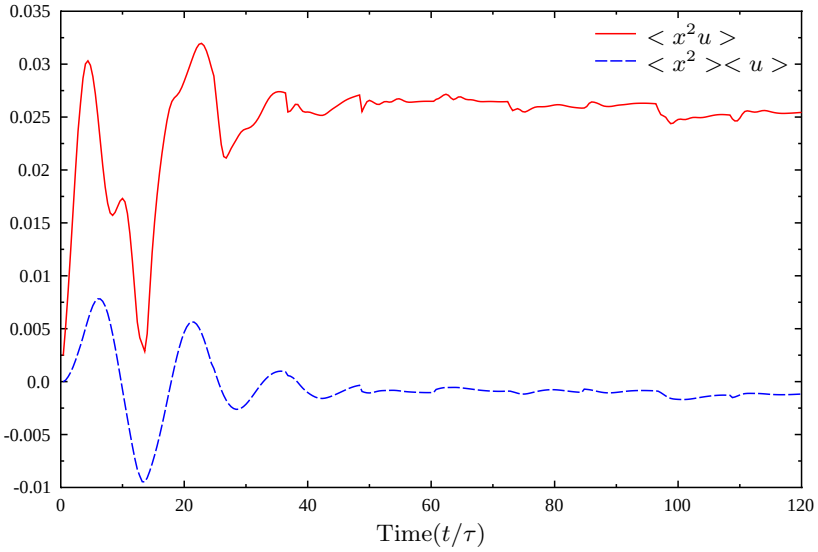

Figure 3.24: Comparison from FEM: $\eta = 1$

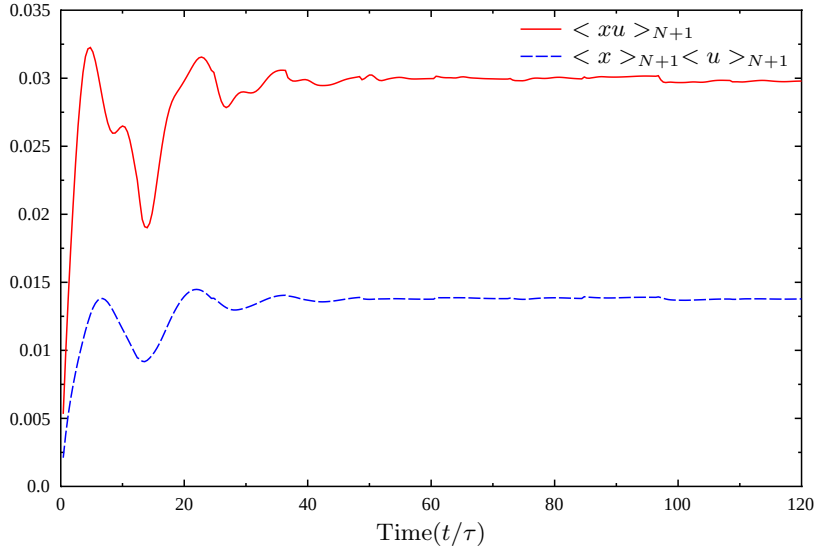

Figure 3.25: Comparison from FEM: $\eta = 1$

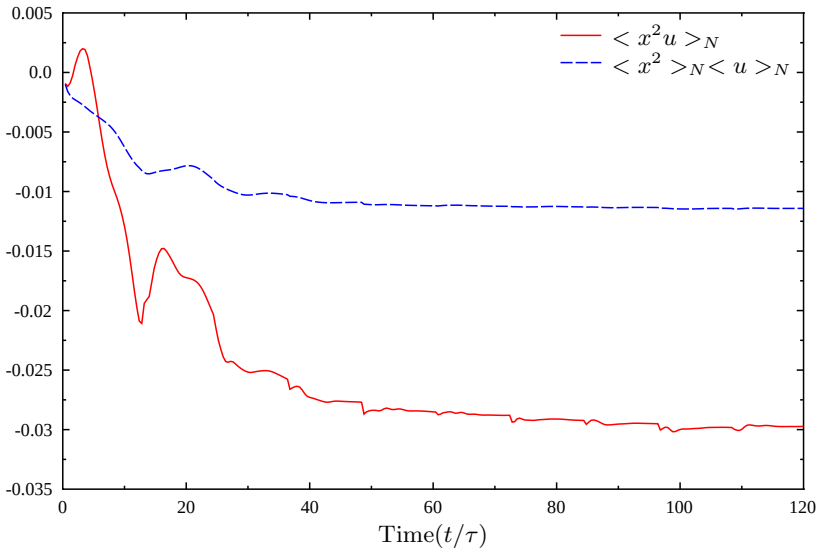

Figure 3.26: Comparison from FEM: $\eta = 1$

as the system approaches the steady state. This result, combined with the behavior of the mean displacement is further confirmation that, indeed, the system reaches a steady state. Now on comparing Figs. 3.3, 3.5, 3.13 and 3.22 we conclude that the SET damps the resonator most effectively for $\eta = 1$. We also mention a point here that is taken up for further discussion in the next subsection. In the linear case (Fig 3.3), the steady state value of the displacement is precisely the mean value during the first period. As the strength of the nonlinearity is increased, the steady state mean values tend to increase as seen from Figs. 3.5, 3.13 and 3.21. Therefore, apart from the conclusion that the resonator approaches the steady state more rapidly in the presence of nonlinearity, we also conclude that the damping mechanism undergoes qualitative changes as the strength of the nonlinearity is increased.

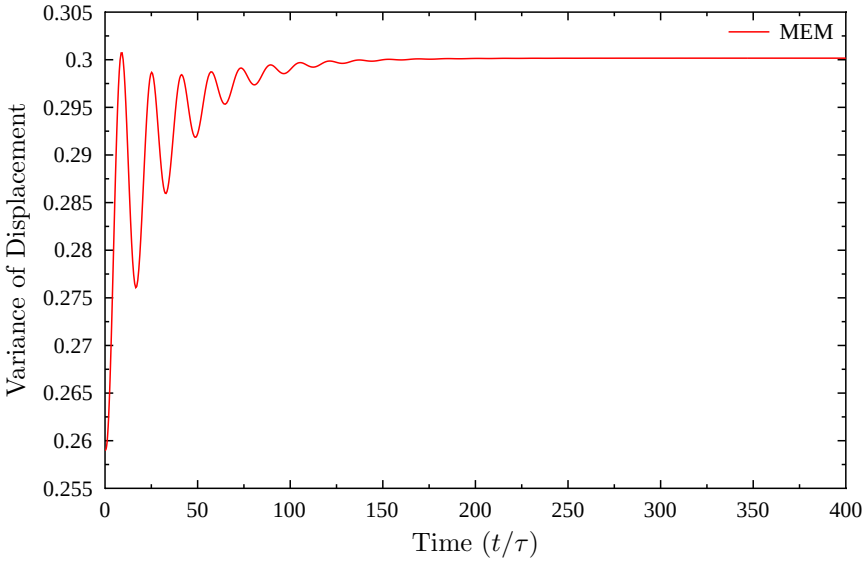

Figure 3.27: Evolution of Variance of Displacement: $\eta = 1.0$

3.9 Discussion of the Results: The Single-Well Duffing Case

The analysis of the single-well Duffing resonator carried out in the previous sections leads us to the following conclusions.

Firstly, we conclude that within the framework of our model, nonlinear motion of the resonator corresponding to a single-well Duffing potential results in the SET-nanoresonator system evolving into a steady state. In other words, we see that one of the main conclusions of the ABZ model holds under the generalization to the single-well Duffing potential.

Secondly, while the resonator motion is damped by the SET in the single-well Duffing case just as in the ABZ model, significantly, the rate of damping is much higher in the nonlinear case. Furthermore, the rate of damping markedly increases with the effective nonlinearity in the system (represented by the parameter η). It is also to be noted here that the increased efficacy of the SET in damping the nonlinear resonator motion is further evidenced by the fact that the mean amplitude of the first period of oscillation of

the resonator decreases with increasing η. Whereas we observe a value of approximately 0.605 (Figure 3.1) for the first period of resonator oscillation in the linear case, this reduces to approximately 0.54 (Figure 3.21) when $\eta = 1$.

Thirdly, it is important to note that the higher rate of damping arises exclusively due to the SET-resonator interaction since we have not included any extrinsic source of damping in our model.

The fourth point is that our results are obtained for relatively weak coupling between the SET and the resonator ($\kappa = 0.1$). Hence we conclude that nonlinearity in the resonator motion significantly impacts the dynamics of the coupled system even for weak coupling between the SET and the resonator. This is noteworthy since usually nonlinear effects are associated with strongly coupled systems.

The fifth point is the implication of our results for SET sensitivity from a practical viewpoint. The SET can be effectively used as a displacement detector for the nanoresonator only after the steady state is achieved for the coupled dynamics. The conclusion that this steady state is achieved more rapidly in the nonlinear case seems to indicate that the coupled system would work better as a sensor in the nonlinear regime.

The sixth point is an important conclusion with respect to the temperature of the oscillator in the steady state. This aspect is discussed in detail in Chapter 6 and here we provide a brief overview. It follows from statistical mechanics that temperature can be defined for a system only when the system is in equilibrium with a thermal bath when the temperature of the system is identical with the temperature of the bath. This is a consequence of the well known theorem on equipartition of energy [39], [58]. In the case of our resonator, we see that it reaches a steady state due to interaction with the SET. We observe from Figs 3.11, 3.19 and 3.27 that the steady state value of the variance of the displacement attained by the oscillator decreases with increasing η. The difference in numerical values is not large as seen from the figures but it exists. Since in the steady state the variance is directly proportional to the absolute temperature of the oscillator (as will be seen in detail in Chapter 6), we conclude that non-vanishing η in fact pushes the oscillator to a state of lower temperature as compared to the linear

case. As was discussed in the introduction, the cooling of nanomechanical resonators continues to be a very important issue and our analysis indicates that better cooling of the resonator is achieved in the nonlinear regime.

The seventh point is the observation from Figs. 3.5, 3.13 and 3.22 that the steady state mean value of the resonator displacement tends to increase with the strength of the nonlinearity. This points to a qualitative change in the damping phenomenon in the strongly nonlinear regime. We believe this to be an important observation unique to the nonlinear regime characterized by the single-well Duffing potential.

This discussion concludes the chapter.

Chapter 4

Generalization of the ABZ Model - The Double-Well Duffing Case

4.1 Introduction

In this chapter we consider the nonlinear extension of the ABZ model [3] where we model the resonator as a double-well Duffing oscillator. As discussed in Chapter 3, this situation, mathematically characterized by the quartic potential term in the Duffing Hamiltonian being subtracted from the harmonic oscillator potential, gives rise to qualitatively different dynamics. Hence it is of interest to investigate the dynamics of the SET-resonator system in this potential. It is also noteworthy that this potential term (denoted by $V(x)$), essentially given by $V(x) = \left(x^2 - \beta x^4\right)$, where x is the resonator displacement and β is a constant that governs the strength of the nonlinearity, gives rise to a force term in the equation of motion given by $F(x) = dV(x)/dx = 2x - 4\beta x^3$. Comparing this with the MacLaurin series expansion of $\sin(x)$ we see that the double-well Duffing potential yields a force term that is an approximation of the potential term in the equation of motion of a strongly nonlinear pendulum given by $\sin x = x - x^3/3! + x^5/5! - ....$ The pendulum being the quintessential model for strongly nonlinear behavior, the double-well Duffing potential enters the picture as a useful approximation in practical situations that demand a reasonable model in the strongly nonlinear regime.

The framework for this chapter is similar to that of the previous one. We are interested in solving for the motion of the resonator. To this end, we solve the moment evolution equations 3.68 for negative values of η. In Section 2 we present the results for different values of η, carefully chosen in order to highlight the dynamical effects

of interest. At the outset it needs to be noted that, given the complicated nature of the double-well potential compared to the single-well case, generating FEM solutions turns out to be quite challenging. However, the qualitative agreement between the two methods continues to hold thereby providing us with sufficient grounds to employ the MEM to reach conclusions about the dynamics. This is exemplified by the case of $\eta = -0.04$ where we provide a direct comparison of the FEM and MEM solutions. It is also important to note here that qualitative changes in the behavior of solutions manifest themselves very early in the dynamics in the double-well Duffing case and hence agreement between the two approaches for even short initial time intervals is adequate to establish the validity of the MEM for our purposes. As a result of extensive numerical experimentation, it is observed that, in contrast to the single-well Duffing case, the results here demonstrate a high degree of sensitivity to the numerical value of η. In fact, we encounter the remarkable dynamical phenomenon of the onset of instability below the threshold value of $\eta = -0.11$. Indeed, we observe the existence of a periodic attractor (a limit cycle, in other words) in the position-velocity space (phase space) of the resonator at precisely $\eta = -0.11$. Physically, this corresponds to a dynamic equilibrium state for the SET-resonator system, one in which no energy exchange occurs between the SET and resonator. However, for any value of η lower than the critical value we see the onset of instability. Physically, the instability corresponds to a situation where the SET begins to pump energy into the resonator driving the latter to oscillations with amplitudes that diverge in time. We summarize our results in Section 3 and conclude the chapter in Section 4 with a discussion of the results.

4.2 The FEM and MEM Solutions

4.2.1 $\eta = -0.04$

We begin with the case of the nonlinearity represented by $\eta = -0.04$ where we could expect the SET to damp the resonator motion in a manner reminiscent of the linear case.

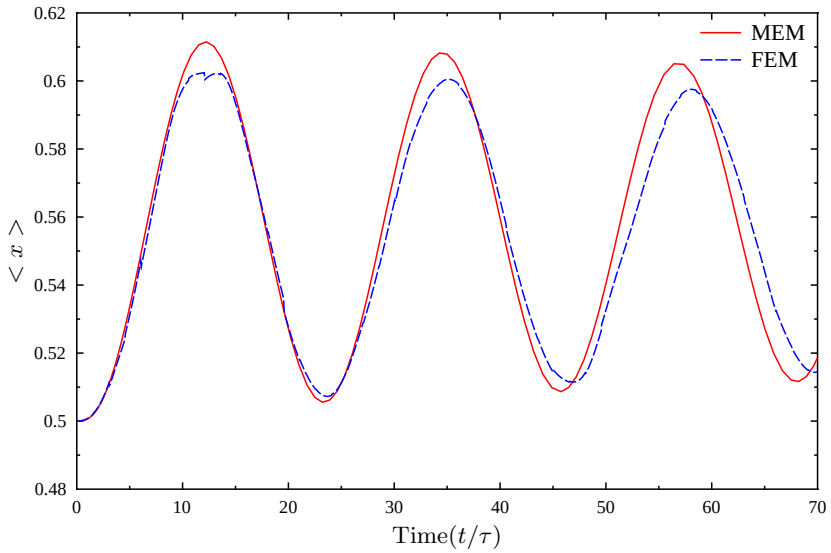

Figure 4.1: Mean Displacement of the Resonator: $\eta = -0.04$

In Fig 4.1 we present a comparison of the time evolution of the mean resonator displacement for the case $\eta = -0.04$ obtained from the FEM and the MEM. Comparing the two solutions the first observation is that the FEM solution is less conservative with respect to the magnitude of the displacement in comparison with the MEM solution. While the difference in peak amplitudes between the solutions remains almost steady at 1.6 percent during the first three cycles, the two solutions begin to step out of phase after about two cycles. It needs to be pointed out here that the double-well Duffing being a more complicated type of nonlinearity than the single-well case, significant numerical difficulties in the form of disagreement between the FEM and MEM solutions occur in the former case. However, referring to our observations in the introductory section of this chapter, the degree of agreement observed in Fig 4.1 is adequate for us to proceed to present the full MEM solution in Fig 4.2 for resonator displacement plotted until $t/\tau = 400$. The key point is that our primary interest is in the qualitative behavior of the solutions in the various regimes and this is faithfully recorded by the MEM solution.

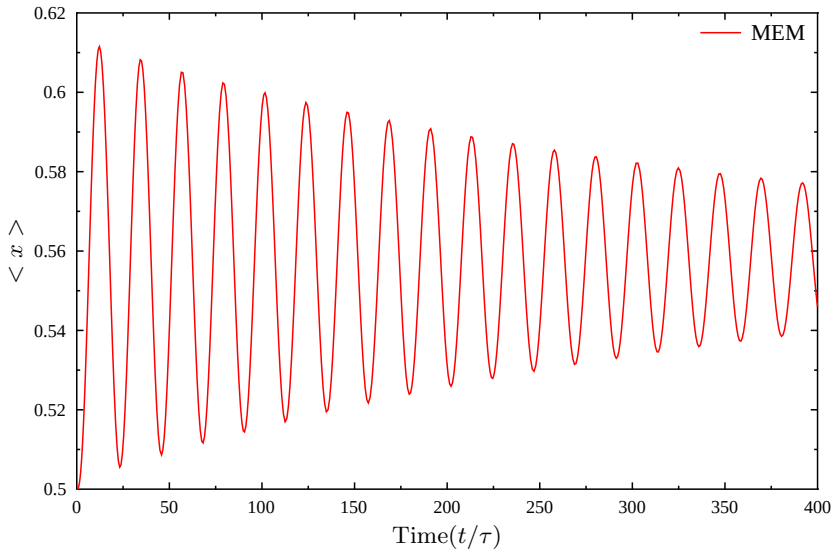

Figure 4.2: Mean Displacement of the Resonator: $\eta = -0.04$

It is clear from Fig 4.2 that the SET damps the resonator motion resulting in a steady state for the system. For a direct comparison with the linear case we refer to Fig 4.3 from which we draw the interesting conclusion that it takes more time for the system to reach a steady state in the case of $\eta = -0.04$. In other words, the SET damps the resonator motion much more effectively in the linear case than in the presence of the double-well Duffing nonlinearity. As will be evident from the cases that follow, this is a precursor to the dramatic changes in the resonator dynamics triggered by variations in η in the double-well Duffing case. Moreover, we note here the contrast with the single-well Duffing case where the presence of nonlinearity enhances the damping effect thereby forcing the system to the steady state more rapidly.

Yet another important aspect of resonator motion as it approaches the steady state is the behavior of the system in the position-velocity space (the phase portrait). We present the phase portrait in Fig 4.4. From the figure it is evident that the system approaches the equilibrium point described by the co-ordinates $(0.56, 0.0)$ in the phase

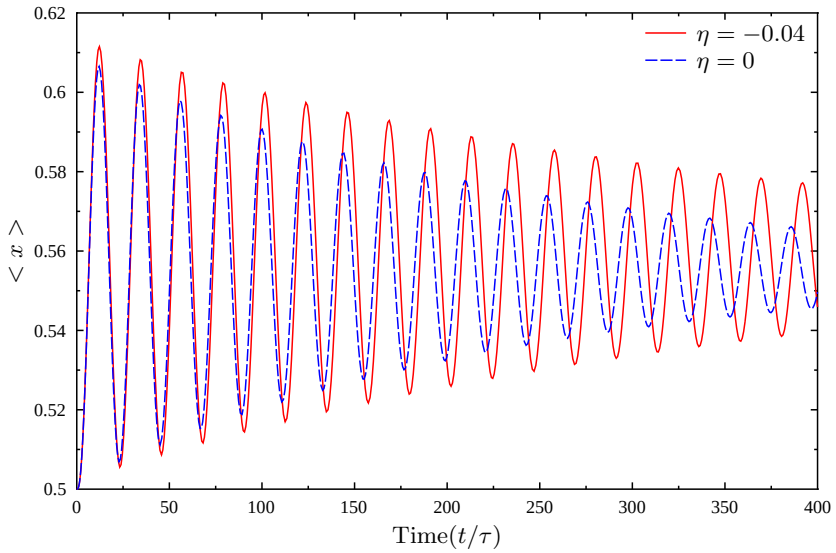

Figure 4.3: Comparison of Mean Displacement of the Resonator

plane. This is quite consistent with the response of the resonator (compare Fig 4.2) and the equilibrium point in this case falls under the category of the focus (also known as the spiral)[57],[34].

4.2.2 $\eta = -0.09$

In order to investigate further the reticence of the SET in damping the resonator motion in the double-well Duffing potential, we now increase the magnitude (absolute value) of the nonlinearity to $\eta = -0.09$. The result is presented in Fig 4.5. Evidently, the SET is increasingly ineffective in damping the resonator motion as the magnitude of η is increased.

4.2.3 $\eta = -0.11$

We now present the most interesting case of $\eta = -0.11$. The mean resonator displacement versus time is presented in Fig 4.6. As seen from the figure, the resonator motion

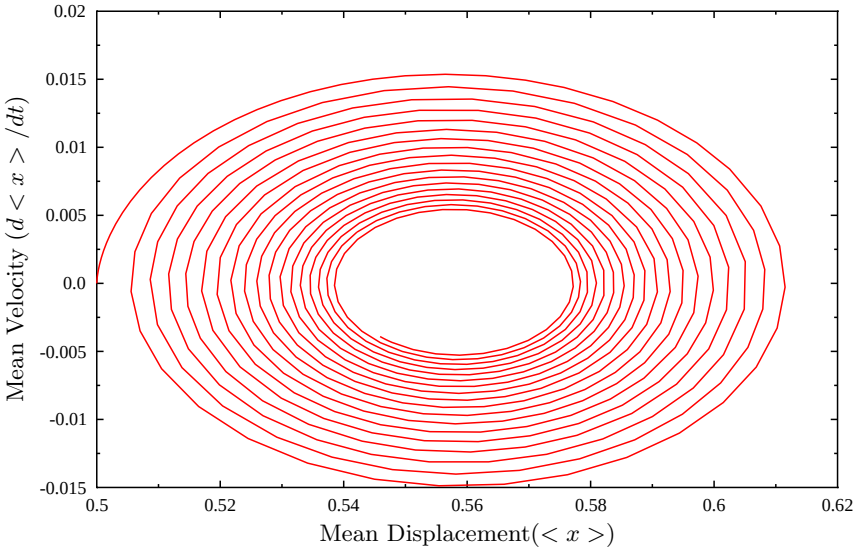

Figure 4.4: Phase Portrait: $\eta = -0.04$

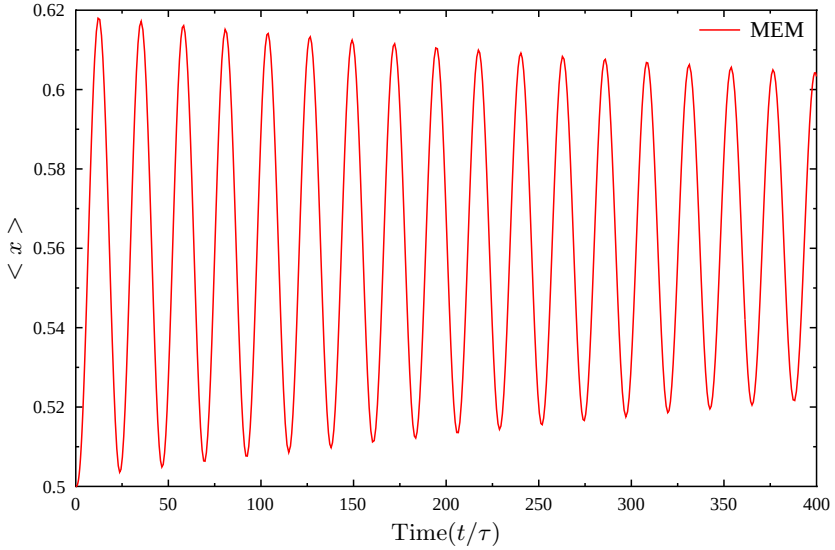

Figure 4.5: Mean Displacement of the Resonator: $\eta = -0.09$

is totally undamped in this case. In other words, no energy transfer occurs between the SET and the resonator and the coupled system is in a state of dynamic equilibrium with the resonator exhibiting self-sustained oscillations. The implications of this important result are taken up for discussion in the final section of this chapter. The presence of self-sustained oscillations in a nonlinear dynamical system is strongly indicative of a periodic attractor (also known as a limit cycle) in the phase space [57], [34]. Hence we examine the phase space (mean position-velocity space) of the SET-resonator system in this case and indeed discover the presence of a limit cycle as seen from Fig 4.7. We note here that the existence of such periodic attractors is a unique feature of nonlinear systems. Furthermore, it is noteworthy that while limit cycles are well understood in the context of deterministic systems, the cycle in our case has emerged in the averaged dynamics of a stochastic system.

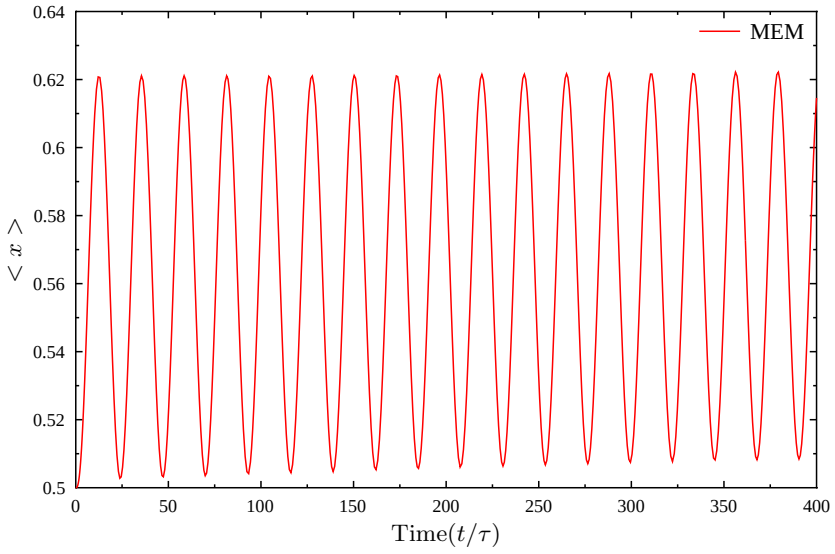

Figure 4.6: Mean Displacement of the Resonator: $\eta = -0.11$

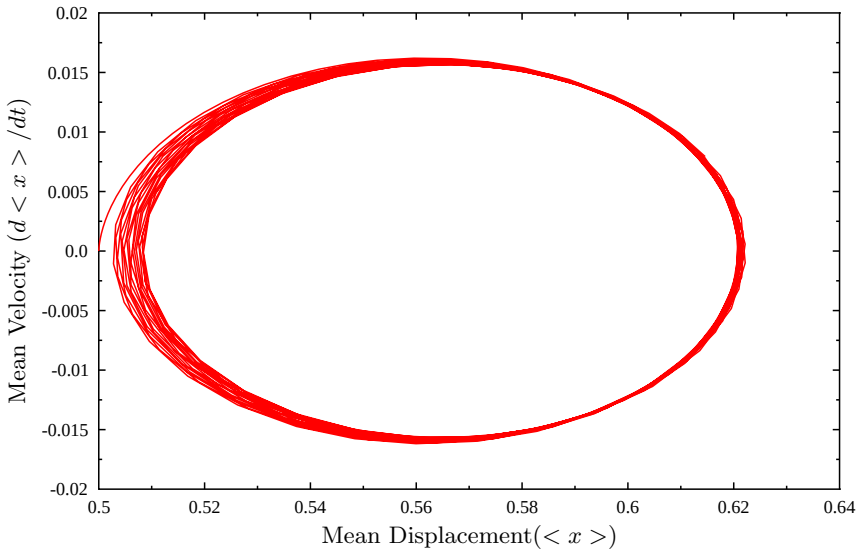

Figure 4.7: Phase Portrait: $\eta = -0.11$

4.2.4 $\eta = -0.25$

Given the existence of a periodic solution for $\eta = -0.11$, it is natural to ask the question of what happens when the modulus of η is increased further. Here we present the results for the case $\eta = -0.25$. The mean resonator displacement versus time is presented in Fig 4.8 and the phase portrait is given in Fig 4.9. Remarkably, we observe the emergence of instability in this case. From Fig 4.8 we see that the resonator exhibits oscillation, the magnitude of which grows unboundedly. This is corroborated by the phase portrait in Fig 4.9 which indicates an unstable focus. Physically, this corresponds to the situation that the SET continuously supplies energy to the oscillator.

4.3 Summary of the Results

Our results in the previous section clearly point to the fact that the dynamics of the SET-resonator system is uniquely sensitive to the strength of the nonlinearity in the

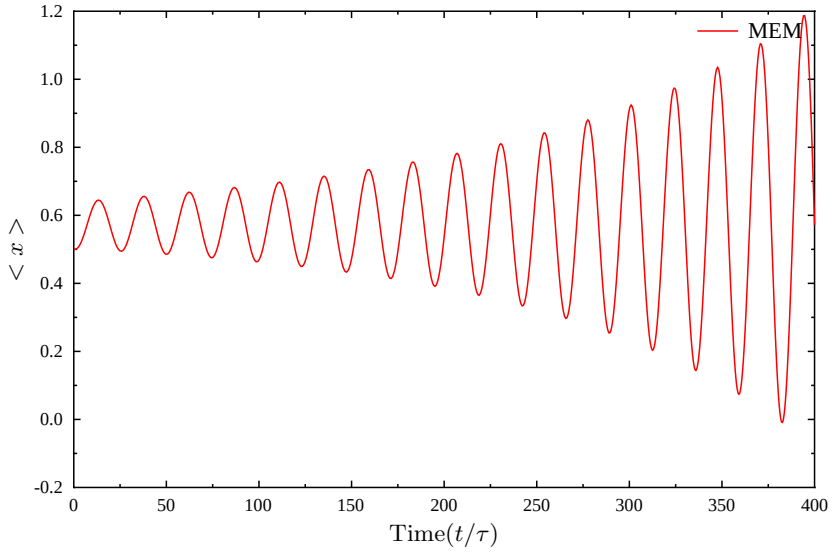

Figure 4.8: Mean Displacement of the Resonator: $\eta = -0.25$

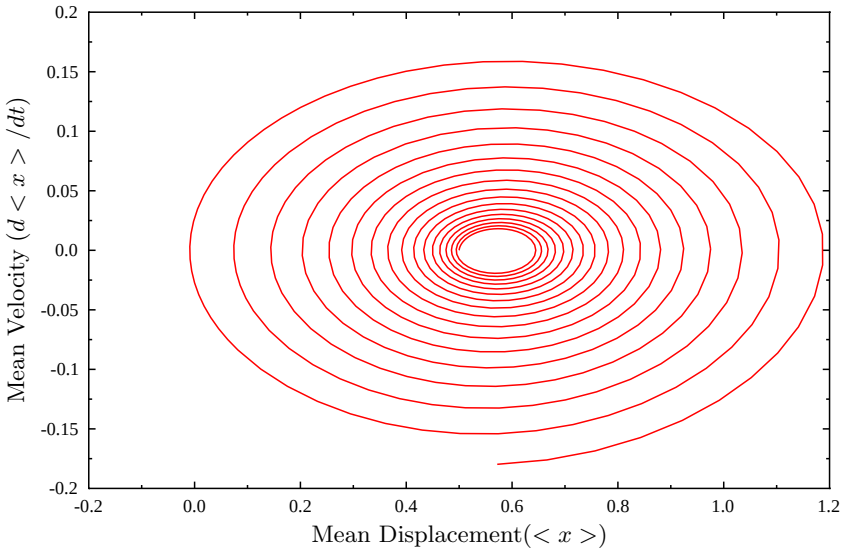

Figure 4.9: Phase Portrait: $\eta = -0.25$

double-well Duffing case. Early evidence of the inability of the SET to damp the resonator motion was observed in Fig 4.3 from which we concluded that even when compared to the case of a weakly nonlinear double-well Duffing potential, the system reaches the steady state much faster in the presence of a linear harmonic potential. The ability of the SET to effectively damp the resonator motion deteriorated further, with an increase in the magnitude of the strength of the nonlinearity. Finally, at $\eta = -0.11$ we observed that the resonator had attained a dynamical state of equilibrium with the SET and there was no energy transfer in either direction. When the magnitude of the strength of the nonlinearity was increased further, we witnessed a dynamical instability at $\eta = -0.25$. Indeed the instability sets in for any value of η less than -0.11 but we choose to demonstrate it at $\eta = -0.25$ for enhanced clarity of the results. While these results are taken up for discussion in the concluding section of this chapter, we note here that the SET-resonator system first reaching a state of dynamical equilibrium followed by the onset of instability are the key results in the double-well Duffing case.

4.4 Conclusions

In this chapter we dealt with the case of the double-well Duffing potential. The first conclusion is the expected one that, in the presence of very weak nonlinearity the SET damps the resonator and the coupled system reaches a steady state. Therefore, the basic conclusions of the ABZ model hold in the weakly nonlinear case. However, in the presence of the double-well Duffing potential the SET finds it harder to damp the resonator motion than in the linear case.

The second conclusion is that the inability of the SET to damp the resonator becomes acute as the strength of the nonlinearity is increased. For the parameter values that we have consistently adhered to in this dissertation ($\epsilon = 0.3$ and $\kappa = 0.1$), we observed that for a critical value of $\eta = -0.11$, the SET and the resonator reach a state of dynamical equilibrium characterized by the presence of a limit cycle in the phase space. Indeed, in comparison with the linear harmonic and the single-well Duffing potentials, this phenomenon is unique to the double-well Duffing regime.

The third conclusion is the onset of instability below the critical value of $\eta = -0.11$. Again, such a clear onset of instability is observed only in the double-well Duffing regime. There has been a lot of recent interest in the phenomenon of the SET pumping energy into the resonator in specific dynamical regimes (for instance, [20]) and our analysis points to a specific situation where this can happen via the onset of instability in the SET-resonator system. In the broad context of nonlinear dynamics of NEMS, knowledge of the existence of such instabilities can be expected to aid the design and operation of these systems.

Chapter 5

The Damping Process

5.1 Introduction

As is evident from our discussions in the previous chapters, an important aspect of the SET-resonator interaction is that in the cases of the linear harmonic potential as well as the single-well Duffing potential the SET damps the motion of the resonator thereby driving the system to a steady state. Since measurements using the system are best realized in a steady state, the phenomenon of damping is of import in the study of nanoresonators. Moreover, from our results in Chapters 3 and 4 we concluded that the damping rate gets significantly enhanced in the presence of the Duffing type of nonlinearity. This chapter is devoted to a more detailed examination of the damping process that drives the resonator to the steady state when coupled to the SET.

Our prime motivation for this exercise arises from the fact that in order to approach the dynamics of the resonator from the Langevin point of view (which is the subject of the next chapter), one needs to introduce explicitly a damping term into the equation of motion. While a linear damping term of the form $c\dot{x}$ has been used in the linear regime in the literature(see for instance Aldridge and Cleland [1], Clerk and Bennett [20], Scheible *et al.* [52], Usmani *et al.* [7]), in the light of our results in the previous chapters it is not *a priori* obvious that such a term would be adequate in the Duffing regime. Hence, what is essentially sought here is an indication of the type of damping term which, when introduced into the Langevin equation, would provide a reasonable model for the resonator motion in the Duffing regime.

Since we already have the results from our generalization of the ABZ model to the nonlinear regime, the attempt is to use those results to draw conclusions about

the nature and characteristics of the damping process. This also provides consistency when the conclusions from the generalized ABZ model and the Langevin approach are compared in the final analysis. However, the ABZ model involves a system of coupled master equations and to begin with makes no analytical statement about damping. Therefore, it is not straightforward to draw conclusions about the damping term from the ABZ model. We solve this problem by fitting the numerical data from the generalized ABZ model to the dynamics of the Duffing resonator with various types of damping terms and look for the best fit. It is important to note here that the ABZ model when generalized to the Duffing regime is quite a complicated one (one deals with a nonlinear system of nine ODEs even after having made simplifying approximations in order to obtain moment closure) and therefore when we attempt to fit the solution of the original complicated system with the solution of a single ODE, at best we only expect a qualitative agreement between the two solutions.

The effort in this chapter is further motivated by the fact that nonlinear damping terms have been proposed in the literature in the context of nanomechanical resonators. For instance, Lifshitz and Cross [44] consider a damping term of the form $x^2\dot{x}$ in their deterministic model of a system of coupled mesoscopic oscillators. A similar term is considered in the more recent work of Zaitsev and Buks [60] which explicitly treats nonlinear damping effects in a nanomechanical resonator.

5.2 Damping in the Generalized ABZ Model

Damping of the resonator motion by the SET driving the former to a steady state is one of the key conclusions of the ABZ model. However, the model makes no explicit reference to the nature of the damping mechanism except for the conclusion (after the equations of the model have been solved) that the resonator behaves like a linearly damped harmonic oscillator. This situation is due to the fact that the basis of the ABZ model is a set of master equations, the solutions to which describe probabilistically the motion of the resonator under the influence of the interaction with the SET. In other words, in the ABZ model one has no direct access to the equation of motion of

the resonator. As a consequence the particular nature of the damping term remains unventilated throughout the analysis until one solves the model to obtain the time evolution of the mean displacement of the resonator.

Since we observed enhanced damping in our results from the generalization of the ABZ model to the Duffing regime and since we require an explicit form of the damping term in order to build a Langevin model, we need to clarify the nature of damping in the Duffing regime. To this end we carry out the following exercise. Firstly, we use the data on the mean displacement (x) from the MEM solutions to compute the mean velocity ($\dot{x}$) and the mean acceleration ($\ddot{x}$) at every time step. In the next step assume the equation of motion for the resonator. We note here that since we are dealing with a resonator in the Duffing regime we know that form of the acceleration and the stiffness terms in the assumed equation of motion. If we denote the displacement of the resonator by y, the acceleration term will be of the form $\alpha_1 \ddot{y}$ and the stiffness term will be of the form $\alpha_3 y + \alpha_4 y^3$ where α_1, α_3 and α_4 are unknown constant coefficients. The next step is to assume different forms of the damping term and to fit the data obtained from the MEM solutions to the assumed equation.

In other words, we use the MEM solution data to numerically obtain the unknown coefficients α_i. This leads to a realization of the assumed equation of motion which can then be immediately solved. Comparing the solution of the assumed equation of motion to the original MEM solution and repeating the process as necessary with different types of damping terms one then arrives at an optimal damping term that best fits the MEM solution. Indeed, this anstaz may be repeated for different values of η (the strength of the nonlinearity) to obtain a more complete picture of the dissipation process in the Duffing regime.

We reiterate here that since the original system of moment evolution equations is a complicated one and the above mentioned procedure attempts to recreate all the characteristics of the system of moment equations by replacing it with an assumed single equation, what is expected here is qualitative agreement between the solutions. Furthermore, it cannot be expected that the solutions obtained by the fitting method will

be in agreement with the MEM solutions for arbitrarily long time intervals. However, qualitative understanding of the damping mechanism is sufficient for the purposes of introducing an appropriate damping term into the Langevin model. The numerical code for the entire fitting process described above is written in MATLAB and is provided in Appendix E. We note here that the fit obtained by this procedure is a least squares fit.

To further elucidate the above anstaz we now consider the example where we assume a linear damping term of the form $\alpha_2\dot{y}$. The assumed equation of motion for the resonator then becomes:

$$\alpha_1\ddot{y} + \alpha_2\dot{y} + \alpha_3 y + \alpha_4 y^3 = 0. \tag{5.1}$$

Now the data obtained from the MEM solution is used to numerically obtain the unknown coefficients α_1, α_2, α_3 and α_4. Once these are obtained, Eqn 5.1 may be solved numerically to obtain the resonator response $y(t)$. Comparing $y(t)$ with the response obtained from the MEM solution $x(t)$ one checks whether the assumed damping term $\alpha_2\dot{y}$ adequately captures the response obtained from the MEM solution. If the fit is unsatisfactory the damping term is to be replaced by a different one (say $\alpha_5 y^2\dot{y}$) and the process is to be repeated until a reasonable fit is obtained.

5.3 Results

In this section we carry out the procedure described in the previous section for the various cases of the Duffing regime. In Figs. 5.1 to 5.6 we present the results of a linear damping term fit (of the form $\alpha_2\dot{y}$ where α_2 is a constant) for the cases $\eta = 0.0$, $\eta = 0.25$, $\eta = 0.50$, $\eta = 0.6$, $\eta = 0.75$ and $\eta = 1.0$ respectively. The MEM solution in all these cases corresponds to $\kappa = 0.1$ and $\epsilon = 0.3$.

It is evident from Figs. 5.1 to 5.6 that a linear damping term of the form $\alpha_2\dot{y}$ progressively fails to capture the resonator response as the strength of the nonlinearity η is increased. While we observe good agreement between the MEM solution and the solution generated by the fitting procedure in the linear case of $\eta = 0$ (Fig. 5.1) until time $t/\tau = 80$, the agreement between the two solutions holds very well only until

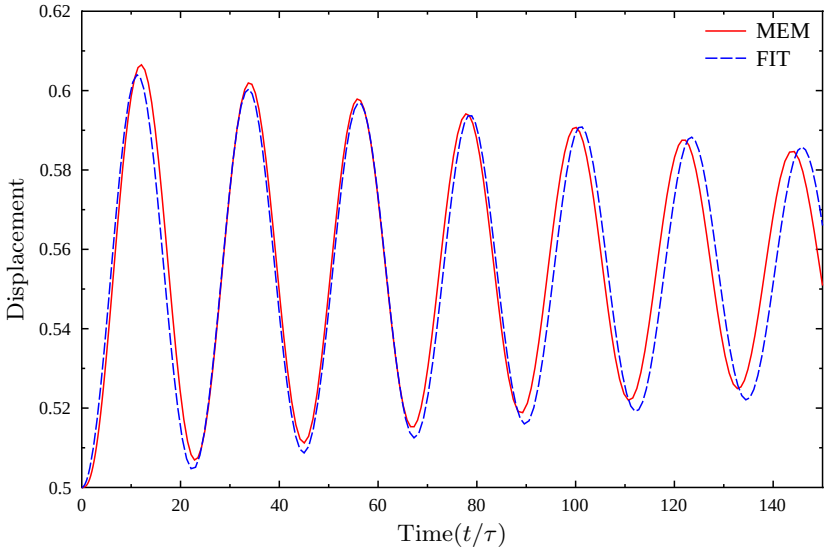

Figure 5.1: Linear Fit: $\eta = 0$.

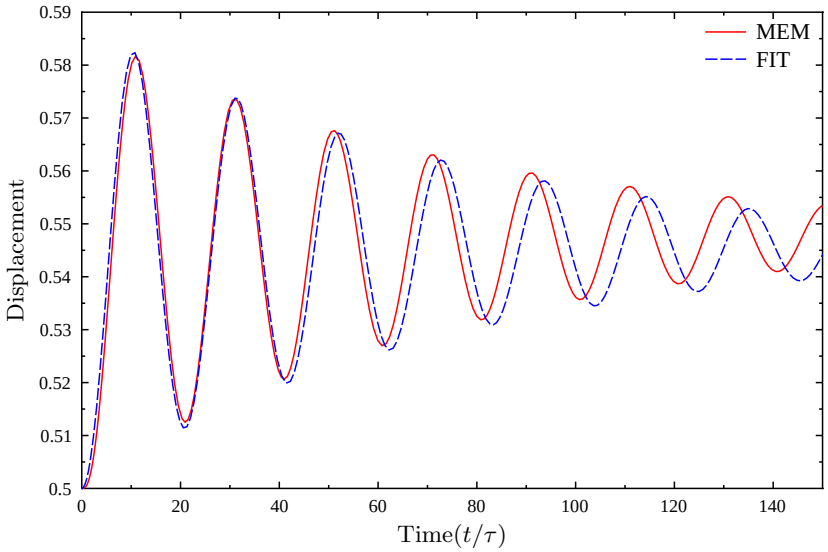

Figure 5.2: Linear Fit: $\eta = 0.25$.

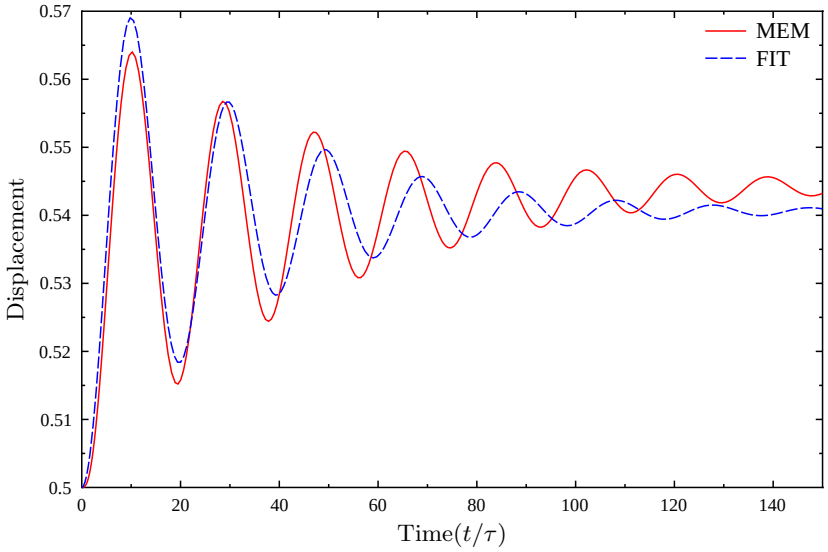

Figure 5.3: Linear Fit: $\eta = 0.50$.

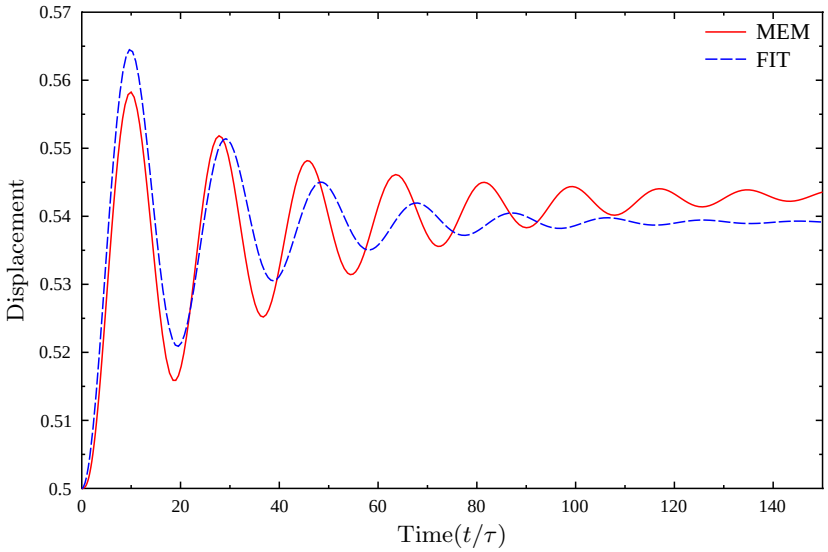

Figure 5.4: Linear Fit: $\eta = 0.60$.

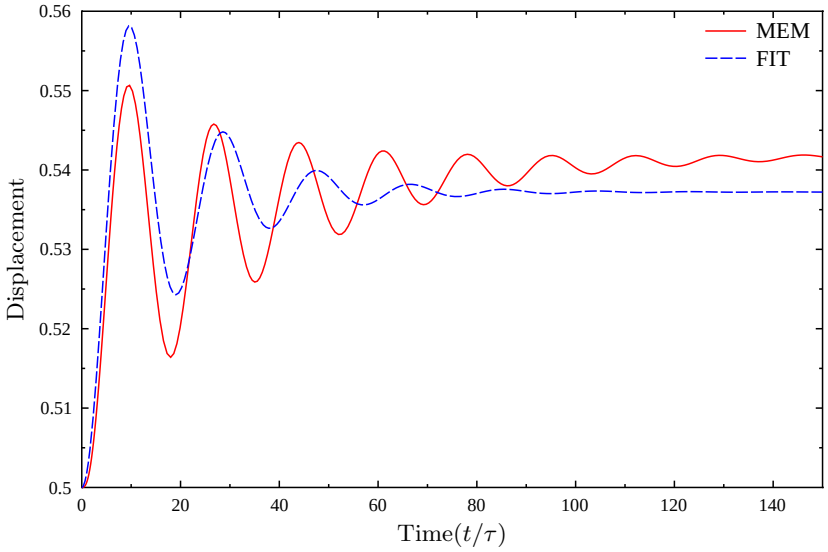

Figure 5.5: Linear Fit: $\eta = 0.75$.

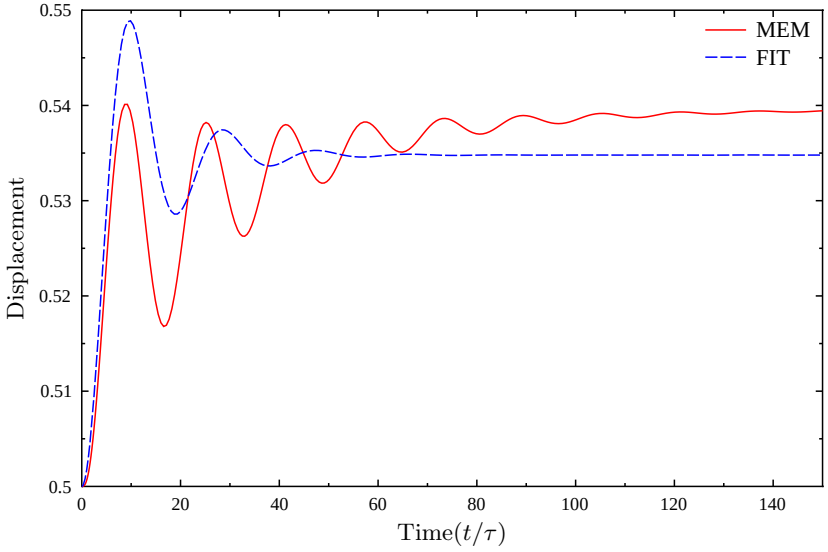

Figure 5.6: Linear Fit: $\eta = 1.0$.

time $t/\tau = 40$ when $\eta = 0.25$. However, the qualitative nature of the two solutions, exemplified by the characteristic that the mean resonator displacement as the system approaches the steady state is about half of the peak mean displacement amplitude in the first period of oscillation, is in agreement only until around $\eta = 0.6$. This is evident from the solutions in the $\eta = 0.75$ and $\eta = 1.0$ cases.

Let us first consider the $\eta = 0.75$ case (Fig 5.5). We first note that both displacement and time in this discussion are scaled, unitless quantities. In the MEM solution, the peak amplitude in the first period is approximately 0.55 whereas the steady state mean displacement is approximately 0.54. The difference between the two is about 0.01. However, in the case of the solution generated by the fit, this difference is approximately 0.023. In other words, the fit solution clearly fails to capture the phenomenon that the mean displacement of the resonator in the steady state gets closer to the peak amplitude in the first period as the strength of the nonlinearity is increased. Further evidence of this is provided by the case $\eta = 1.0$ (Fig 5.6). The steady state mean resonator displacement in this case is almost exactly the same value of the peak amplitude in the first period while the fit solution fails to capture this phenomenon. We also note here that the higher order damping terms such as $\alpha y\dot{y}$, $\alpha y^2\dot{y}$ where α is a constant are unable to provide a solution in this strongly nonlinear single-well Duffing regime that fit well with the MEM solution. The main conclusion from this discussion is that a linear damping term of the form $\alpha\dot{y}$ is optimal in the single-well Duffing regime for $0 \leq \eta \leq 0.6$ but cannot be employed with confidence for the cases of stronger nonlinearities.

As a further check on the fit analysis, we now present the results of using a linear damping term of the form $\alpha\dot{y}$ in the double-well Duffing regime. From our results in Chapter 4 we know that among the values of η considered, the most interesting MEM solutions in this regime correspond to $\eta = -0.11$ and $\eta = -0.25$. We recall that $\eta = -0.11$ corresponds to a state of dynamical equilibrium between the SET and the resonator with no energy transfer taking place in either direction. The case of $\eta = -0.25$ belonged to the unstable regime where the SET continuously pumps energy into the resonator. In Fig 5.7 and Fig 5.8 we present comparisons of the MEM solutions with

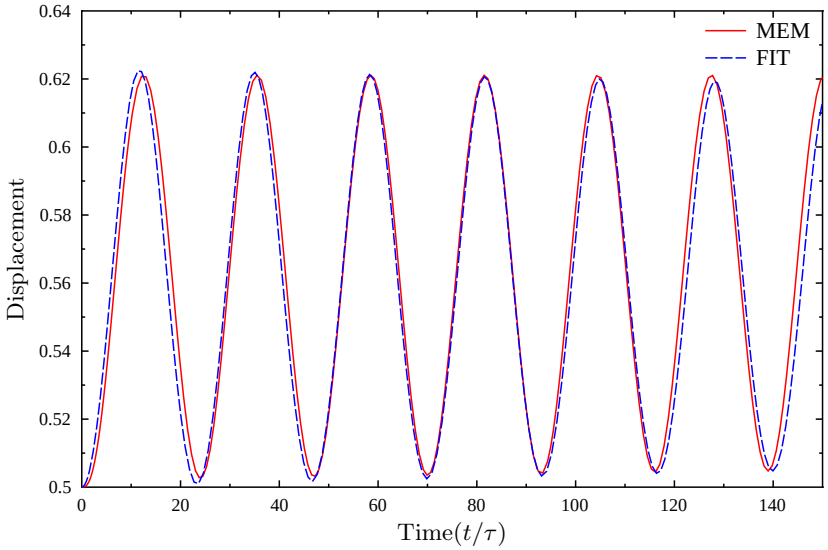

Figure 5.7: Linear Fit: $\eta = -0.11$.

the fit solutions using a linear damping term.

From Fig 5.7 it is seen that the fit solution captures remarkably well the situation of a dynamical equilibrium between the SET and the resonator at $\eta = -0.11$. It can be observed from Fig 5.8 that the qualitative feature of the instability of the solution corresponding to $\eta = -0.25$ is also predicted accurately by the fit solution.

5.4 Conclusion

In this chapter we investigated the mathematical form of the damping term that characterizes the motion of the resonator in its interaction with the SET motivated by the fact that an explicit form of the damping term is required for setting up a Langevin model for SET-resonator system; the subject of our next chapter. While the results in Chapters 3 and 4 from our generalization of the ABZ model clearly pointed to enhanced damping in the single-well Duffing case and the onset of instability in certain

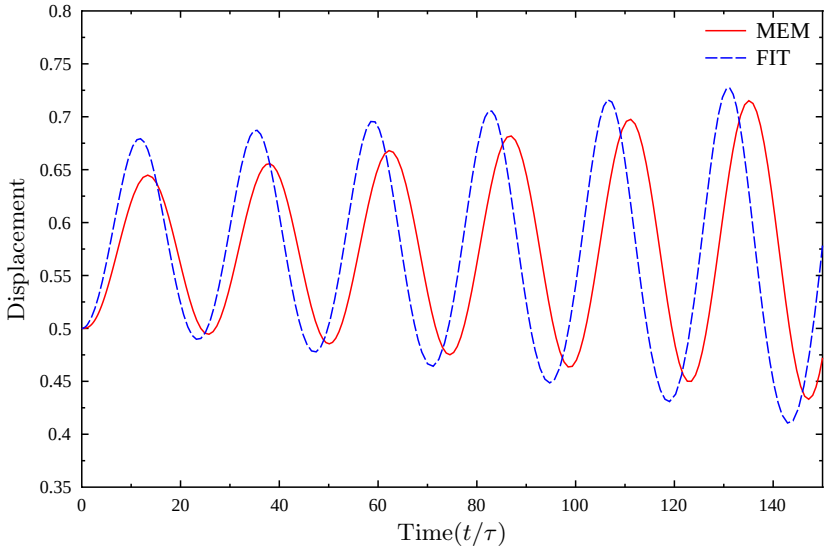

Figure 5.8: Linear Fit: $\eta = -0.25$.

regimes in the double-well Duffing case, the framework of the ABZ model makes no reference to the actual form of the damping term. We therefore fit the results to a single ODE and concluded that a linear damping term of the form $\alpha\dot{y}$ adequately captures the observed damping in the resonator motion in both the single-well and double-well Duffing regimes. However, in the single-well Duffing case (which is the case of primary interest) the linear damping term is effective only for nonlinearities characterized by the interval $0 \leq \eta \leq 0.6$. The Langevin model developed in the next chapter is based on this important conclusion.

Chapter 6

The Langevin Approach

6.1 Introduction

In this chapter we consider a Langevin approach to the dynamics of the nanoresonator-SET system. The focus of the discussion in this approach is on the stochastic motion of the resonator under the influence of a random force imparted on it by the tunneling electrons in the SET. As is customary in a first treatment of stochastic dynamical systems [31], this random force is modeled as a white-noise stochastic process. Hence one obtains a stochastic differential equation for the motion of the resonator which, following the seminal work of Langevin in the context of Brownian motion, is known in the literature as the Langevin equation. A key result in stochastic analysis is the canonical way in which one obtains a partial differential equation satisfied by the probability density function associated with a given Langevin equation [31]. The solution of this partial differential equation, known as the Fokker-Planck equation, yields the conditional probability density function of the stochastic process in question, thereby solving the dynamical problem. It is to be noted that closed form analytical solutions to the Fokker-Planck equation are generally considered hard to obtain, particularly so for nonlinear systems.

The Langevin equation represents a first principles approach to the problem since the starting point is a differential equation of motion for the resonator based on Newton's Second Law of motion. However, in contrast to the generalization of the ABZ model that was considered in the previous chapters, the Langevin equation for the resonator motion does not address in as much detail the interaction between the SET

and the resonator. On the other hand, it is precisely this characteristic that eliminates the need for the specific assumptions about the SET-resonator interaction that are essential for the ABZ model. Moreover, the Langevin approach has been applied to the linear regime of resonator motion in the literature [19], [20],[9]. In particular, [19] considers a generic position detector operating in the linear regime (of which a SET may be considered as a specific example) coupled to a nanomechanical resonator and concludes that the resonator motion is well approximated by a Langevin equation. This is established based on a rigorous quantum field theoretical calculation that lies outside the scope of our discussion. In [9] a Fokker-Planck equation for the resonator motion is derived starting from the ABZ master equations and employing an approximation method known as the Born-Markov approximation.

The focus of our investigation being the Duffing regime, we begin in Sec 2 by writing the Langevin equation for a generic nanoresonator in this regime assuming that the resonator is weakly coupled to the SET. A key point in the Langevin equation is the introduction of a damping term appropriate for the dynamics under consideration. We turn to the results of the previous chapter to assure ourselves that a linear damping term best suits our model with the caveat that the discussion does not include the strongly nonlinear regime. Using the standard theory of stochastic differential equations we then obtain straightforward passage to the Fokker-Planck equation. In Sec 3 we obtain the non-dimensional form of the equation. In Sec 4, we solve the equation for the steady state analytically, in closed form. In Sec 5 we obtain a numerical solution in the time dependent case using the FEM developed in the master equation approach and show that the resonator attains a steady state more rapidly in the nonlinear case. Indeed, this is consistent with our results from the master equation approach considered previously.

We recall from our discussion in the introductory chapter that the effective temperature of the resonator is a quantity of great importance in applications. In the linear case, the equipartition of energy theorem from statistical mechanics allows one to define the effective temperature of the resonator in the steady state. While this classical result resists extension to the case of arbitrarily nonlinear systems, the fact that we have a

closed form, steady state solution to the Fokker-Planck equation may be exploited to invoke a generalization of the equipartition of energy theorem in order to define an effective temperature for the resonator. We note here, parenthetically, that the existence of the steady state solution and the generalization of the equipartition theorem are both hinged on the fact that the Duffing resonator is a Hamiltonian system, albeit a nonlinear one. Thus we show, in Sec 6, that the resonator in fact attains a lower steady state effective temperature in the presence of nonlinearity. We conclude the chapter in Sec 7 with an overall discussion of our results from the Langevin approach, a comparison with those obtained from the ABZ method and the implications of the cooling effects in the nonlinear regime.

6.2 The Langevin and Fokker-Planck Equations

Consider a Duffing nanoresonator of mass m, damping coefficient γ, stiffness $k = {\omega_0}^2$ and nonlinear coefficient α (identical to the coefficient used in deriving the master equations), moving under the influence of a random force $F(t)$ provided by the SET. We shall work in a scale in which the mass of the resonator is taken to be unity. Denoting the displacement of the resonator as x and assuming a linear damping term in the weak-coupling limit of the interaction between the SET and the resonator, the Langevin equation can be written as:

$$\ddot{x} + \gamma\dot{x} + {\omega_0}^2\left(x + \alpha x^3\right) = F(t). \tag{6.1}$$

We note here that since $\ddot{x}$ has dimensions $\left(LT^{-2}\right)$, the term $\gamma\dot{x}$ must have the identical dimensions. Hence γ has dimensions $\left(T^{-1}\right)$.

Following standard practice in Langevin dynamics we now assume that $F(t)$ is a white noise process, the canonical mathematical representation of which is as the integral of an incremental Wiener process dW. In other words, $F(t)dt = dW$. The Wiener process is central to a consistent mathematical description of stochastic processes in general and the Brownian motion in particular. For a detailed discussion of this process and its connection to Langevin dynamics we refer to the classical review article

by Chandrasekhar [13], the modern works of Gardiner [31], Risken [51], Oksendal [48], Sobczyk [54] and the masters thesis of the author [50]. The above references also discuss the fundamental aspects of stochastic differential equations (SDEs). The Langevin equation being a particular example of a SDE, it follows that the theory of SDEs is fully applicable in its case. The principal idea here is that associated with a system of SDEs, there exists a partial differential equation (the Fokker-Planck equation) that is uniquely satisfied by the probability density function corresponding to the SDE system. Hence, solving the PDE for the probability density essentially solves the problem of stochastic motion posed by the Langevin equation. Presently we derive the Fokker-Planck equation for our system with the note that the references given above provide the theoretical basis and methodological validation for our procedure.

Converting Eqn 6.1 into a first order system of stochastic differential equations and using the notation $\dot{x} = y$, we write in matrix form:

$$\begin{pmatrix} dx \\ dy \end{pmatrix} = \begin{pmatrix} y \\ -\gamma y - {\omega_0}^2 \left(x + \alpha x^3 \right) \end{pmatrix} dt + \begin{pmatrix} 0 & 0 \\ 0 & 1 \end{pmatrix} \begin{pmatrix} 0 \\ dW \end{pmatrix}. \tag{6.2}$$

Now, a standard system of stochastic differential equations (see, for instance, [31]) is given by:

$$d\bar{x} = \bar{A}dt + \tilde{B}d\bar{W}, \tag{6.3}$$

where $\bar{x}$ is a vector-valued random process driven by the vector valued Wiener process $d\bar{W}$. Here, $\bar{A}$ is called the drift vector and $\tilde{B}$ the diffusion matrix. It is known that the probability density function P corresponding to Eqn 6.3 satisfies the following Fokker-Planck equation:

$$\frac{\partial P}{\partial t} = -\sum_i \frac{\partial}{\partial x_i} \left[A_i P \right] + \frac{1}{2} \sum_{i,j} \frac{\partial^2}{\partial x_i \partial x_j} \left[\left(BB^T \right)_{ij} P \right]. \tag{6.4}$$

Comparing Eqn 6.2 and Eqn 6.3 we write:

$$\bar{A} = \begin{pmatrix} A_1 \\ A_2 \end{pmatrix} = \begin{pmatrix} y \\ -\gamma y - {\omega_0}^2 \left(x + \alpha x^3 \right) \end{pmatrix} \tag{6.5}$$

where we use the notation A_1 and A_2 to denote the components of $\bar{A}$ with respect to the variables x and y respectively. We also have:

$$\tilde{B} = \begin{pmatrix} 0 & 0 \\ 0 & 1 \end{pmatrix}. \tag{6.6}$$

This yields:

$$\tilde{B}\tilde{B}^T = \begin{pmatrix} 0 & 0 \\ 0 & 1 \end{pmatrix}. \tag{6.7}$$

Using Eqn 6.7 the second term on the RHS of Eqn 6.4 can be written as:

$$\frac{1}{2}\sum_{i,j}\frac{\partial^2}{\partial x_i \partial x_j}\left[\left(\tilde{B}\tilde{B}^T\right)_{ij} P\right] = \frac{\partial^2 P}{\partial y^2}. \tag{6.8}$$

We now consider the first term on the RHS of Eqn 6.4 to write:

$$\begin{aligned} -\sum_i \frac{\partial}{\partial x_i}\left[A_i P\right] &= -\left[\frac{\partial}{\partial x}\left(A_1 P\right) + \frac{\partial}{\partial y}\left(A_2 P\right)\right] \\ &= -\left[\frac{\partial}{\partial x}\left(yP\right) - \frac{\partial}{\partial y}\left(\gamma y P + {\omega_0}^2\left\{x + \alpha x^3\right\}P\right)\right] \\ &= -y\frac{\partial P}{\partial x} + \gamma\left(P + y\frac{\partial P}{\partial y}\right) + {\omega_0}^2\left(x + \alpha x^3\right)\frac{\partial P}{\partial y}. \end{aligned} \tag{6.9}$$

Substituting Eqns 6.8 and 6.9 into Eqn 6.4 we may write the Fokker-Planck equation as:

$$\frac{\partial P}{\partial t} = -y\frac{\partial P}{\partial x} + \gamma\left(P + y\frac{\partial P}{\partial y}\right) + {\omega_0}^2\left(x + \alpha x^3\right)\frac{\partial P}{\partial y} + \frac{1}{2}\frac{\partial^2 P}{\partial y^2}. \tag{6.10}$$

It is of interest to compare Eqn 6.10 with Fokker-Planck equations obtained in the literature for linear motion of the nanoresonator. Blencowe [9] derives the following Fokker-Planck equation starting from the master equation formalism and carrying out a perturbative approximation technique borrowed from quantum mechanics known as the Born-Markov approximation.

$$\frac{\partial P}{\partial t} = \left[{\omega_R}^2 x\frac{\partial}{\partial v} - v\frac{\partial}{\partial x} + \gamma_{SET}\frac{\partial}{\partial v}v + \frac{\gamma_{SET}k_B T_{SET}}{m}\frac{\partial^2}{\partial v^2}\right]P, \tag{6.11}$$

where v stands for the velocity (which we denote in Eqn 6.10 by y), ω_R is a constant known as the renormalized oscillator frequency, γ_{SET} is another constant called the damping rate and $\gamma_{SET}k_B T_{SET}/m$ is yet another constant that involves the damping

rate, the Boltzmann constant k_B, the temperature of the SET (T_{SET}) and m the mass of the resonator. We note that Eqn 6.10 that we derived using the standard formalism of stochastic calculus is identical in form to Eqn 6.11 derived in [9] if we set the nonlinear coefficient α equal to zero. The apparent difference between the two equations exists only in the co-efficients since Eqn 6.11 is derived using a different technique. It is to be noted, however, that even though the Markov approximation does not appear explicitly in the derivation of Eqn 6.10 the defining characteristic of a Markov process (viz. that the conditional probability of the stochastic process attaining a given state in the next instant of time is dependent exclusively on the current state and on none of the previous states in its time history) is an inherent assumption in the correspondence between Eqns 6.3 and 6.4 [13],[31],[48],[51],[54].

Clerk and Bennett [20], as part of their quite general model for the SET-resonator system also derive a Fokker-Planck equation for the nanoresonator. Their model takes into account the damping effects on the resonator due to interaction with the SET as well as with the environment. Moreover, since they are interested in the strong-coupling regime of the SET-resonator interaction, they postulate that in this regime the damping coefficient γ and the diffusion coefficient D in the Fokker-Planck equation both become functions of x. The equation they obtain is given by:

$$\frac{\partial w}{\partial t} = \left[-\frac{p}{m}\frac{\partial}{\partial x} + \frac{\partial}{\partial p}\left(m\Omega^2 x + \left(\gamma_0 + \gamma\left(x\right)\right) p \right) \right] w + \left(D_0 + D\left(x\right)\right) \frac{\partial^2}{\partial p^2} w, \qquad (6.12)$$

where w denotes the probability density function, m is the mass of the resonator, p stands for momentum (equal to my in our notation), γ_0 and D_0 are the damping and diffusion coefficients due to the environment and $\gamma\left(x\right)$ and $D\left(x\right)$ are the damping and diffusion coefficients due to the interaction of the resonator with the SET. Since our model does not consider environmental effects on the resonator, in comparing Eqns 6.10 and 6.12 we can ignore the terms with coefficients γ_0 and D_0. Moreover, since we are interested in the weak-coupling regime we do not consider position dependent damping or diffusion coefficients. Keeping these two factors in mind we see that, if we restrict ourselves to the linear regime, the Fokker-Planck equation that we derive is similar to the one obtained in the Clerk-Bennett model.

6.3 The Fokker-Planck Equation in Scaled Form

Consider the scaling transformation of the variables x, y and t:

$$\begin{aligned} x' &= \frac{x}{x_0} \\ y' &= \frac{y}{y_0} \\ \epsilon &= \omega_0 \tau \\ t' &= \frac{t}{\tau}. \end{aligned} \tag{6.13}$$

Here τ is the characteristic time scale of the problem which is the electron tunneling time in the SET and x_0 is the characteristic length scale which is the magnitude of the displacement of the resonator induced by a tunneling electron. Similarly $y_0 = x_0/\tau$ represents the characteristic velocity of the problem. We recall that these scales were discussed in the chapters on the master equation approach. We can write that derivatives in the new variables as:

$$\begin{aligned} \frac{\partial}{\partial t} &= \frac{1}{\tau}\frac{\partial}{\partial t'} \\ \frac{\partial}{\partial x} &= \frac{1}{x_0}\frac{\partial}{\partial x'} \\ \frac{\partial}{\partial y} &= \frac{1}{y_0}\frac{\partial}{\partial y'} \\ \frac{\partial^2}{\partial^2 y} &= \frac{1}{{y_0}^2}\frac{\partial^2}{\partial^2 y'}. \end{aligned} \tag{6.14}$$

Substituting Eqns 6.13 and 6.14 into Eqn 6.10 we write:

$$\frac{1}{\tau}\frac{\partial P}{\partial t'} = -\frac{y_0}{x_0}y'\frac{\partial P}{\partial x'} + \gamma\left(P + y_0 y'\frac{1}{y_0}\frac{\partial P}{\partial y'}\right) + {\omega_0}^2 x_0 x'\frac{1}{y_0}\frac{\partial P}{\partial y'} + {\omega_0}^2\alpha {x_0}^3 x'^3\frac{1}{y_0}\frac{\partial P}{\partial y'} + \frac{1}{2{y_0}^2}\frac{\partial^2 P}{\partial y'^2}, \tag{6.15}$$

and with characteristic velocity as $y_0 = x_0/\tau$ we can then write:

$$\frac{1}{\tau}\frac{\partial P}{\partial t'} = -\frac{1}{\tau}y'\frac{\partial P}{\partial x'} + \gamma\left(P + y'\frac{\partial P}{\partial y'}\right) + {\omega_0}^2\tau\left(x' + \alpha {x_0}^2 x'^3\right)\frac{\partial P}{\partial y'} + \frac{1}{2{y_0}^2}\frac{\partial^2 P}{\partial y'^2}. \tag{6.16}$$

Multiplying throughout by τ, recalling the definitions $\epsilon = \omega_0\tau$ and $\alpha {x_0}^2 = \eta$ from the master equation approach and dropping the primes we can write:

$$\frac{\partial P}{\partial t} = -y\frac{\partial P}{\partial x} + \gamma\tau\left(P + y\frac{\partial P}{\partial y}\right) + \epsilon^2\left(x + \eta x^3\right)\frac{\partial P}{\partial y} + \frac{\tau}{2{y_0}^2}\frac{\partial^2 P}{\partial y^2}. \tag{6.17}$$

Considering the fact that all the coefficients in Eqn 6.17 are constant with respect to a given SET-nanoresonator system, we now define the following parameters:

$$\begin{aligned} \delta &= \gamma\tau \\ \rho &= \frac{\tau}{2{y_0}^2}. \end{aligned} \tag{6.18}$$

It is noted here that as obtained here, ρ is a dimensional quantity. However, if one were to consider a weighting factor for the random force $F(t)$ in Eqn 6.1, then one would obtain a non-dimensional parameter in the place of ρ. Using the above definitions we finally write the Fokker-Planck equation as:

$$\frac{\partial P}{\partial t} = -y\frac{\partial P}{\partial x} + \left[\delta y + \epsilon^2\left(x + \eta x^3\right)\right]\frac{\partial P}{\partial y} + \delta P + \rho\frac{\partial^2 P}{\partial y^2}. \tag{6.19}$$

6.4 Analytical Solution in the Steady State

The problem of solving for the stochastic dynamics of the SET-nanoresonator system in the Duffing regime has now essentially been reduced to solving the Fokker-Planck equation 6.19. Despite the study of equations involving differential operators of the Fokker-Planck type being a classical subject, the area continues to be one of active current research. For instance, the work of Soize [55] provides a detailed account of the steady state solutions of such equations in an abstract setting. While the article by Fuller [29] in 1969 comprehensively surveys the developments till that time, a more recent account is provided by Zhu [61] with focus on those equations that arise in the context of Hamiltonian systems. The key point of interest to us in the above references is that while Fokker-Planck equations turn out to be quite formidable in general, they admit steady state solutions in the case of dissipative Hamiltonian systems. Drawing reassurance from this generic result, we now attempt to obtain steady state solutions of Eqn 6.19 using the straightforward method of separation of variables. Even though we expect a steady state solution, we begin by assuming a time-dependent solution. As will be seen, the solution that emerges from our method is a steady state solution.

Let us assume a solution to Eqn 6.19 of the form:

$$P\left(x, y, t\right) = a\left(t\right) f\left(x\right) \exp\left(-\beta y^2\right). \tag{6.20}$$

Here β is an as yet undetermined constant. We also observe here that the assumption of exponential dependence on y of the solution is motivated by the fact that the second derivative in the Fokker-Planck operator on the RHS of Eqn 6.19 (the diffusion term, in other words) involves the variable y alone.

From Eqn 6.20 we may write:

$$\begin{aligned}
\frac{\partial P}{\partial t} &= a_t f(x) \exp\left(-\beta y^2\right); \\
\frac{\partial P}{\partial x} &= a(t) f_x \exp\left(-\beta y^2\right); \\
\frac{\partial P}{\partial y} &= -2\beta y a(t) f(x) \exp\left(-\beta y^2\right); \\
\frac{\partial^2 P}{\partial y^2} &= -2\beta a(t) f(x) \left(1 - 2\beta y^2\right) \exp\left(-\beta y^2\right).
\end{aligned} \tag{6.21}$$

Substituting Eqns 6.21 into Eqn 6.19 and using the simpler notation $a(t) = a$ and $f(x) = f$ we obtain:

$$\begin{aligned}
a_t f \exp\left(-\beta y^2\right) = -y a f_x \exp\left(-\beta y^2\right) - \left[\delta y + \epsilon^2\left(x + \eta x^3\right)\right] 2\beta a f \exp\left(-\beta y^2\right) \\
+\delta a f \exp\left(-\beta y^2\right) - 2\beta\rho a f \left(1 - 2\beta y^2\right) \exp\left(-\beta y^2\right).
\end{aligned} \tag{6.22}$$

Cancelling $\exp\left(-\beta y^2\right)$ on both sides we obtain:

$$a_t f = -y a f_x - \left[\delta y + \epsilon^2\left(x + \eta x^3\right)\right] 2\beta a f + \delta a f - 2\beta\rho a f \left(1 - 2\beta y^2\right). \tag{6.23}$$

Dividing both sides by f, we then obtain:

$$a_t = \left[-a\frac{f_x}{f} - 2a\beta\epsilon^2\left(x + \eta x^3\right)\right] y + 2a\beta\left(2\rho\beta - \delta\right) y^2 + a\left(\delta - 2\rho\beta\right). \tag{6.24}$$

Equating the coefficients of y^2 on both sides of the reduced Eqn 6.24 gives:

$$\begin{aligned}
2a\beta\left(2\rho\beta - \delta\right) &= 0 \\
\Rightarrow 2\rho\beta &= \delta.
\end{aligned} \tag{6.25}$$

Equating the coefficients of y^0 (i.e., the constants) on both sides of Eqn 6.24 and using Eqn 6.25 gives:

$$a_t = a\left(\delta - 2\beta\rho\right) \tag{6.26}$$

$$= 0. \tag{6.27}$$

$$\Rightarrow a = K, \text{an arbitrary constant.} \tag{6.28}$$

We note here that even though we started off with the assumption that a is a function of time, the solution has returned a constant value for a. Thus what we obtain is a steady state solution.

Equating the coefficients of y on both sides of Eqn 6.24 we have:

$$-a\left[\frac{f_x}{f}+2\beta\epsilon^2\left(x+\eta x^3\right)\right]=0 \tag{6.29}$$

$$\Rightarrow \frac{f_x}{f}=-2\beta\epsilon^2\left(x+\eta x^3\right) \tag{6.30}$$

$$\Rightarrow f(x)=C_0\exp\left[-2\beta\epsilon^2\left(\frac{x^2}{2}+\frac{\eta}{4}x^4\right)\right]. \tag{6.31}$$

Here C_0 is an arbitrary constant. Using Eqns 6.25, 6.26 and 6.29 and absorbing the product of the constants K and C_0 into another constant C, we can write the steady-state probability density as:

$$P\left(x,y\right)=C\exp\left[-2\beta\epsilon^2\left(\frac{x^2}{2}+\frac{\eta}{4}x^4\right)\right]\exp\left[-\beta y^2\right]. \tag{6.32}$$

It can be shown (please see Appendix F for the MAPLE file showing the calculation) that if we set $\beta=1$, the expression for $P\left(x,y\right)$ given in Eqn 6.33 identically satisfies the Fokker-Planck equation 6.19 with LHS set to zero. Hence we write our solution in the final form as:

$$P\left(x,y\right)=C\exp\left[-2\epsilon^2\left(\frac{x^2}{2}+\frac{\eta}{4}x^4\right)\right]\exp\left[-y^2\right]. \tag{6.33}$$

We note here that the constant C can be explicitly obtained by invoking the normalization condition on P. However, the explicit value of C is not required for our purposes. The steady state closed form solution derived above turns out to be of particular value in a discussion of the effective temperature attained by the system in the steady state. We shall utilize this solution in Section 6 to define an effective temperature for the system as well as to show that a lower effective temperature is obtained in the presence of nonlinearity.

6.5 Time Dependent FEM Solution

In this section we present a numerical time dependent solution to the Fokker-Planck equation 6.19 using the FEM developed in the master equation approach. In order to

solve the equation, we first need numerical values for the constant coefficients δ and ρ in Eqn 6.19. We turn to the experimental results of La Haye et al. [41], Schwab [53] and the Fokker-Planck equation derived by Blencowe [9] to obtain estimates of these values. We note here that since, to the best of our knowledge, no experiment reports on values for these coefficients in the Duffing regime, we base our estimates on the data and calculations available in the linear regime.

In order to estimate the coefficients we use the typical values as reported by Schwab [53]. If we consider a resonator with a frequency of $\omega = 60\ MHz$ and recall the definition of ϵ from the master equation formalism as $\epsilon = \omega\tau$ and assume $\epsilon = 0.3$ as in the ABZ case, we obtain an estimate of the electron tunneling time as $\tau = 0.3/60E6 = 5E-9\ s$. Since in most current experiments the resonator is very weakly coupled to the SET, we assume $\kappa = 0.1$ and $\epsilon = 0.3$. Using a result of Blencowe [9] we can then compute the unscaled damping coefficient as:

$$\begin{aligned} \gamma_{SET} &= \kappa\epsilon\omega \\ &= 1.8E6\ Hz. \end{aligned} \tag{6.34}$$

Hence we obtain the scaled damping coefficient δ (which has no units) as [9]:

$$\begin{aligned} \delta &= \gamma_{SET}\ \tau \\ &= 9E-3. \end{aligned} \tag{6.35}$$

Assuming a characteristic displacement of $x_0 = 100\ nm$[53], along with a tunneling time $\tau = 5E{-}9$, one obtains the characteristic velocity $y_0 = 20\ m/s$. Hence we compute the scaled diffusion coefficient as:

$$\begin{aligned} \rho &= \frac{\tau}{2{y_0}^2} \\ &= 6E-12. \end{aligned} \tag{6.36}$$

We recall here that our results from the master equation approach and our subsequent analysis of the damping mechanism in the SET-resonator system pointed to the fact that the assumption of linear damping is categorically valid only in the presence of weak to moderately strong ($0 \leq \eta \leq 0.6$) nonlinearities in the resonator motion. Hence

we restrict ourselves to the range of η as defined above. For the FEM, based on our estimates discussed above we assume values of the same order of magnitude as obtained from our calculations as $\delta = 5E-3$ and $\rho = 1E-12$. The initial condition for the probability density function is chosen to be a sharply peaked Gaussian density with mean 0.5 and variance 0.00625. We note here that the fact that we are dealing with a partial differential equation in the nonlinear regime makes the task of generating consistent FEM solutions a very challenging one. The absence of experimental results in the nonlinear regime that could guide the choice of δ and ρ compounds the problem. Moreover, the convergence of the FEM solutions was found to be sensitive to the choice of δ and ρ in the nonlinear regime. Hence, in order to obtain consistent results, the above values for the parameters as well as the initial conditions were chosen based on a detailed numerical investigation. It is also noted here that while the value of ρ that we have obtained is extremely small, the use of a weighting factor for the random force $F(t)$ can increase the value of ρ. While a more detailed analysis incorporating the weighting factor will be of value in future work, here we do not expect our results to be significantly affected by this feature. The results from the numerical computations are presented in Fig 6.1 to Fig 6.4. In the figures the mean displacement of the resonator is plotted against time for values of η in the range 0 to 0.6. The effect of the nonlinearity is to drive the system to the steady state more rapidly. However, this may not be apparent from a cursory glance at the figures since the difference is not enormous. Hence, in order to establish this, in the following figure we compare the solutions obtained for $\eta = 0$ and $\eta = 0.6$. Thus this figure shows a juxtaposition of the solutions shown in Fig 6.1 and Fig 6.4. It is clear from Fig 6.5 that our conclusion from the master equation approach that the resonator attains a steady state much more rapidly in the presence of nonlinearity is validated by the Langevin approach as well. The differences in amplitude and phase between the solutions evidently indicate that the damping process is accelerated in the presence of nonlinearity. Thus far, the ABZ and the Langevin models agree. However it is of interest here to contrast their conclusions as well. From Fig 6.5 it is seen that the mean resonator displacement tends to zero

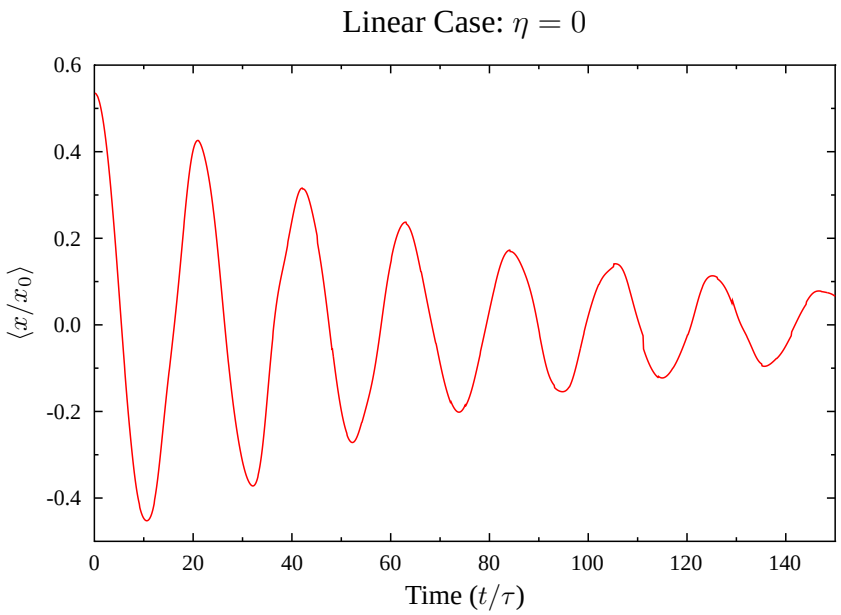

Figure 6.1: FEM Results: Mean Displacement vs Time

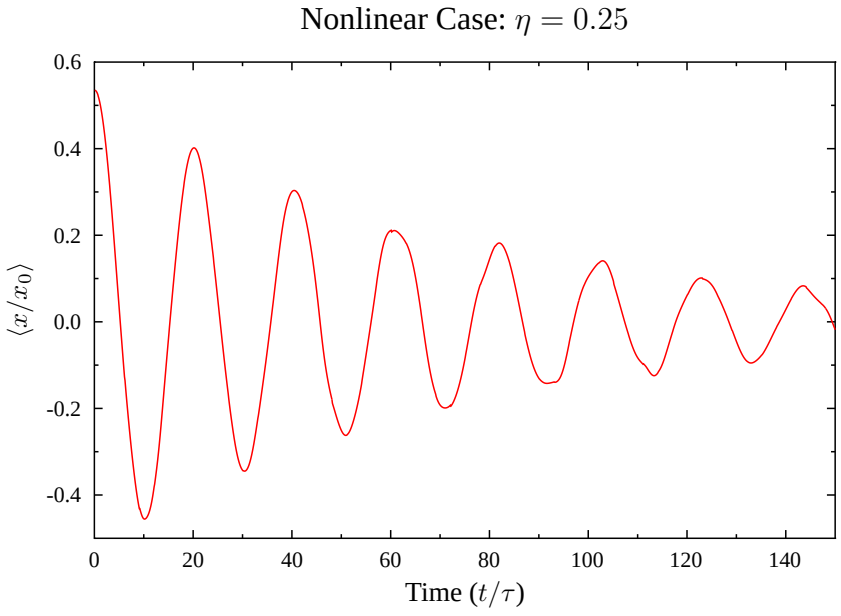

Figure 6.2: FEM Results: Mean Displacement vs Time

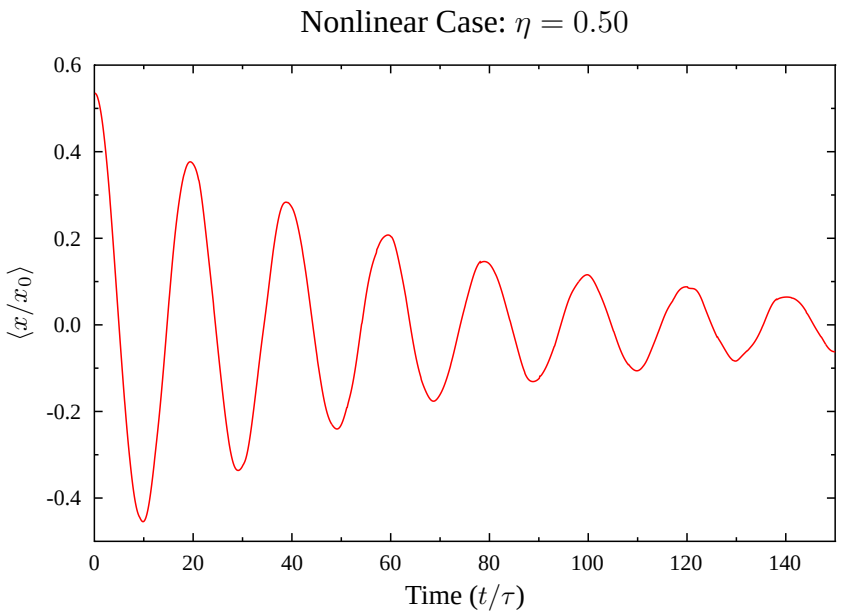

Figure 6.3: FEM Results: Mean Displacement vs Time

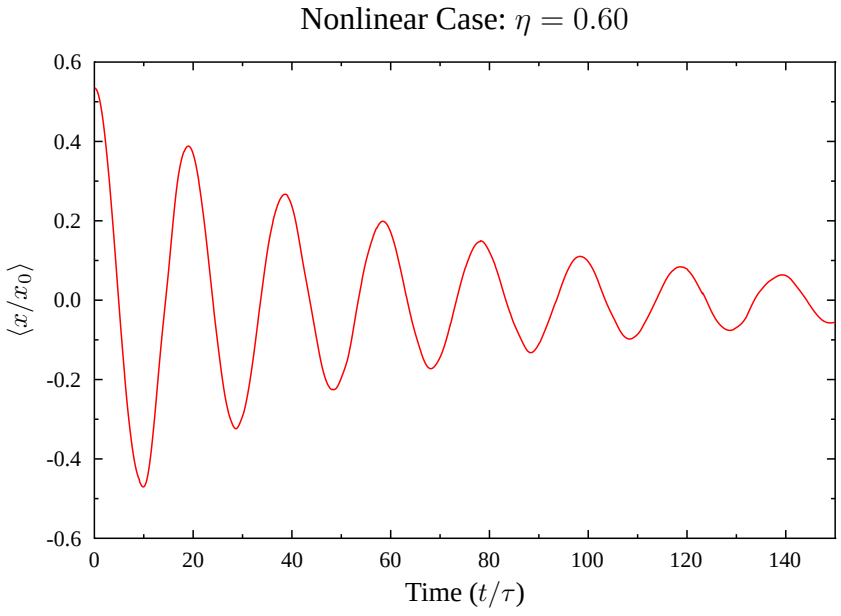

Figure 6.4: FEM Results: Mean Displacement vs Time

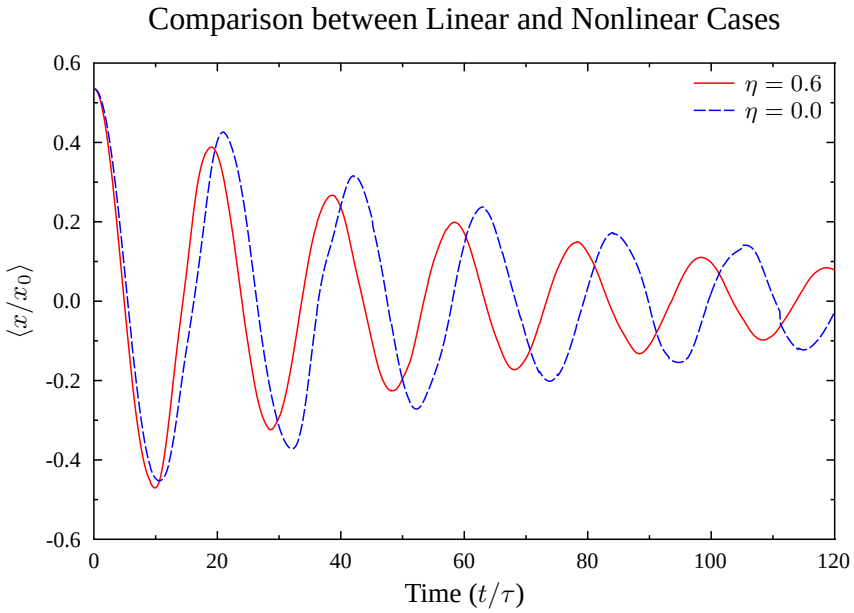

Figure 6.5: FEM Results: Mean Displacement vs Time

as the system evolves in time to a steady state whereas in the ABZ model, the steady state corresponds to a non-zero value for the mean displacement (Fig 3.3). This is due to the fact that, in the Langevin model, the damping mechanism represented by the $\gamma\dot{x}$ term in Eqn 6.1 dominates when compared with the energy provided to the resonator (represented by the random forcing term $F(t)$). In other words, there exists asymmetry between the processes that transfer energy to and from the resonator. Indeed, this is another consequence of having introduced a damping term by hand into the Langevin equation. However, we emphasize that the conclusion that the steady state is attained more rapidly in the presence of nonlinearity holds despite this asymmetry in the energy transfer mechanism between the SET and the resonator.

It is a generic principle of stochastic analysis that the behavior of both the first and second moments of a random variable ought to be taken into consideration in drawing conclusions about the dynamical behavior of the variable. Hence, we present in Fig 6.6, a comparison of the evolution of the variances of the resonator displacement between

the linear and nonlinear cases.

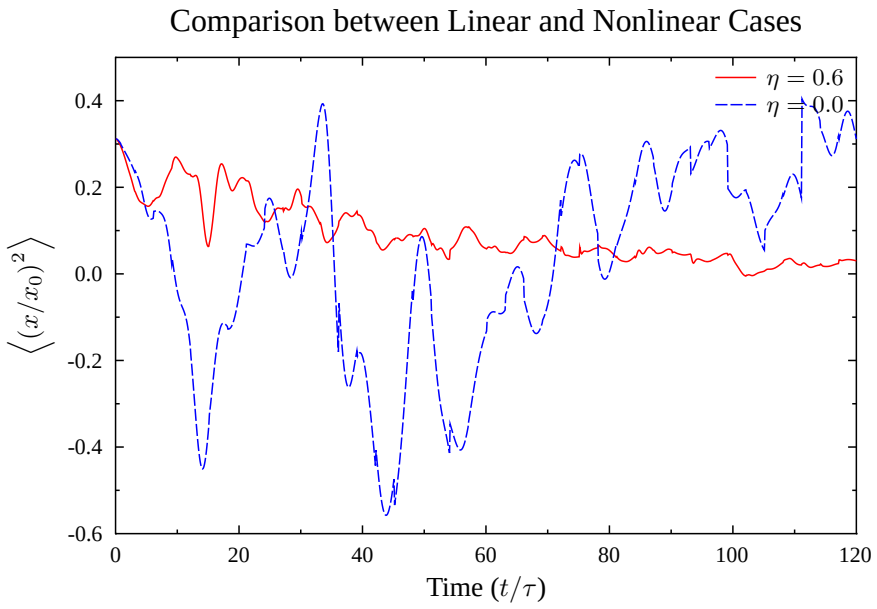

Figure 6.6: FEM Results: Variance of Displacement vs Time

We note from Fig 6.6 that the variance of the resonator displacement shows lesser variation with respect to time in the nonlinear case and that it approaches zero as the system tends to the steady state. This implies that, probabilistically, there is less uncertainty associated with the mean resonator displacement in the nonlinear case when compared with the linear case.

Finally, to further convince ourselves of the validity of our conclusions, we compare the behavior of the variance of the velocity between the linear and the nonlinear cases. In Fig 6.7, we present a comparison of the variances of the velocities.

Indeed, Fig 6.7 provides further evidence that the nonlinear case gives rise to statistically more robust dynamics since the variance of the velocity shows smaller fluctuations as the steady state is approached.

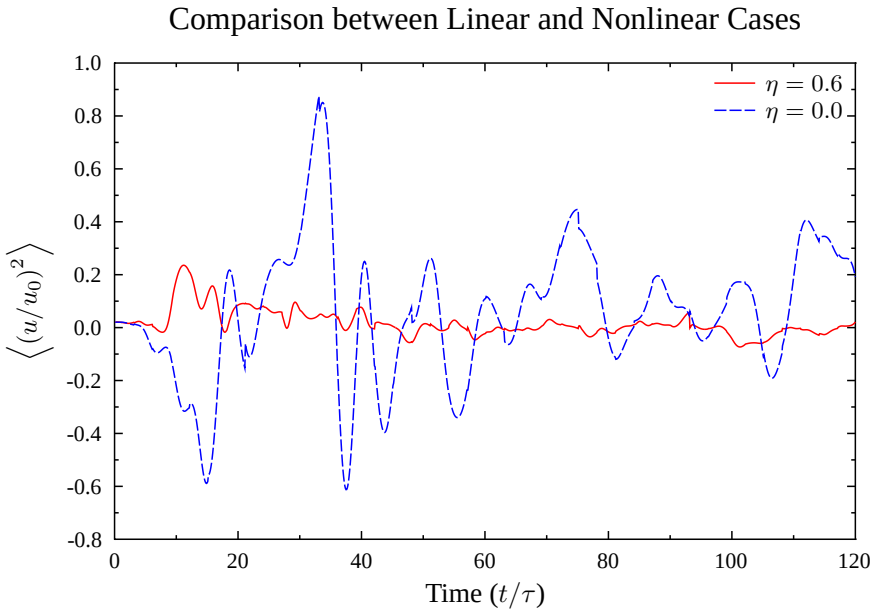

Figure 6.7: FEM Results: Variance of Velocity vs Time

6.6 Temperature

As discussed in Chapter 1, the effective temperature of the SET-resonator system is a quantity of great interest both from the theoretical and practical points of view. In this section we are primarily interested in the effect of the Duffing nonlinearity on the steady state temperature of the resonator. In particular, we would like to examine whether the presence of nonlinearity results in a lower effective temperature. As will be seen below, the definition of temperature involves analytical expressions for the mean energy in the steady state and of course these can be computed only if one has access to the steady state probability density of the system. Thus, we can embark on this exercise precisely because we have obtained the steady state density in Eqn 6.33. The fact that the Duffing resonator is a Hamiltonian system also plays a crucial role.

The classical result from statistical mechanics that allows the definition of effective temperature of a dynamical system is the theorem of equipartition of energy [58],[39]. In its most general form, the equipartition theorem may be stated as follows. Consider

a Hamiltonian system with energy $H(x_1, x_2, .., x_n)$, where $(x_1, x_2, .., x_n)$ are the generalized co-ordinates that describe the system. In thermal equilibrium, for all indices m and n, the theorem asserts:

$$\left\langle x_m \frac{\partial H}{\partial x_n} \right\rangle = \delta_{mn} k_B T, \tag{6.37}$$

where δ_{mn} is the Kronecker delta symbol, k_B is the Boltzmann constant and T is the absolute temperature. Using the definition of the Kronecker delta, that it equals unity when $m = n$ and vanishes otherwise, we can write Eqn 6.37 equivalently as:

$$\begin{aligned} \left\langle x_n \frac{\partial H}{\partial x_n} \right\rangle &= k_B T \; \forall \; n \\ \left\langle x_m \frac{\partial H}{\partial x_n} \right\rangle &= 0 \; \forall \; m \neq n. \end{aligned} \tag{6.38}$$

A distinguishing feature of Hamiltonian mechanics is the binary classification of all generalized co-ordinates into generalized position co-ordinates and generalized momenta, each of the latter being canonically conjugate to the corresponding position. In terms of the generalized position co-ordinates $q_1, q_2, .., q_n$ and conjugate momenta $p_1, p_2, .., p_n$ the Hamiltonian can be expressed as $H(p_1, p_2, .., p_n; q_1, q_2, .., q_n)$. Keeping in mind that each of the p_k and q_k are independent co-ordinates, we can write the first of Eqns 6.38 explicitly as:

$$\begin{aligned} \left\langle p_k \frac{\partial H}{\partial p_k} \right\rangle &= \left\langle q_k \frac{\partial H}{\partial q_k} \right\rangle \\ &= k_B T, \; \forall \; k \text{ from 1 to } n. \end{aligned} \tag{6.39}$$

Now, let us consider a linear harmonic oscillator with mass m, spring constant k, displacement given by q and momentum $p = mv$, where v is the velocity. Recalling that the Hamiltonian is nothing but the sum of the kinetic and potential energies of the system, we can write:

$$H = \frac{p^2}{2m} + \frac{1}{2} k q^2. \tag{6.40}$$

Substituting Eqn 6.40 into Eqn 6.39 followed by an elementary calculation yields:

$$\frac{1}{2} \left\langle m v^2 \right\rangle = \frac{1}{2} \left\langle k q^2 \right\rangle = k_B T. \tag{6.41}$$

Hence, for a harmonic oscillator in equilibrium with a thermal bath (in other words, the oscillator is in a steady state) the mean kinetic energy equals the mean potential energy

which is proportional to the absolute temperature. This is the fundamental result that is invoked to define an equilibrium effective temperature for the SET-resonator system (see, for instance, Armour et. al [3], Blencowe [9]).

It bears repetition that the method is hinged on the following features of the system: (1) it is Hamiltonian, (2) there exists a steady state, the probability density corresponding to which is known and (3) the mean values given within angled brackets in Eqn 6.39 exist and are finite. The condition (3) is a recognition of the fact that computing the mean values implies computing integrals involving the probability densities and that these integrals need not, necessarily, converge to yield finite values.

In the case of the Duffing oscillator, we are assured of the conditions (1) and (2). In what follows we compute the quantities in Eqn 6.39, verify that finite mean values emerge and thereby obtain a definition of the effective temperature of the system. Consider a Duffing resonator with mass m, frequency ω_0 and nonlinear parameter β. The Hamiltonian is given by:

$$H = \frac{p^2}{2m} + \frac{1}{2} m {\omega_0}^2 \left(x^2 + \beta x^4\right). \tag{6.42}$$

Differentiating H with respect to p and recalling that the momentum $p = m\dot{x} = my$ where we have introduced the notation $\dot{x} = y$ for the velocity, we can write:

$$\begin{aligned} \frac{\partial H}{\partial p} &= \frac{p}{m} = \frac{m\dot{x}}{m} \\ &= y. \end{aligned} \tag{6.43}$$

Hence we have:

$$p\,\frac{\partial H}{\partial p} = my^2. \tag{6.44}$$

We recall that the steady state density was derived as (Eqn 6.33):

$$P\left(x, y\right) = C \exp\left[-2\epsilon^2 \left(\frac{x^2}{2} + \frac{\eta}{4} x^4\right)\right] \exp\left[-y^2\right]. \tag{6.45}$$

Using Eqn 6.44 and Eqn 6.45 in Eqn 6.39 we obtain:

$$\begin{aligned} \left\langle p \frac{\partial H}{\partial p} \right\rangle &= mC \int_{-\infty}^{\infty} \int_{-\infty}^{\infty} e^{-2\epsilon^2 \left(\frac{x^2}{2} + \frac{\eta}{4} x^4\right)} e^{-y^2} y^2 dx dy \\ &= mC \int_{-\infty}^{\infty} e^{-y^2} y^2 dy \int_{-\infty}^{\infty} e^{-2\epsilon^2 \left(\frac{x^2}{2} + \frac{\eta}{4} x^4\right)} dx \\ &= k_B T. \end{aligned} \tag{6.46}$$

The first integral on the RHS of Eqn 6.46 is a standard one given by:

$$\int_{-\infty}^{\infty} z^2 e^{-az^2} dz = \frac{1}{2}\sqrt{\frac{\pi}{a^3}}, \tag{6.47}$$

where a is a constant. Substituting $a = 1$, we can write the first integral in the RHS of Eqn 6.46 as:

$$\int_{-\infty}^{\infty} y^2 e^{-y^2} dy = \frac{\sqrt{\pi}}{2}. \tag{6.48}$$

Defining a new constant

$$\Lambda = mC\frac{\sqrt{\pi}}{2}\frac{1}{k_B}, \tag{6.49}$$

we can define the steady state effective temperature of the resonator as:

$$T = \Lambda \int_{-\infty}^{\infty} e^{-2\epsilon^2\left(\frac{x^2}{2}+\frac{\eta}{4}x^4\right)} dx. \tag{6.50}$$

It is evident from Eqn 6.50 that the effective temperature is directly proportional to the value of the integral which we denote by I. In the following figure we plot the value of I versus the strength of the nonlinearity measured by η between 0 and 1. For the sake of consistency we maintained $\epsilon = 0.3$ in this calculation as well. It turns out that I is indeed convergent in this case ($\forall\ \eta \geq 0$) and furthermore, is a monotonically decreasing function of η. We also note here that I fails to converge for $\eta < 0$ and hence this approach to defining an effective temperature for the resonator is not valid in the double-well Duffing regime.

Thus Fig 6.8 leads us to the conclusion that in the presence of the single-well Duffing type of nonlinearity the resonator attains a lower steady state effective temperature. This is an important conclusion since, as we have repeatedly emphasized in this dissertation, a major focus of current research in NEMS is the cooling of mesoscopic systems and the above result indicates that better cooling could be achieved in the nonlinear regime.

It is interesting to note here how our results from Chapter 3 were indicative of the present result. From our results in Chapter 3, comparing the variance of the displacement in the steady state as the strength of the nonlinearity is increased it is seen from Figs. 3.11, 3.19 and 3.27 that progressively lower values are obtained. Intuitively, a

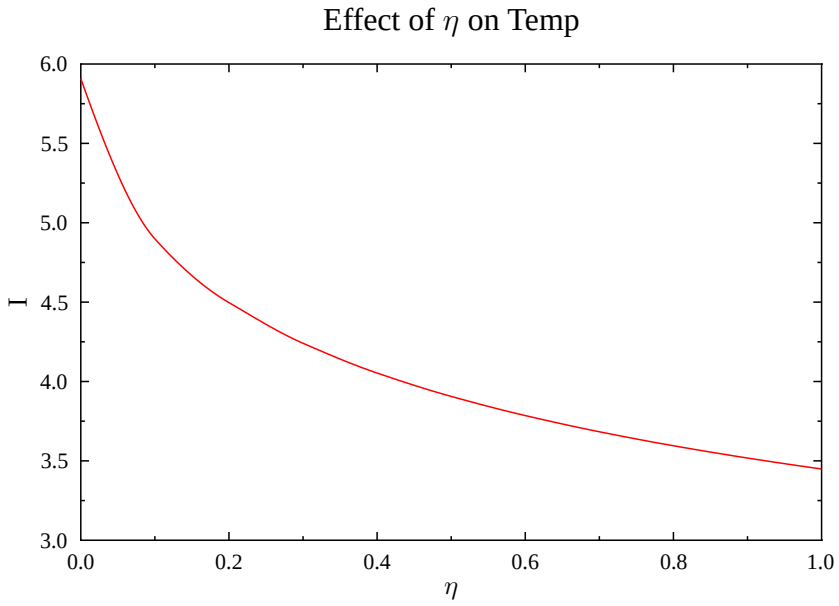

Figure 6.8: Effect of nonlinearity on Temperature

lower value for the variance of the displacement in the steady state corresponds to a lower effective temperature for the system. However, the applicability of the generalized form of the equipartition theorem in this case is what allows us to put this conclusion on a firm theoretical basis.

Finally, we note from Fig 6.8 that significant percentage drop in the temperature is observed even in the presence of relatively weak nonlinearity ($0 < \eta < 0.5$). While indicating the sensitivity of the steady state temperature to the presence of nonlinearity, this behavior is also of importance from the practical point of view since the weakly nonlinear regime is the most readily accessible in practical situations.

6.7 Conclusion

In this chapter we approached the dynamics of the SET-resonator system from a Langevin point of view. Starting with the Langevin equation for the resonator motion, we derived the corresponding Fokker-Planck equation and obtained an analytical closed

form solution for the response density function in the time-independent case. In the time-dependent case, we obtained FEM solutions for the mean and the mean squared displacements. Comparing with the solutions obtained from the master equation approach it was found that the two methods led to similar conclusions. In particular, the conclusion that the SET-resonator system approaches the steady state more rapidly in the presence of nonlinearity was well supported by the Langevin model. Finally, taking advantage of the fact that we obtained a closed form analytical steady state solution for the response density function, we invoked a generalization of the equipartition of energy theorem from statistical mechanics to reach the important conclusion that the system attains a lower steady state effective temperature in the presence of nonlinearity in the single-well Duffing case. As noted earlier, such an approach to defining an effective temperature is not valid in the double-well Duffing regime since the integrals involved in the definition fail to converge in that case.

Chapter 7

Conclusions and Future Work

7.1 Conclusions

1. The results obtained in this dissertation show that the ABZ model for the coupled dynamics of the SET-nanoresonator system afford a generalization to the Duffing regime.

2. In the single-well Duffing case, the SET damps the resonator at a significantly higher rate when compared to the linear regime. Furthermore, the rate of damping markedly increases with the strength of the effective nonlinearity in the system. The latter is characterized by a new parameter that emerged from our analysis which we have called η.

3. The higher rate of damping arises exclusively due to the interaction of the resonator with the SET since no extrinsic source of damping, such as environmental effects, are considered in our model.

4. Since our results are obtained for relatively weak coupling between the SET and the resonator, our results demonstrate that nonlinear resonator motion significantly impacts the coupled dynamics even if the SET and the resonator are weakly coupled to each other. This is important since usually nonlinear effects are associated with strongly coupled systems.

5. The SET-resonator system can be effectively used in sensory applications only after the coupled dynamics has achieved a steady state. Since our results show that due to enhanced damping the steady state is attained much more rapidly in

the single-well Duffing case, this indicates that the system is likely to work as a better sensor in the nonlinear regime.

6. From our solutions we observe a qualitative change in the damping mechanism in the strongly nonlinear regime of the single-well Duffing case. This is an important result both from the perspective of analytical modelling in the strongly nonlinear regime as well as the point of view of applications.

7. In the double-well Duffing case, our results show that in the presence of very weak nonlinearity, the SET damps the oscillator and the system reaches a steady state. However, in comparison with the linear case, the SET finds it harder to damp the motion of the resonator. The inability of the SET to damp the resonator becomes acute as the strength of the nonlinearity is increased.

8. For a critical value of $\eta = -0.11$ in the double-well Duffing case, we observe the remarkable phenomenon that the SET and the resonator attain a state of dynamical equilibrium with no energy exchange taking place between the two. This is characterized by the appearance of a limit cycle in the phase space. Below this critical value of $\eta = -0.11$, we observe the onset of instability which is physically characterized by the SET continuously pumping energy into the resonator. The phenomenon of the resonator gaining energy from the SET is called the SET back-action and is a topic of great current interest. While back-action arising from unique processes in the SET have been discussed in the literature, our results show that the phenomenon can arise from instabilities in the nonlinear regime.

9. The mathematical nature of the damping term is latent in the master equation formalism of the ABZ model. We conclude from a fit analysis that a linear damping term of the form $\alpha\dot{x}$ adequately models the resonator behavior in the single-well Duffing regime only for a parameter range defined by $0 \leq \eta \leq 0.6$. This is consistent with our earlier result that qualitative changes in the damping mechanism occur in the strongly nonlinear regime.

10. Our results using the Langevin approach, when compared with the ones we obtained from the generalized ABZ model, confirm that the SET-resonator system approaches the steady state more rapidly in the single-well Duffing case.

11. We obtained an analytical closed form solution to the steady state Fokker-Planck equation for the probability density function in the Langevin approach. Using this solution in combination with the theorem of equipartition of energy we conclude that the SET-resonator system attains a lower effective steady state temperature in the single-well Duffing case. This result is significant in the context of cooling of nanomechanical resonators.

7.2 Future Work

1. Our generalization of the ABZ model is applicable exclusively to the case of weak coupling between the SET and the resonator. While this is currently the most readily experimentally realizable regime, there is a lot of interest (see, for instance [25]) in the strong coupling regime. The analysis of Duffing nonlinearities in the strong coupling regime is a problem for future work.

2. The ABZ model could further be generalized to the case of very strong nonlinearities, for instance the one represented by the full pendulum potential $\cos x$. This would provide an extreme case from the point of view of nonlinear behavior.

3. In our generalization of the ABZ model to the Duffing regime we assumed that only linear terms in the resonator Hamiltonian influence the tunnelling rates in the SET. This was dictated by the fact that currently little is known about the nonlinear behavior of the SET itself. As our understanding of the SET improves, the scope exists for developing fully nonlinear models of the SET-resonator interaction.

4. Highly sophisticated variants of the SET have been used in very recent experiments [46]. In particular, a device known as the superconducting SET (SSET) has

proved itself to be of immense value in NEMS. The tunnelling process in a SSET is a superconducting process and therefore of a higher order of complexity when compared to those in a SET. While the Clerk-Bennett [20] model is applicable to the SSET, it has been unable to account for some anomalies observed in recent experiments with a SSET-resonator system. It is possible that nonlinear considerations can better account for these experimental results. Overall, the nonlinear dynamics of a nanomechanical resonator coupled to a SSET is an important open problem.

5. An important aspect of NEMS that has not been discussed in this dissertation is that of control. The application of mathematical control theory to quantum systems with a view towards controlling systems like NEMS is an emerging and exciting area of current research. In particular, the principles of quantum control have been applied to the SET-resonator system by Hopkins and co-workers [36] in the linear regime to show that better cooling may be achieved by monitoring the position of the resonator and then using this information to realize feedback control. The enhanced damping effects that we observed in the ABZ framework and the explicit cooling results of the Langevin approach provide a compelling case to attempt to apply the ideas of Hopkins *et al.* [36] to the nonlinear regime.

6. The single-well Duffing regime is readily accessible in current experiments and it is of importance to obtain experimental validation of the results obtained in this dissertation.

The above discussion concludes the chapter and the dissertation.

Appendix A

Derivation of Moment Evolution Equations

A.1 Basic Equations

The basic equations used in the derivation of the moment evolution equations are reproduced here from Chapter 3. Also we note that all integrations in the calculations are carried out in the interval $(-\infty, \infty)$.

$$\begin{aligned}\frac{\partial P_N}{\partial t} &= \epsilon^2 \left[x + \eta x^3\right] \frac{\partial P_N}{\partial u} \\ &\quad - u\frac{\partial P_N}{\partial x} + \left[\frac{P_{N+1}}{2} - \frac{P_N}{2} - \kappa x P\right].\end{aligned} \tag{A.1}$$

$$\begin{aligned}\frac{\partial P_{N+1}}{\partial t} &= \epsilon^2 \left[(x-1) + \eta\,(x-1)^3\right] \frac{\partial P_{N+1}}{\partial u} \\ &\quad - u\frac{\partial P_{N+1}}{\partial x} - \left[\frac{P_{N+1}}{2} - \frac{P_N}{2} - \kappa x P\right].\end{aligned} \tag{A.2}$$

$$\frac{\partial P}{\partial t} = \epsilon^2 x\frac{\partial P}{\partial u} + \epsilon^2\eta x^3\frac{\partial P}{\partial u} - \epsilon^2\,(1+\eta)\,\frac{\partial P_{N+1}}{\partial u} + 3\epsilon^2\eta x\frac{\partial P_{N+1}}{\partial u} - 3\epsilon^2\eta x^2\frac{\partial P_{N+1}}{\partial u} - u\frac{\partial P}{\partial x}. \tag{A.3}$$

For a random process s governed by the density P, at every instant of time,

$$\int dx \int du\; s\frac{\partial P}{\partial t} = \frac{d\langle s\rangle}{dt}. \tag{A.4}$$

Also, for arbitrary functions $f\,(x)$ and $g\,(u)$ of the random variables x and u, we have:

$$\int f\,(x)\,dx \int \frac{\partial P_{N+1}}{\partial u}du = \int f\,(x)\,dx \int dP_{N+1} = 0. \tag{A.5}$$

$$\int g\,(u)\,du \int \frac{\partial P_{N+1}}{\partial x}dx = \int g\,(u)\,du \int dP_{N+1} = 0. \tag{A.6}$$

In Eqns. A.5 and A.6 the results hold even if P_{N+1} is replaced with P_N or P. Also we recall from Chapter 3 that we assume that the densities vanish asymptotically:

$$P|_{-\infty}^{\infty} \;=\; P_N|_{-\infty}^{\infty} \;=\; P_{N+1}|_{-\infty}^{\infty} = 0. \tag{A.7}$$

A.2 $\langle P \rangle_{N+1}$

Integrating both sides of Eqn. A.2 w.r.t x and u in the limits $(-\infty, \infty)$ and using Eqns. A.4, A.5, A.6,

$$\begin{aligned}\frac{d}{dt}\langle P \rangle_{N+1} &= -\int\int dxduP_{N+1} + 0.5\int\int dxduP + \kappa\int\int dxduxP \\ &= -\langle P \rangle_{N+1} + 0.5 + \kappa\langle x \rangle.\end{aligned}$$

A.3 $\langle x^3 \rangle$

Multiplying both sides of Eqn A.3 by x^3, integrating w.r.t x and u in the limits $(-\infty, \infty)$ and using Eqns. A.4, A.5, A.6,

$$\begin{aligned}\frac{d}{dt}\langle x^3 \rangle &= -\int udu\int x^3\frac{\partial P}{\partial x}dx \\ &= -\int udu\int x^3 dP \\ &= -\int udu\left[x^3P|_{-\infty}^{\infty} - \int 3x^2Pdx\right] \\ &= 3\int\int x^2uPdxdu \\ &= 3\langle x^2u \rangle.\end{aligned}$$

A.4 $\langle x \rangle_{N+1}$

Multiplying both sides of Eqn. A.2 by x we obtain:

$$\begin{aligned}x\frac{\partial P_{N+1}}{\partial t} = \epsilon^2 x\left[(x-1) + \eta\,(x-1)^3\right]\frac{\partial P_{N+1}}{\partial x} \\ - xP_{N+1} + (0.5 + \kappa x)xP.\end{aligned}$$

Integrating both sides w.r.t. x and u in the limits $(-\infty, \infty)$ and using Eqns. A.4 and A.5,

$$\frac{d}{dt}\langle x \rangle = 0 - \int udu\int x\frac{\partial P_{N+1}}{\partial x}dx - \langle x \rangle + 0.5\langle x \rangle + \kappa\langle x^2 \rangle. \tag{A.8}$$

Now,

$$\begin{aligned} -\int udu \int x\frac{\partial P_{N+1}}{\partial x}dx &= -\int udu \int x dP_{N+1} \\ &= \int udu \left[xP_{N+1}|_{-\infty}^{\infty} - \int P_{N+1}dx \right] \\ &= \langle u \rangle_{N+1} . \end{aligned} \tag{A.9}$$

$\Rightarrow$

$$\frac{d}{dt}\langle x \rangle_{N+1} = \langle u \rangle_{N+1} - \langle x \rangle_{N+1} + 0.5\langle x \rangle + \kappa \langle x^2 \rangle. \tag{A.10}$$

A.5 $\langle x^2 \rangle_{N+1}$

Multiplying both sides of Eqn. A.2 by x^2 we obtain:

$$\begin{aligned} x^2\frac{\partial P_{N+1}}{\partial t} = \epsilon^2 x^2 \left[(x-1) + \eta(x-1)^3 \right] \frac{\partial P_{N+1}}{\partial u} - ux^2\frac{\partial P_{N+1}}{\partial x} \\ - x^2 P_{N+1} + (0.5 + \kappa x)x^2 P. \end{aligned} \tag{A.11}$$

Integrating both sides in the limits $(-\infty, \infty)$ w.r.t. x and u and using Eqns. A.4 and A.5, we then obtain,

$$\frac{d}{dt}\langle x^2 \rangle = 0 - \int udu \int x^2 \frac{\partial P_{N+1}}{\partial x} - \langle x^2 \rangle + 0.5\langle x^2 \rangle + \kappa \langle x^3 \rangle. \tag{A.12}$$

Now,

$$\begin{aligned} -\int udu \int x^2\frac{\partial P_{N+1}}{\partial x}dx &= -\int udu \int x^2 dP_{N+1} \\ &= -\int udu \left[x^2 P_{N+1}|_{-\infty}^{\infty} - \int 2xP_{N+1}dx \right] \\ &= 2\int uxP_{N+1}dxdu \\ &= 2\langle ux \rangle_{N+1}. \end{aligned} \tag{A.13}$$

$\Rightarrow$

$$\frac{d}{dt}\langle x^2 \rangle = 2\langle ux \rangle_{N+1} - \langle x^2 \rangle_{N+1} + 0.5\langle x^2 \rangle + \kappa \langle x^3 \rangle. \tag{A.14}$$

A.6 $\langle x^2 \rangle$

Multiplying both sides of A.3 by x^2, integrating over x and u in the limits $(-\infty, \infty)$ and using Eqn. A.5,

$$\begin{aligned}
\frac{d}{dt}\langle x^2 \rangle &= -\int u du \int x^2 \frac{\partial P}{\partial x} dx \\
&= -\int u du \left[x^2 P|_{-\infty}^{\infty} - \int 2xP dx \right] \\
&= 2\int uxP dx du \\
&= 2\int uxP dx du \\
&= 2\langle ux \rangle.
\end{aligned} \tag{A.15}$$

A.7 $\langle u \rangle_N$

Using $P = P_N + P_{N+1}$ to replace P_{N+1} in the last term on the RHS of Eqn. A.1, we first write:

$$\frac{dP_N}{dt} = \epsilon^2 \left[x + \eta x^3 \right] \frac{\partial P_N}{\partial u} - u \frac{\partial P_N}{\partial x} + \left[(0.5 - \kappa x)P - P_N \right]. \tag{A.16}$$

Multiplying both sides by u and integrating w.r.t. x and u in the limits $(-\infty, \infty)$, let us denote the terms on the RHS by T_1, T_2, T_3, T_4 and T_5.

$$\begin{aligned}
T_1 &= \epsilon^2 \int (x + \eta x^3) dx \int \frac{\partial P_N}{\partial u} u du \\
&= \epsilon^2 \int (x + \eta x^3) dx \int u dP_N \\
&= \epsilon^2 \int (x + \eta x^3) dx \left[uP_N|_{-\infty}^{\infty} - \int P_N du \right] \\
&= \epsilon^2 \int \int (x + \eta x^3) P_N dx du \\
&= -\epsilon^2 \left[\langle x \rangle_N + \eta \langle x^3 \rangle_N \right].
\end{aligned} \tag{A.17}$$

$$\begin{aligned}
T_2 &= -\int u^2 du \int \frac{\partial P_N}{\partial x} dx \\
&= -\int u^2 du \int dP_N \\
&= -\int u^2 du P_N|_{-\infty}^{\infty} = 0.
\end{aligned} \tag{A.18}$$

$$T_3 = 0.5 \int\int uPdxdu = 0.5\langle u\rangle. \tag{A.19}$$

$$T_4 = -\kappa \int\int xuPdxdu = -\kappa\langle xu\rangle. \tag{A.20}$$

$$T_5 = -\int\int uP_N dxdu = -\langle u\rangle_N. \tag{A.21}$$

Collecting the terms and using Eqn. A.4,

$$\frac{d}{dt}\langle u\rangle_N = -\epsilon^2\left[\langle x\rangle_N + \eta\langle x^3\rangle_N\right] + 0.5\langle u\rangle - \kappa\langle xu\rangle - \langle u\rangle_N. \tag{A.22}$$

A.8 $\langle u\rangle_{N+1}$

Recalling $P = P_N + P_{N+1}$ we write:

$$\begin{aligned}\langle u\rangle &= \int\int uPdxdu \\ &= \int\int u(P_N + P_{N+1})dxdu \\ &= \langle u\rangle_N + \langle u\rangle_{N+1}.\end{aligned} \tag{A.23}$$

$\Rightarrow$

$$\frac{d}{dt}\langle u\rangle_{N+1} = \frac{d}{dt}\langle u\rangle + \frac{d}{dt}\langle u\rangle_N. \tag{A.24}$$

A.9 $\langle x^3\rangle_N$

Multiplying both sides of Eqn. A.1 by x^3, integrating over x and u in the limits $(-\infty, \infty)$ and using Eqn. A.5,

$$\begin{aligned}\frac{d}{dt}\langle x^3\rangle_N &= -\int udu \int x^3 \frac{\partial P_N}{\partial x}dx \\ &= -\int udu \int x^3 dP_N \\ &= -\int udu \left[x^3 P_N|_{-\infty}^{\infty} - \int P_N 3x^2 dx\right] \\ &= 3\int\int x^2 uP_N dxdu \\ &= 3\langle x^2 u\rangle_N.\end{aligned} \tag{A.25}$$

Appendix B

Freefem++ Code: FEM

B.1 The Linear Case

```
// file convects.edp
// Characteristics Galerkin
// BEST FOR LINEAR CASE- No initial Adaptmesh, later AM with
// if (i < 10 || (i%30)==0 ) { Th=adaptmesh(Th,p); }

border C(t=0, 2*pi) { x=5.0*cos(t);  y=5.0*sin(t); };
mesh Th = buildmesh(C(500));
fespace Vh(Th,P1);
Vh p0 = exp(-((x-0.5)^2+y^2)/(2*0.00625))/(2*pi*0.00625);
//Th=adaptmesh(Th,p0);
real norm = 2*int2d(Th)(p0);
Vh p1 = (exp(-((x-0.5)^2+y^2)/(2*0.00625))/(2*pi*0.00625))/norm, p2=p1;
Vh p,p1old, p2old,q1,q2;
real np; //  =max(p1,p2);

//cout<<"Initial: I(p) " <<  2*int2d(Th)(p0)<<endl;
//cout<<"Initial: I(x*p) "<< 2*int2d(Th)(x*p0)<<endl;
//cout<<"Initial: I(u*p) "<< 2*int2d(Th)(y*p0)<<endl;
real dt = 0.05, t=0, k=0.1, e=0.3, eta=0.0;

Vh u1 = y, u2 = -e*e*(x + eta*x^3);
```

```
Vh u3 = y, u4 = -e*e*((x-1) + eta*(x-1)^3);


problem lin(p1,p2,q1,q2)=
   int2d(Th)(
        (p1*q1+p2*q2)/dt
        -(p2*(0.5-k*x)-p1*(0.5+k*x))*q1
        -(p1*(0.5+k*x)-p2*(0.5-k*x))*q2)
  + int2d(Th)(
        -q1*convect([u1,u2],-dt,p1old)/dt
        -q2*convect([u3,u4],-dt,p2old)/dt)
  +on(C,p1=0,p2=0);


{
ofstream fp3("lin.dat");
  for(int i=0;i<3000;i++){
     t=t+dt;
     p1old=p1;
     p2old=p2;
     lin;
     np=int2d(Th)(p1+p2);
     p1=p1/np; p2=p2/np;
     fp3<<t<<"  "<<int2d(Th)(x*(p1+p2))<<endl;
     p=max(p1,p2);
     if (i < 10 || (i%30)==0 ) { Th=adaptmesh(Th,p); }
   }
}
real pp=int2d(Th)(p1+p2);
p1=p1/pp; p2=p2/pp;
{
```

```
ofstream fp1("p1lin.dat");
for(int i=1;i<500;i++) fp1<<-5+i*0.1<<"  "<<p1(-5+i*0.1,0)<<endl;
ofstream fp2("p2lin.dat");
for(int i=1;i<500;i++) fp2<<-5+i*0.1<<"  "<<p2(-5+i*0.1,0)<<endl;
}
```

B.2 The Single - Well Duffing Case

```
// file convects.edp
// Characteristics Galerkin
border C(t=0, 2*pi) { x=5.0*cos(t);  y=5.0*sin(t); };
mesh Th = buildmesh(C(500));
fespace Vh(Th,P1);

Vh p0 = exp(-((x-0.5)^2+y^2)/(2*0.00625))/(2*pi*0.00625);
//Th=adaptmesh(Th,p0);
real norm = 2*int2d(Th)(p0);
Vh p1 = (exp(-((x-0.5)^2+y^2)/(2*0.00625))/(2*pi*0.00625))/norm,
   p2=p1;
Vh p,p1old, p2old,q1,q2;
real np; //  =max(p1,p2);

//cout<<"Initial: I(p) " <<  2*int2d(Th)(p0)<<endl;
//cout<<"Initial: I(x*p) "<< 2*int2d(Th)(x*p0)<<endl;
//cout<<"Initial: I(u*p) "<< 2*int2d(Th)(y*p0)<<endl;

//Th=adaptmesh(Th,p1);

//plot(Th);
```

```
real dt = 0.4, t=0., k=0.1, e=0.3, eta=1.0;

Vh u1 = y, u2 = -e*e*(x + eta*x^3);
Vh u3 = y, u4 = -e*e*((x-1) + eta*(x-1)^3);

problem lin(p1,p2,q1,q2)=
   int2d(Th)(
         (p1*q1+p2*q2)/dt
         -(p2*(0.5-k*x)-p1*(0.5+k*x))*q1
         -(p1*(0.5+k*x)-p2*(0.5-k*x))*q2)
  + int2d(Th)(
         -q1*convect([u1,u2],-dt,p1old)/dt
         -q2*convect([u3,u4],-dt,p2old)/dt)
  +on(C,p1=0,p2=0);

{
ofstream fp3("1pt4.dat");
  for(int i=0;i<1000;i++){
     t=t+dt;
     p1old=p1;
     p2old=p2;
     lin;
     np=int2d(Th)(p1+p2);
     p1=p1/np; p2=p2/np;
     fp3<<t<<"  "<<int2d(Th)(x*(p1+p2))<<" "
     <<int2d(Th)(((x^2)*y)*(p1+p2))<<" "
     <<int2d(Th)((x^2)*(p1+p2))*int2d(Th)(y*(p1+p2))<<" "
     <<int2d(Th)((x*y)*(p1+p2))<<"  "
```

```
     <<int2d(Th)(x*(p1+p2))*int2d(Th)(y*(p1+p2))<<" "
     <<int2d(Th)((x*y)*p2)<<" "
     <<int2d(Th)(x*p2)*int2d(Th)(y*p2)<<"  "
     <<int2d(Th)(((x^2)*y)*(p1))<<"  "
     <<int2d(Th)((x^2)*(p1))*int2d(Th)(y*(p1))<<endl;
     p=max(p1,p2);
     if (i < 10 || (i%30)==0 ) { Th=adaptmesh(Th,p); }
   }
}

//plot(p1);

real pp=int2d(Th)(p1+p2);
p1=p1/pp; p2=p2/pp;
{
ofstream fp1("p1duff.dat");
for(int i=1;i<701;i++) fp1<<-5+i*0.1<<"  "<<p1(-5+i*0.1,0)<<endl;
ofstream fp2("p2duff.dat");
for(int i=1;i<701;i++) fp2<<-5+i*0.1<<"  "<<p2(-5+i*0.1,0)<<endl;
}
```

B.3 The Double-Well Duffing Case

```
// Characteristics Galerkin
border C(t=0, 2*pi) { x=5.0*cos(t);  y=5.0*sin(t); };
mesh Th = buildmesh(C(500));
fespace Vh(Th,P1);

Vh p0 = exp(-((x-0.5)^2+y^2)/(2*0.00625))/(2*pi*0.00625);
Th=adaptmesh(Th,p0);
```

```
real norm = 2*int2d(Th)(p0);
Vh p1 = (exp(-((x-0.5)^2+y^2)/(2*0.00625))/(2*pi*0.00625))/norm,
   p2=p1;
Vh p,p1old, p2old,q1,q2;
real np; //  =max(p1,p2);

//cout<<"Initial: I(p) " <<  2*int2d(Th)(p0)<<endl;
//cout<<"Initial: I(x*p) "<< 2*int2d(Th)(x*p0)<<endl;
//cout<<"Initial: I(u*p) "<< 2*int2d(Th)(y*p0)<<endl;

//Th=adaptmesh(Th,p1);

//plot(Th);


real dt = 0.05, t=0., k=0.1, e=0.3, eta=-0.04;

Vh u1 = y, u2 = -e*e*(x + eta*x^3);
Vh u3 = y, u4 = -e*e*((x-1) + eta*(x-1)^3);

problem lin(p1,p2,q1,q2)=
   int2d(Th)(
        (p1*q1+p2*q2)/dt
        -(p2*(0.5-k*x)-p1*(0.5+k*x))*q1
        -(p1*(0.5+k*x)-p2*(0.5-k*x))*q2)
  + int2d(Th)(
        -q1*convect([u1,u2],-dt,p1old)/dt
        -q2*convect([u3,u4],-dt,p2old)/dt)
  +on(C,p1=0,p2=0);
```

```
{
ofstream fp3("pt05-am.dat");
  for(int i=0;i<2400;i++){
     t=t+dt;
     p1old=p1;
     p2old=p2;
     lin;
     np=int2d(Th)(p1+p2);
     p1=p1/np; p2=p2/np;
     fp3<<t<<"  "<<int2d(Th)(x*(p1+p2))<<"  "
     <<int2d(Th)(((x^2)*y)*(p1+p2))<<"  "
     <<int2d(Th)((x^2)*(p1+p2))*int2d(Th)(y*(p1+p2))<<"  "
     <<int2d(Th)((x*y)*(p1+p2))<<"  "
     <<int2d(Th)(x*(p1+p2))*int2d(Th)(y*(p1+p2))<<"  "
     <<int2d(Th)((x*y)*p2)<<"  "
     <<int2d(Th)(x*p2)*int2d(Th)(y*p2)<<"  "
     <<int2d(Th)(((x^2)*y)*(p1))<<"  "
     <<int2d(Th)((x^2)*(p1))*int2d(Th)(y*(p1))<<endl;
     p=max(p1,p2);
     if (i < 10 || (i%30)==0 ) { Th=adaptmesh(Th,p); }
   }
}

plot(p1);
real pp=int2d(Th)(p1+p2);
p1=p1/pp; p2=p2/pp;
{
ofstream fp1("p1duff.dat");
```

```
for(int i=1;i<701;i++) fp1<<-5+i*0.1<<"  "<<p1(-5+i*0.1,0)<<endl;
ofstream fp2("p2duff.dat");
for(int i=1;i<701;i++) fp2<<-5+i*0.1<<"  "<<p2(-5+i*0.1,0)<<endl;
}
```

B.4 The Fokker-Planck Equation

```
// Characteristics Galerkin
// For Solving Fokker-Planck Equations

border C(t=0, 2*pi) { x=15.0*cos(t);  y=15.0*sin(t); };
mesh Th = buildmesh(C(300));
fespace Vh(Th,P1);

Vh p0 = exp(-((x-0.5)^2+y^2)/(2*0.00625))/(2*pi*0.00625);
//Th=adaptmesh(Th,p0);
real norm = int2d(Th)(p0);
Vh p = (exp(-((x-0.5)^2+y^2)/(2*0.00625))/(2*pi*0.00625))/norm;
Vh pold,q;
real np; //  =max(p1,p2);

//cout<<"Initial: I(p) " <<  2*int2d(Th)(p0)<<endl;
//cout<<"Initial: I(x*p) "<< 2*int2d(Th)(x*p0)<<endl;
//cout<<"Initial: I(u*p) "<< 2*int2d(Th)(y*p0)<<endl;

//Th=adaptmesh(Th,p1);

//plot(Th);
```

```
real dt = 0.1, t=0., k=0.1, e=0.3, delta= 0.005,
     rho= 0.000000000001, eta=0.6;

Vh u1 = y, u2 = -(delta)*y -e*e*(x + eta*x^3);

problem fokker(p,q)=
   int2d(Th)(
        (p*q)/dt
        -(p*delta)*q
        - rho*dy(p)*dy(q))
  + int2d(Th)(
        -q*convect([u1,u2],-dt,pold)/dt)
  +on(C,p=0);

{
ofstream fp3("etapt6.dat");
  for(int i=0;i<1500;i++){
     t=t+dt;
     pold=p;
     fokker;
     np=int2d(Th)(p);
     fp3<<t<<"  "<<int2d(Th)(x*(p))<<"  "
     <<int2d(Th)(x^2*p)<<"  "
     <<int2d(Th)(y*p)<<" "
     <<int2d(Th)(y^2*p)<<endl;
     if (i < 10 || (i%30)==0 ) { Th=adaptmesh(Th,p); }
   }
}
```

Appendix C

MATLAB Code For Moment Evolution Equations

C.1 Linear Case

```
% MATLAB Code For MEM
% e = \epsilon; k =\kappa; n = \eta
% Time [0 400]
% Initial Conds: [0.5;0.0;0.5;0.134;0.25;0.129;0.256;0.0;0.067]

function dx = linear(t,x)
dx = zeros(9,1);
e = 0.3;
k = 0.1;
n = 0.0;
dx(1) = x(2);
dx(2) = -(e^2)*(x(1) + n*x(4)) + (e^2)*(1+n)* x(3)
        - 3*(e^2)*n*x(5) + 3*(e^2)*n*x(6);
dx(3) = -x(3) +0.5 + k*x(1);
dx(4) = 3*x(2)*x(7);
dx(5) = x(2)- x(8) - x(5) +(0.5)*x(1) + k*x(7);
dx(6) = 2 * (x(2)-x(8))*x(5) - x(6) + (0.5)*x(7) + k*x(4);
dx(7) = 2*x(2)*x(1);
dx(8) = -e^2*(x(1) - x(5) + n*x(9)) + (0.5)*x(2) - k*x(1)*x(2) - x(8);
dx(9) = 3*(x(7)-x(6))*x(8);
```

C.2 Single-Well Duffing Case

```
% MATLAB Code For MEM
% e = \epsilon; k =\kappa; n = \eta
% Time [0 400]
% Initial Conds: [0.5;0.0;0.5;0.134;0.25;0.129;0.256;0.0;0.067]

function dx = duffhard(t,x)
dx = zeros(9,1);
e = 0.3;
k = 0.1;
n = 1.0;
dx(1) = x(2);
dx(2) = -(e^2)*(x(1) + n*x(4)) + (e^2)*(1+n)* x(3)
        - 3*(e^2)*n*x(5) + 3*(e^2)*n*x(6);
dx(3) = -x(3) +0.5 + k*x(1);
dx(4) = 3*x(2)*x(7);
dx(5) = x(2)- x(8) - x(5) +(0.5)*x(1) + k*x(7);
dx(6) = 2 * (x(2)-x(8))*x(5) - x(6) + (0.5)*x(7) + k*x(4);
dx(7) = 2*x(2)*x(1);
dx(8) = -e^2*(x(1) - x(5) + n*x(9)) + (0.5)*x(2) - k*x(1)*x(2) - x(8);
dx(9) = 3*(x(7)-x(6))*x(8);
```

C.3 Double-Well Duffing Case

```
% MATLAB Code For MEM
% e = \epsilon; k =\kappa; n = \eta
% Time [0 400]
% Initial Conds: [0.5;0.0;0.5;0.134;0.25;0.129;0.256;0.0;0.067]
```

```
function dx = duffsoft(t,x)

dx = zeros(9,1);

e = 0.3;

k = 0.1;

n = -0.25;

dx(1) = x(2);

dx(2) = -(e^2)*(x(1) + n*x(4)) + (e^2)*(1+n)* x(3)

        - 3*(e^2)*n*x(5) + 3*(e^2)*n*x(6);

dx(3) = -x(3) +0.5 + k*x(1);

dx(4) = 3*x(2)*x(7);

dx(5) = x(2)- x(8) - x(5) +(0.5)*x(1) + k*x(7);

dx(6) = 2 * (x(2)-x(8))*x(5) - x(6) + (0.5)*x(7) + k*x(4);

dx(7) = 2*x(2)*x(1);

dx(8) = -e^2*(x(1) - x(5) + n*x(9)) + (0.5)*x(2) - k*x(1)*x(2) - x(8);

dx(9) = 3*(x(7)-x(6))*x(8);
```

Appendix D

MAPLE Code: Initial Conditions For MEM

```
> restart:
> c:=625/10^5: g:=(x,u)-> exp(-((x-1/2)^2+u^2)/2/c)/(2*Pi*c):

> b1:=int(int(x*g(x,u),u=-infinity..infinity),x=-infinity..infinity):
b2:=int(int(u*g(x,u),u=-infinity..infinity),x=-infinity..infinity):
# int(int(x*g(x,u),u=-infinity..infinity),x=-infinity..infinity):
b3:=0.5:
b4:=int(int(x^3*g(x,u),u=-infinity..infinity),x=-infinity..infinity):
b5:=b1/2:
b6:=int(int(x^2*g(x,u),u=-infinity..infinity),x=-infinity..infinity)/2:
b7:=2.0*b6:
b8:=b2/2.:
b9:=b4/2.:

#Initial Conditions given by:
> 'x1(0)'=evalf(b1);'x2(0)'=evalf(b2);'x3(0)'=evalf(b3);
  'x4(0)'=evalf(b4);'x5(0)'=evalf(b5);'x6(0)'=evalf(b6);
  'x7(0)'=evalf(b7);'x8(0)'=evalf(b8);'x9(0)'=evalf(b9);

#To Check Normalization
> int(int(g(x,u),u=-infinity..infinity),x=-infinity..infinity);
```

Appendix E

MATLAB Code: Fit Analysis

E.1 Main Code

```
% To obtain best fit DE and solve
% Step 1: Solve moment eqns (duffhard.m)
% Step 2: Use data to get \ddot{x} and \dot{x}
% Step 3: Fit data to U_{11}\ddot{x} + U_{21}\dot{x} + x + U_{31} = 0
%         - Line 28 generates the best fit U
% Step 4: Use the coeffs of U to solve
%         U_{11}\ddot{x} + U_{21}\dot{x} + x + U_{31} = 0
%         using (newfitduff.m).
% Step 5: Plot disp vs time in both cases.


 clear all;%clc;
 global U;
 [T,X]=ode45(@duffhard,[0 200],
             [0.5;0.0;0.5;0.134;0.25;0.129;0.256;0.0;0.067]);
e = 0.3;
k = 0.1;
n = -0.25;
 x=X(:,1);
 xdot=X(:,2);
 xddot= -(e^2)*(X(:,1) + n*X(:,4))
        + (e^2)*(1+n)*X(:,3) - 3*(e^2)*n*X(:,5) + 3*(e^2)*n*X(:,6);
```

```
 %A=[xdot, x.*xdot, x, x.^3];
 %A=[xdot, x.^2.*xdot, x, x.^3, ones(561,1)];
 A=[xddot, xdot, x.^3];
 %A=[xdot, x.*xdot, x.^2.*xdot, x.^3.*xdot, x, x.^3, ones(561,1)];
 %A=[xdot, x.*xdot, x, x.^3, ones(561,1)];
 %A=[xdot, x.*xdot, x, x.^3];
 %A=[xdot, x, x.^3];
 B=-[x];
 % A*U=B
 %%U=A\B
 U = pinv(A)*B
% dy = newfitduff(U)
plot(T,X(:,1),'r');hold on;
 [t,y] = ode45(@newfitduff, [0 200], [0.5;0.]);
 plot(t,y(:,1),'g--');legend('X','y');
```

E.2 To Obtain Fit Solution

```
function dy = newfitduff(t,y)
global U;
dy = zeros(2,1);
dy(1) = y(2);
dy(2) = (- y(1) - U(2,1)*y(2) - U(3,1)*y(1)^3 )/U(1,1);
```

E.3 Original MEM Solution

```
% e = \epsilon; k =\kappa; n = \eta
% Time [0 400]
% Initial Conds: [0.5;0.0;0.5;0.134;0.25;0.129;0.256;0.0;0.067]
function dx = duffhard(t,x)
dx = zeros(9,1);
```

```
e = 0.3;

k = 0.1;

n = -0.25;

dx(1) = x(2);

dx(2) = -(e^2)*(x(1) + n*x(4)) + (e^2)*(1+n)* x(3)

        - 3*(e^2)*n*x(5) + 3*(e^2)*n*x(6);

dx(3) = -x(3) +0.5 + k*x(1);

dx(4) = 3*x(2)*x(7);

dx(5) = x(2)- x(8) - x(5) +(0.5)*x(1) + k*x(7);

dx(6) = 2 * (x(2)-x(8))*x(5) - x(6) + (0.5)*x(7) + k*x(4);

dx(7) = 2*x(2)*x(1);

dx(8) = -e^2*(x(1) - x(5) + n*x(9))

        + (0.5)*x(2) - k*x(1)*x(2) - x(8);

dx(9) = 3*(x(7)-x(6))*x(8);
```

Appendix F

MAPLE Code: Steady State Solution For Fokker-Planck Equation

```
> restart;

> beta:=1;


> P:= C*exp(-beta*y^2)*exp(-2*beta*epsilon^2*(x^2/2 + eta*x^4/4));


> LHS:=diff(P,t);


> RHS:= -y*diff(P,x) + (delta*y+ epsilon^2*(x+eta*x^3))*diff(P,y)
        +delta*P +delta*diff(P,y$2)/2*beta;


> res:= RHS-LHS;


> simplify(res);
```

References

[1] J. S. Aldridge and A. N. Cleland. Noise enabled precision measurements of a duffing nanomechanical resonator. *Phys. Rev. Lett.*, 94:156403, 2005.

[2] M. Amman, R. Wilkins, E. Ben-Jacob, P. D. Maker, and R. C. Jaklevic. Analytic solution for the current-voltage characteristic of two mesoscopic tunnel junctions coupled in series. *Phys. Rev. B.*, 43:1146–1149, 1991.

[3] A. D. Armour, M. P. Blencowe, and Y. Zhang. Classical dynamics of a nanomechanical resonator coupled to a single electron transistor. *Phys. Rev. B.*, 69:125313, 2004.

[4] A. D. Armour and A. MacKinnon. Transport via a quantum shuttle. *Phys. Rev. B*, 66:035333, 2002.

[5] D. V. Averin and K. K. Likharev. Coulomb blockade of single-electron tunneling, and coherent oscillations in small tunnel junctions. *Jour. Low Temp. Phys.*, 62:345–373, 1986.

[6] E. Ben-Jacob, D. J. Bergman, B. J. Matkowsky, and Z. Schuss. Master-equation approach to shot noise in josephson junctions. *Phys. Rev. B*, 34:1572–1581, 1986.

[7] Ya. M. Blanter, O. Usmani, and Yu. V. Nazarov. Single-electron tunneling with strong mechanical feedback. *Phys. Rev. Lett.*, 93:136802, 2004.

[8] M. P. Blencowe. Nanomechanical quantum limits. *Science*, 304:56–57, 2004.

[9] M. P. Blencowe. Nanoelectromechanical systems. *Contemporary Physics*, 46:249–264, 2005.

[10] R. H. Blick, A. Erbe, L. Pescini, and et.al. Nanostructured silicon for studying fundamental aspects of nanomechanics. *J. Phys.: Cond. Matter.*, 14:R905–R945, 2002.

[11] T. Brandes and N. Lambert. Steering of a bosonic mode with a double quantum dot. *Phys. Rev. B*, 67:125323, 2003.

[12] E. Buks and M. L. Roukes. Electricallu tunable collective response in a coupled micromechanical array. *Jour. Micromech. Sys.*, 11:802–807, 2002.

[13] S. Chandrasekhar. Stochastic problems in physics and astronomy. *Rev. Mod. Phys.*, 15:1–89, 1943.

[14] A. Cho. Researchers race to put the quantum into mechanics. *Science*, 299:36–37, 2003.

[15] A. N. Cleland. *Foundations of Nanomechanics*. Springer, Heidelberg, 2002.

[16] A. N. Cleland and M. R. Geller. Superconducting qubit storage and entanglement with nanomechanical resonators. *Phys. Rev. Lett.*, 93:070501, 2004.

[17] A. N. Cleland and M. L. Roukes. A nanometre scale mechanical electrometer. *Nature*, 392:160–162, 1998.

[18] A. N. Cleland and M. L. Roukes. Noise processes in nanomechanical resonators. *J. App. Phys.*, 92:2758–2769, 2002.

[19] A. A. Clerk. Quantum-limited position detection and amplification: A linear response perspective. *Phys. Rev. B.*, 70:245306, 2004.

[20] A. A. Clerk and S. Bennett. Quantum nano-electromechanics with electrons, quasiparticles and cooper pairs: effective bath descriptions and strong feedback effects. *New J. Phys.*, 7:238, 2005.

[21] A. A. Clerk and S. M. Girvin. Shot noise of a tunnel junction displacement detector. *Phys. Rev. B.*, 70:121303, 2004.

[22] R. Courant and D. Hilbert. *Methods of Mathematical Physics - Vol.2*. John Wiley and Sons, New York, 1989.

[23] H. G. Craighead. Nanoelectromechanical systems. *Science*, 290:1532–1535, 2000.

[24] A. J. Davies. *The Finite Element Method: A First Approach*. Oxford University Press, Oxford, UK, 1980.

[25] C. B. Doiron, W. Belzig, and C. Bruder. Electrical transport through a single electron transistor strongly coupled to an oscillator. *Phys. Rev. B.*, 74:205336, 2006.

[26] K. L. Ekinci, X. M. H. Huang, and M. L. Roukes. Ultrasensitive nanoelectromechanical mass detection. *App. Phys. Lett.*, 84:4469–4471, 2004.

[27] A. Erbe, H. Krommer, A. Kraus, and et.al. Mechanical mixing in nonlinear nanomechanical resonators. *Applied Phys. Lett.*, 77:3102–3104, 2000.

[28] D. K. Ferry and S. M. Goodnick. *Transport in Nanostructures*. CUP, Cambridge, 1997.

[29] A. T. Fuller. Analysis of nonlinear stochastic systems by means of the Fokker-Planck equation. *Int. Jour. Control*, 9:603–655, 1969.

[30] T.A. Fulton and G. J. Dolan. Observation of single-electron charging effects in small tunnel junctions. *Phys. Rev. Lett.*, 59:109–112, 1987.

[31] C. W. Gardiner. *Handbook of Stochastic Methods*. Springer-Verlag, Berlin, 1985.

[32] H. Goldstein. *Classical mechanics*. Addison-Wesley Publishing Co., Reading, Mass., second edition, 1980. Addison-Wesley Series in Physics.

[33] L. Y. Gorelik, A. Isacsson, M. V. Voinova, B. Kasemo, R. I. Shekhter, and M. Jonson. Shuttle mechanism for charge transport in coulomb blockade nanostructures. *Phys. Rev. Lett.*, 80:4526, 1998.

[34] J. Guckenheimer and P. Holmes. *Nonlinear Oscillations, Dynamical Systems, and Bifurcations of Vector Fields*. Springer-Verlag, New York, 1983.

[35] F. Hecht, O. Pironneau, A. LeHyaric, and K. Ohtsuka. *freefem++ Manual*. University of Paris, Paris, 2005.

[36] A. Hopkins, K. Jacobs, S. Habib, and K. Schwab. Feedback cooling of a nanomechanical resonator. *Phys. Rev. B.*, 68:235328, 2003.

[37] X. M. H. Huang, C. A. Zorman, M. Mehregany, and et al. Nanodevice motion at microwave frequencies. *Nature*, 421:496, 2003.

[38] A. Isacsson, L. Y. Gorelik, , M. V. Voinova, B. Kasemo, R. I. Shekhter, and M. Jonson. Shuttle instability in self assembled coulomb blockade nanostructures. *Physica B*, 255:150, 1998.

[39] C. Kittel. *Elementary Statistical Physics*. Wiley, New York, 1961.

[40] R. G. Knobel and A. N. Cleland. Nanometre scale displacement sensing using a single electron transistor. *Nature*, 424:291, 2003.

[41] M. D. LaHaye, O. Buu, B. Camarota, and K. C. Schwab. Approaching the quantum limit of a nanomechanical resonator. *Science*, 304:74–77, 2004.

[42] L. D. Landau and E. M. Lifshitz. *Course of theoretical physics. Vol. 1*. Pergamon Press, Oxford, second edition, 1987.

[43] R. J. Leveque. *Finite Volume Methods for Hyperbolic Problems*. Cambridge University Press, Cambridge-UK, 2002.

[44] R. Lifshitz and M. C. Cross. Response of parametrically driven nonlinear coupled oscillators with application to micromechanical and nanomechanical resonator arrays. *Phys. Rev. B.*, 67:134302, 2003.

[45] J. D. Logan. *An Introduction to Nonlinear Partial Differential Equations*. John Wiley and Sons, New York, 1994.

[46] A. Naik, O. Buu, M. D. LaHaye, and et.al. Cooling a nanomechanical resonator with quantum back-action. *Nature*, 443:193–196, 2006.

[47] T. Nord, L. Y. Gorelik, R. I. Shekhter, and M. Jonson. Electromechanics of charge shuttling in dissipative nanostructures. *Phys. Rev. B.*, 65:165312, 1991.

[48] Bernt Øksendal. *Stochastic differential equations*. Universitext. Springer-Verlag, Berlin, sixth edition, 2003. An introduction with applications.

[49] V. Peano and M. Thorwat. Macroscopic quantum effects in a strongly driven nanomechanical resonator. *Phys. Rev. B.*, 70:235401, 2004.

[50] S. Ramakrishnan. Stochastic analysis of non-holonomic dynamical systems. Master's thesis, The Johns Hopkins University, 2001.

[51] H. Risken. *The Fokker-Planck Equation*. Springer-Verlag, Berlin, 1984.

[52] D. V. Scheible, A. Erbe, R. H. Blick, and G. Corso. Evidence of a nanomechanical resonator being driven into chaotic response via the ruelle takens route. *Applied Phys. Lett.*, 81:1884–1886, 2002.

[53] K. Schwab. Spring constant and damping constant tuning of nanomechanical resonators using a single-electron transistor. *App. Phys. Lett.*, 80:1276–1278, 2002.

[54] Kazimierz Sobczyk. *Stochastic differential equations*, volume 40 of *Mathematics and its Applications (East European Series)*. Kluwer Academic Publishers Group, Dordrecht, 1991. With applications to physics and engineering.

[55] C. Soize. *The Fokker-Planck equation for stochastic dynamical systems and its explicit steady state solutions*, volume 17 of *Series on Advances in Mathematics for Applied Sciences*. World Scientific Publishing Co. Inc., River Edge, NJ, 1994.

[56] G. Strang and G. J. Fix. *An Analysis of the Finite Element Method*. Prentice-Hall, Englewood Cliffs, NJ, 1973.

[57] S. H. Strogatz. *Nonlinear Dynamics and Chaos*. Perseus, Cambridge MA, 1994.

[58] R. C. Tolman. *The principles of statistical mechanics*. Dover Publications Inc., New York, 1979. Reprint of the 1938 original.

[59] E. T. Whittaker. *A treatise on the analytical dynamics of particles and rigid bodies*. Cambridge Mathematical Library. Cambridge University Press, Cambridge, 1988. With an introduction to the problem of three bodies, Reprint of the 1937 edition, With a foreword by William McCrea.

[60] S. Zaitsev, R. Almog, O. Schtempluck, and E. Buks. Nonlinear dynamics in nanomechanical oscillators. In W. Badawy and W. Moussa, editors, *Proceedings of the International Conference on MEMS, NANO and Smart Systems*, pages 387–391. IEEE Computer Society, 2005.

[61] W. Q. Zhu. Nonlinear stochastic dynamics and control in hamiltonian formulation. *Trans. ASME*, 59:230–248, 2006.

Vita

Subramanian Ramakrishnan

1992 B. Tech. (Mechanical Engineering), Mahatma Gandhi University, Kerala, India.

1996-99 M.Sc. (Mechanical Engineering), University of Calgary, Calgary, Canada.

1999-01 M.S.E. (Mechanical Engineering), Johns Hopkins University, Baltimore, USA.

2002-04 Project Specialist, MCS Inc., Houston, USA.

2004-07 Ph. D. in Mechanical Engineering, Rutgers, The State University of New Jersey, New Brunswick, USA.